ELECTROCHEMICAL AND ELECTRON TRANSFER INVESTIGATIONS OF COPPER PROTEINS

Thesis by

Cynthia Strong St. Clair

In Partial Fulfillment of the Requirements

for the Degree of

Doctor of Philosophy

California Institute of Technology

Pasadena, California

1989

(Submitted April 3, 1989)

Acknowledgements

First of all, I would like to thank Harry for his support and encouragement. I am also grateful to many past and present members of the Gray group and other people at Caltech for their friendship, assistance, and support. Thanks are especially due to Mike, Erica, Bruce, Mary, and Van. I would also like to thank the members of WorldWork and its previous incarnations for many enjoyable hours of commiseration on the state of the world, and for some wonderful potlucks.

I am very grateful for the expert assistance of Dave Malerba with the electrochemical instrumentation, Adel Naylor for her patient assistance with Biograf, and Walther Ellis for his collaboration on the azurin electrochemistry.

The time I've spent at Caltech has been tremendously enriched by many people outside of Caltech. In particular, I would like to acknowledge the people at Casa Grande and at All Saints for their friendship and for helping me to learn about many things other than chemistry.

I would like to thank my parents, Bob and Sara Jane Strong, for their constant encouragement and their faith in me, and for supporting me in many ways. Finally, I would like to thank my husband, Marty, for patiently supporting me, for valuing my goal of a liberal arts college job, and for his love and friendship.

ABSTRACT

A study of the pH and temperature dependence of the redox potentials of azurins from five species of bacteria has been performed. The variations in the potentials with pH have been interpreted in terms of electrostatic interactions between the copper site and titrating histidine residues, including the effects of substitutions in the amino acid sequences of the proteins on the electrostatic interactions. A comparison of the observed pH dependences with predictions based on histidine pK_a values known for *Pseudomonas aeruginosa* (Pae), *Alcaligenes denitrificans* (Ade), and *Alcaligenes faecalis* (Afa) azurins indicates that the Pae and Ade redox potentials exhibit pH dependences in line with electrostatic arguments, while Afa azurin exhibits more complex behavior. Redox enthalpies and entropies for four of the azurins at low and high pH values have also been obtained. Based on these results in conjuction with the variable pH experiments, it appears that *Bordetella bronchiseptica* azurin may undergo a more substantial conformational change with pH than has been observed for other species of azurin.

The temperature dependence of the redox potential of bovine erythrocyte superoxide dismutase (SOD) has been determined at pH 7.0, with potassium ferricyanide as the mediator. The following thermodynamic parameters have been obtained (T = 25°C): $E^{\circ\prime}$ = 403±5 mV vs. NHE, $\Delta G^{\circ\prime}$ = -9.31 kcal/mol, $\Delta H^{\circ\prime}$ = -21.4 kcal/mol, $\Delta S^{\circ\prime}$ = -40.7 eu, $\Delta S^{\circ\prime}_{rc}$ = -25.1 eu. It is apparent from these results that $\Delta H^{\circ\prime}$, rather than $\Delta S^{\circ\prime}$, is the dominant factor in establishing the high redox potential of SOD. The large negative enthalpy of reduction may also reflect the factors which give SOD its high specificity toward reduction and oxidation by superoxide.

TABLE OF CONTENTS

LIST OF FIGURES

CHAPTER 1

CHAPTER 4

LIST OF TABLES

CHAPTER 1

CHAPTER 2

CHAPTER 1

INTRODUCTION

Copper is employed in a number of roles in biological systems, including oxygen binding, oxygen reduction, and electron transfer.[1,2] The active sites of many copper-containing proteins can be classified according to their spectroscopic properties as type 1, type 2, or type 3. Examples of proteins with each of these sites are listed in Table 1. Proteins containing the mononuclear type 1 copper site typically function as electron transfer proteins,[1,3] and are characterized by a relatively high redox potential, a small hyperfine coupling constant in the electron paramagnetic resonance spectrum, and an intense blue color, which arises from a ligand to metal charge transfer transition absorption near 600 nm.[1,3] The proteins facilitate rapid interconversion between the oxidation states of copper by providing a rigid coordination environment intermediate between those preferred by copper(I) and copper(II) and by shielding the copper site from solvent.[1,4]

The type 2 copper site is composed of a single solvent-accessible copper ion in an approximately square planar coordination geometry. These sites absorb only weakly in the visible region, and exhibit normal hyperfine coupling constants in the EPR.[2] Type 2 copper is found in conjuction with type 1 and type 3 sites in a class of proteins called the multicopper oxidases, which function in the reduction of dioxygen. Examples of multicopper oxidases include laccase and ceruloplasmin. In the type 3 site, two copper ions occur in close proximity and are strongly antiferromagnetically coupled.[1]

A number of proteins contain copper sites which do not fit into the classification scheme described above. These include Cu-Zn superoxide dismutase (SOD),[5,6] a mammalian protein which catalyzes the dismutation of superoxide (O_2^-) to form H_2O_2 and O_2. Copper in SOD is in an approximately square pyramidal geometry, and shares an imidazole ligand with a nearby zinc ion.[7,8]

Table 1. Examples of copper proteins[a]

Protein	Source	MW(kDa)	Copper sites		
			Type 1	Type 2	Type 3
Plastocyanin	French bean	11	x		
Azurin	*P. aeruginosa*	14	x		
Laccase	*R. vernicifera*	110	x	x	x
Ascorbate oxidase	Cucumber	140	x	x	x
Ceruloplasmin	Human	150	x	x	x
Superoxide dismutase	Bovine	31			

a References 1,2,9

In each protein, the protein structure controls the function of the copper by positioning the copper ligands in the required geometry and controlling the access of solvent to the site. Understanding the mechanisms by which a protein optimizes the copper environment for a particular function is a subject of considerable research. In Chapter 2 of this thesis, this problem is addressed in the bacterial blue (type 1) copper protein azurin, through an electrochemical study of the azurins from five species of bacteria. Azurin has been well characterized structurally, and azurins from different sources exhibit close structural homology.[10] Thus, azurin provides an excellent system in which to study the variation in properties of the copper caused by relatively small changes in the amino acid sequence. Studies of the pH and temperature dependence of the redox potentials of azurins can provide insight into the control of the redox potentials by the protein through electrostatic interactions, variations in copper site geometry, and conformational changes.

Chapter 3 describes a study of the redox thermodynamics of bovine erythrocyte SOD. The redox potential of the copper in SOD is quite high, yet the copper is reduced only slowly by most reducing agents. Since the proposed mechanisms for the dismutation of superoxide by SOD involve alternate reduction and oxidation of the copper ion by superoxide,[7,11] the relative redox-inactivity of the copper site may reflect an important functional property of the enzyme. Determination of the redox thermodynamics of the enzyme provide information on the mechanisms by which the protein achieves a high redox potential and protects the copper site from reduction.

Electron transfer within the azurin molecule is addressed in Chapter 4. The modification of *Pseudomonas aeruginosa* (Pae) azurin with $[Ru(NH_3)_4(py)]^{3+}$ (py = pyridine) is described, as well as the modification of *Alcaligenes denitrificans* (Ade) azurin with $[Ru(NH_3)_5]^{3+}$. Results with modified Pae azurin provide an estimate of the variation in electron-transfer rate with driving force. It is anticipated that a study of

intramolecular electron transfer in modified Ade azurin will allow a comparison of electron transfer rates over similar distances (~12 Å) for two pathways through the protein.

REFERENCES

1. Farver, O.; Pecht, I. In "Copper Proteins and Copper Enzymes"; Lontie, R., Ed.; CRC Press, Inc.: Boca Raton, Florida, 1984; Vol. I, Chapter 7.

2. Lontie, R. A.; Groeseneken, D. R. *Topics Current Chem.* **1983,** *108,* 1-33.

3. Adman, E. T. In "Topics in Molecular and Structural Biology"; Harrison, P., Ed.; VCH Verlagsgesellschaft: Weinheim, BRD, 1984; Vol. 1, Chapter 1.

4. Gray, H. B.; Malmstrom, B. G. *Comments Inorg. Chem.* **1983,** *2,* 203-209.

5. Valentine, J. S.; Pantoliano, M. W. In "Metal Ions in Biology"; Spiro, T. G., Ed; Wiley: New York, 1981; Vol. 3, pp. 291-358.

6. Fielden, E. M.; Rotilio, G. In "Copper Proteins and Copper Enzymes"; Lontie, R., Ed.; CRC Press: Boca Raton, Florida, 1984; Vol. 2, Chapter 2.

7. Tainer, J. A.; Getzoff, E. D.; Richardson, J. S.; Richardson, D. C. *Nature* **1983,** *306,* 284-287.

8. Tainer, J. A.; Getzoff, E. D.; Beem, K. M.; Richardson, J. S.; Richardson, D. C. *J. Mol. Biol.* **1982,** *160,* 181-217.

9. Holwerda, R. A.; Wherland, S.; Gray, H. B. *Ann. Rev. Biophys. Bioeng.* **1976,** *5,* 363-396.

10. Adman, E. T.; Turley, S.; Bramson, R.; Petratos, K.; Banner, D.; Tsernoglou, D.; Beppu, T.; Watanabe, B. *J. Biol. Chem.* **1989,** *264,* 87-99.

11. Klug, D.; Rabani, J.; Fridovich, I. *J. Biol. Chem.* **1972,** *247,* 4839-4842.

CHAPTER 2

SPECTROELECTROCHEMICAL STUDIES OF AZURINS

INTRODUCTION

Azurin is a small, copper-containing protein found in several species of bacteria.[1,2] It is one of a class of metalloproteins called the blue copper proteins; other members of this group include amicyanin, from a methylotrophic bacterium, and plastocyanin and stellacyanin, both found in plants. Selected properties of these and other blue copper proteins are listed in Table 1. The blue copper proteins exhibit strikingly similar structural features[3] and share a number of unusual spectroscopic characteristics.

Although a biological role for azurin has not been established unambiguously, other members of the blue copper class are known to function as electron transfer proteins.[1,4] Thus, it is likely that azurin plays an electron transfer role as well, perhaps by receiving electrons from cytochrome c_{551} and transferring them to cytochrome oxidase.[2] The bacterial electron transport chain in which azurin is thought to play a role has not been clearly delineated; however, the terminal electron transport chain of mitochondria has been mapped out in substantial detail. It serves to illustrate the bioenergetic role played by electron transfer proteins, and is illustrated schematically in Figure 1. As electrons flow through the chain from NAD (nicotinamide adenine dinucleotide) to molecular oxygen, there are three points where the free energy change is quite large. At each of these points, the free energy released is used to drive the reaction of adenosine diphosphate (ADP) with inorganic phosphate to form ATP, adenosine triphosphate. ATP serves as a convenient storage system for energy in the cell which can then be used for a variety of functions.

The copper site of *Alcaligenes denitrificans* azurin, as determined by x-ray crystallography, is shown schematically in Figure 2. Two histidine nitrogens and a deprotonated cysteine sulfur form relatively short bonds to copper in an approximately trigonal planar arrangement; longer axial bonds (~3 Å) to copper from a methionine

Table 1. Properties of selected blue copper proteins

Protein	Source	MW (Da)	λ_{max} (nm)	$E^{o'a}$ (mV vs. NHE)	Ref
Azurin	Pseudomonas aeruginosa	14,600	625	308	5,6
Plastocyanin	Phaseolus vulgaris	10,800	597	360	5
Stellacyanin	Rhus vernicifera	20,000	608	191	5,7
Rusticyanin	Thiobacillus ferrooxidans	16,500	597	680	8,9
Amicyanin	Paracoccus denitrificans	11,700	596	180	4
Cucumber basic protein	Cucumber seedlings	10,100	597	317	10,11
Pseudoazurin	Alcaligenes faecalis S-6	12,000	593	-	12

a pH 7.0, 25°C

Figure 1. Schematic diagram of the terminal electron transport chain in mitochondria.[13] At three points in the chain, illustrated by the vertical arrows, the free energy change in particularly large. The free energy released in each of these three steps is used to drive the formation of adenosine triphosphate (ATP).

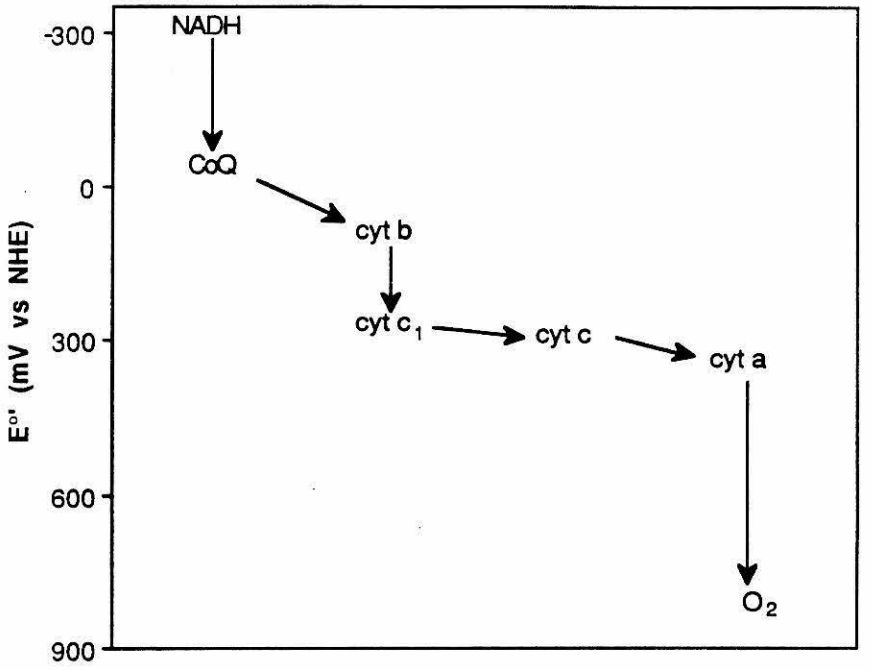
NADH
CoQ
cyt b
cyt c1
cyt c
cyt a
O2
-300
0
300
600
900
E°' (mV vs NHE)

Figure 2. The copper site of *Alcaligenes denitrificans* azurin. His 46, His 117, and Cys 112 are arranged in an approximately trigonal planar geometry. Met 121 and the main-chain carbonyl of Gly 45 form longer, axial bonds to copper.[14-16]

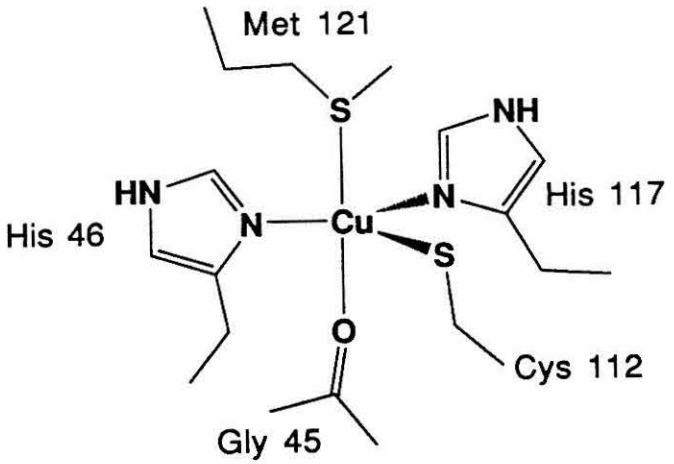
Met 121
S
NH
HN
N
Cu
N
His 117
His 46
S
O
Cys 112
Gly 45

sulfur and the oxygen of a backbone carbonyl complete the coordination sphere. The extent to which the methionine and the carbonyl form bonding interactions with the copper has been the subject of some debate. Based on comparison with model compounds in which Cu-S bond lengths of 2.8 to 3.2 Å are observed, it appears that the Cu-S(Met) interaction in azurin can be considered a bond.[17,18] The copper-oxygen distance is at the upper limit for a bond, when compared to tetragonally distorted copper complexes.[19] Evidence for a Cu-O(carbonyl) bond is provided by the observation of Norris et al.[15] that the carbonyl in question is in a non-polar environment, with no nearby polar groups with which to interact. In addition, a Cu-carbonyl interaction provides an explanation for the presence of a peak with a large downfield shift in the ^{13}C-NMR spectrum of oxidized azurin from *Pseudomonas aeruginosa*.[20] The position of the copper site in the azurin structure is shown in Figure 3; the copper lies near one end of the protein, in the middle of an eight-strand β barrel.

Other members of the blue copper protein class contain copper sites very similar to that of azurin. Of these, the protein for which the highest resolution crystal structure data are available is plastocyanin. In plastocyanin, the three strong bonds are essentially the same as in azurin, but the Cu-S(Met) bond is about 0.2 Å shorter, and the Cu-O bond is not present.[21] The four ligands are arranged in a distorted tetrahedral geometry. The copper sites of cucumber basic protein (CBP)[22] and the *Alcaligenes faecalis* S-6 cupredoxin[3] also consist of two histidines, a methionine, and a cysteine in an approximately tetrahedral arrangement. Suitable crystals of stellacyanin have not been obtained for a crystal structure determination, but the amino acid composition indicates that no methionine is present;[23,24] thus, at least one ligand of the stellacyanin copper site is different from those of the other blue copper proteins.

The relatively low coordination number for copper and the distorted ligand geometry confer a number of unusual properties on the blue copper proteins. The

Figure 3. The structure of *Alcaligenes denitrificans* azurin.[14-16] The eight-strand β barrel is oriented vertically; the α-helical flap is shown on the right. The copper ligands are shown in pink.

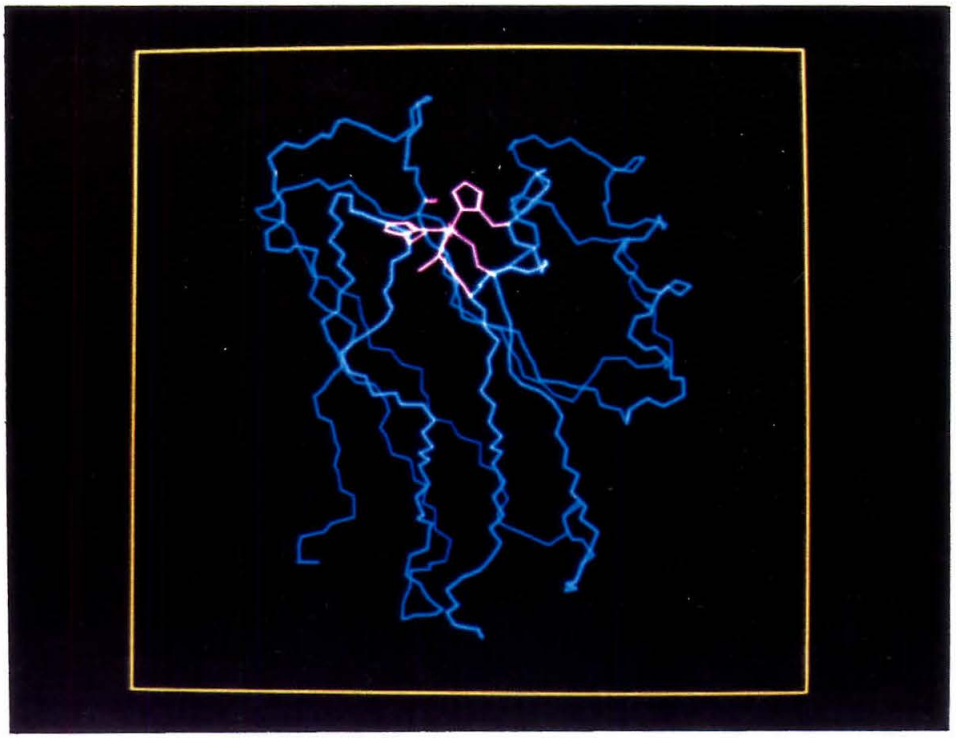

characteristic blue color of the proteins is due to a strong absorption at about 620 nm, which has been assigned as a S(Cys) to copper charge transfer transition. The molar absorptivity of this absorption is 3500-6000 $M^{-1}cm^{-1}$, or about 100 times as large as that found in simple complexes of copper with amino acids or peptides.[25] In the electron paramagnetic resonance studies of the blue copper proteins, an axial spectrum with an extremely narrow hyperfine splitting ($A_{\parallel}$ = 0.006cm^{-1}) is observed. This value of $A_{\parallel}$ is roughly half that found in simple copper complexes, and has been attributed to the high degree of delocalization of the unpaired electron in the copper x^2-y^2 orbital onto a Cys(S)pπ orbital.[26] The blue copper proteins also exhibit relatively high redox potentials, ranging from 180[4] to 680[8] mV versus NHE. The origin of this unusual feature is of particular interest, in light of the role the blue copper proteins play as electron transfer proteins. A high redox potential implies preferential stabilization of the Cu(I) state, which can be attributed in part to the low ligand field at the copper in the blue copper proteins (distorted tetrahedral or trigonal five coordinate with long axial bonds) and the back-bonding interaction between Cu(I) and the methionine sulfur.[27]

The coordination geometry at the copper appears to be mandated by the structure of the protein.[27,28] Thus, when azurin is reduced, the copper-ligand bond distances and other structural features of the protein change very little;[29,30] in fact, removal of the copper from azurin appears to cause very little structural reorganization. Control of the copper site geometry by the protein is effected in part by burying the copper about 6 Å below the surface of the protein. In addition, an extensive network of hydrogen bonds and other interactions with neighboring residues hold the copper ligands fixed.[31] One of the ligand histidines (His 117) in *Alcaligenes denitrificans* azurin is sandwiched between Phe 114 and Met 113, while the methionine ligand (Met 121) is packed tightly against Tyr 15.

The rigidity of the copper site and the inaccessibility of the copper to the solvent also facilitate azurin's participation in the electron transport chain.[32] These two features help to minimize the inner-sphere and outer-sphere contributions, respectively, to the reorganization energy, and thus enhance the rate of electron transfer.

The mechanisms by which the protein constrains the copper site and thus controls the redox function of the protein must ultimately have their origin in the amino acid sequence. The growing body of information on the sequences and structures of blue copper proteins provides an opportunity to attempt to relate redox potential data to structural variations among the proteins. Azurins from several species of bacteria have been isolated and characterized to varying extents. It is apparent from a number of experiments that azurins isolated from different bacteria have similar gross structural features. Thus, the structural differences among the proteins may be small enough that legitimate comparisons among the proteins can be made, allowing redox potentials to be correlated with sequences and structures. Therefore, a detailed study of the redox potentials of azurins from five different species of bacteria was undertaken.

Table 2 lists the five species of bacteria from which azurins were isolated for use in this study. Crystal structure data have been reported for Ade[14-16,33] and Pae[34,35] azurins, at resolutions of 1.8 and 2.7 Å, respectively; a preliminary report of a crystallographic study of Asp azurin has also appeared.[36] The amino acid sequences of all five azurins have been reported; these are aligned in Figure 4. The percent homology of each azurin relative to Ade can be determined from the alignment. These figures are listed in the fourth column of Table 2, and indicate that the amino acid sequence is rather highly conserved. When the positions of the amino acid substitutions are located in the structure of Ade azurin, it is found that all of the changes in internal residues are conservative. Thus, the effective homology among the azurins is higher than the

Table 2. The five species of bacteria from which the azurins used in this study were isolated

Azurin source	Structural data	Sequence data	% homology[a]
Alcaligenes denitrificans	yes[b]	yes	100
Pseudomonas aeruginosa	yes[c]	yes	63.8
Alcaligenes faecalis	no	yes	67.7
Alcaligenes sp.	partial[d]	yes	69.8
Bordetella bronchiseptica	no	yes	64.3

a Relative to Ade; Ref. 6.
b Ref. 14, 15, 16.
c Ref. 34,35.
d Ref. 37.

Figure 4. The sequences of azurins from five species of bacteria.[6] The three-letter abbreviation for each bacterial species is given at the start of each sequence. The amino acid numbers correspond to the Ade sequence.

Ade	1	AQCEA	TIESN	DAMQY	NLKEM	VVDKS	CKQFT	VHLKH	VGKMA	KAVMG
Pae		-E-SV	D-QG-	-Q--F	-TNAI	T----	-----	-N-S-	P-NLP	-N---
Afa		A-DV	S--G-	-S--F	-TKSI	----T	--E--	IN---	T--LP	--A--
Asp		-E-SV	D-AG-	-Q--F	DK--I	T-S--	-----	-N---	P--L-	-N---
Bbr		-E-SV	D-AGT	-Q--F	DK-AI	E-S--	-----	-N---	T--LP	RN---

Ade	46	HNWVL	TKEAD	KEGVA	TDGMN	AGLAQ	DYVKA	GDTRV	IAHTK	VIGGG
Pae		-----	STA--	MQ--V	----A	S--DK	--L-P	D-S--	-----	L--S-
Afa		--V-V	S-KS-	ESA--	----K	---NN	-----	--E--	----S	-----
Asp		-----	--Q--	MQ-AV	N---A	---DN	N---K	D-A--	-----	-----
Bbr		-----	--T--	MQA-E	K--IA	---DN	Q-L--	-----	L----	-L---

Ade	91	ESDSV	TFDVS	KLTPG	EAYAY	FCSFP	GHWAM	MKGTL	KLSN
Pae		-K---	-----	--KE-	-Q-MF	--T--	--S-L	-----	T-K
Afa		-T---	-----	--KE-	-D--F	-----	---SI	----I	E-GS
Asp		-T---	-----	--AA-	-D---	-----	--F-L	---V-	--VD
Bbr		-----	----A	--AA-	DD-TF	-----	--G-L	-----	--VD

numbers in Table 2 indicate. As a result of their high homology, the azurins from different species of bacteria form very similar three-dimensional structures. The similarity between the protein folds is apparent in Figure 5, which shows an overlay of the main chains of Ade and Pae azurins, as constructed from the crystal structure data. If this similarity extends to the other three azurins as well, then the prospect of relating structure to redox potential is promising.

In addition to the variations in redox potential among species of azurin, the dependence of each potential on pH was also examined, in order to assess the importance of electrostatic interactions between the copper and charged residues in controlling the potential. An understanding of the effect of pH on redox potentials may also provide insight into the mechanisms which link electron transfer to proton pumping, as in more complex systems such as cytochrome oxidase.

Finally, a study of the temperature dependence of the azurin potentials at low and high pH was undertaken, in order to sort out the enthalpic and entropic contributions to the redox potentials, and to understand conformational differences among species of azurin and between the high- and low-pH forms of each species.

Electrochemistry of metalloproteins

A common problem in the measurement of metalloprotein redox potentials is the fact that metalloproteins usually do not exchange electrons readily with an electrode surface. Due to their large size, proteins diffuse slowly through solution, and collisions with the electrode are therefore infrequent. As a further result of the protein's large size, a low percentage of the collisions will occur in the proper orientation for transfer of an electron to occur. In addition, since the metal center is often buried several angstroms below the protein surface, the protein may act as insulation between the electrode and the metal center.

Figure 5. Comparison of the structures of Pae (red) and Ade (blue) azurins. The program Biograf (BioDesign, Pasadena, California) was used to determine a least squares fit of the main chain atoms.

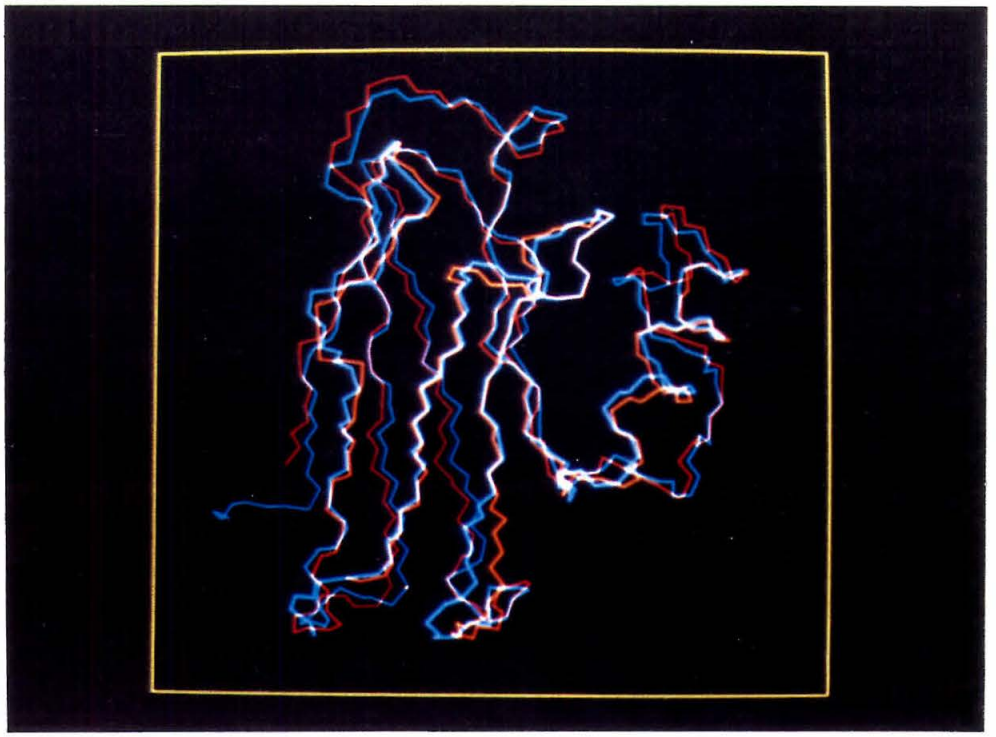

A number of methods have been developed to improve the rate of electron transfer between a protein and an electrode surface.[38] Surface modifications of electrodes have proven promising in studies of the redox potentials of metalloproteins, including several blue copper proteins.

An alternative way to enhance electron exchange between the protein and the electrode is to use a small redox-active molecule, or mediator-titrant, as a catalyst to increase the rate of electron exchange between the protein and the electrode surface. This approach is illustrated in Figure 6. A mediator-titrant is selected which exhibits a redox potential similar to that of the protein of interest, so that both reduction and oxidation can be effectively catalyzed. In addition, a mediator must be chosen which will not interfere with the property of the protein being observed in the electrochemical experiment. Finally, the mediator used must not bind to the protein and perturb the redox potential.

The redox potentials reported in this study were measured by spectroelectrochemistry in the visible region. This technique takes advantage of the fact that oxidized azurin absorbs very strongly at about 625 nm, while reduced azurin does not absorb at that wavelength. In the spectroelectrochemical experiment, a potential is applied across a solution of the protein and mediator, and the concentrations of oxidized and reduced species in solution are allowed to come to equilibrium at that potential. The approach to equilibrium can be monitored by observing the absorbance at a wavelength where the oxidized and reduced forms of the protein have significantly different absorptivities. Once equilibrium has been established, the ratio of the concentrations of oxidized and reduced protein can be determined from the absorption spectrum and the spectra of the fully oxidized and fully reduced protein. For the redox couple

$$ox + ne^- \rightarrow red \qquad (1)$$

Figure 6. A schematic diagram illustrating the use of a mediator-titrant (MT) to catalyze the exchange of electrons between an electrode surface and a protein.

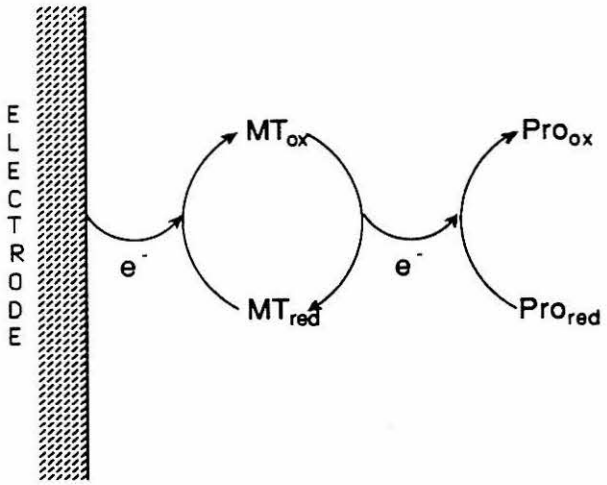
ELECTRODE
e⁻
MT$_{ox}$
MT$_{red}$
e⁻
Pro$_{ox}$
Pro$_{red}$

the Nernst equation is as follows:

$$E_{app} = E^{\circ} - \left(\frac{RT}{nF}\right) \ln \frac{[red]}{[ox]} \qquad (2)$$

where E_{app} is the applied potential, E° is the formal potential of the redox couple, R is the gas constant, n is the number of electrons involved in the reduction, and F is the faraday constant. Thus, a plot of the applied potential versus ln[red]/[ox] will yield E° and the number of electrons involved in the reduction. In accordance with biochemical convention, redox potentials determined at pH 7 are reported as $E^{\circ\prime}$ values; potentials at other pH values are reported as E_{mx}, where x is the pH.

To allow the visible absorption spectrum of the solution to be measured as a potential is applied, an optically transparent thin layer electrode cell is employed. The cell, illustrated schematically in Figure 7, consists of a gold minigrid working electrode sandwiched between two quartz windows. The cell is filled with a solution of mediator and protein and placed in the sample compartment of a spectrophotometer. Two ports at the top of the cell hold the reference and counter electrodes in contact with the protein solution. A copper wire is connected to the gold minigrid to provide an external contact for the working electrode. The sample compartment is typically 0.3 mm thick, allowing rapid diffusion of the species in solution to the electrode surface. Since the spectroelectrochemical cell allows the absorption spectrum of the protein to be monitored continuously, it also provides a convenient way to check for decomposition of the protein during the electrochemical experiment.

pH dependence of redox potentials[39]

When an ionizable group occurs near the metal center in a protein, the redox potential of the protein will be affected by the state of protonation of the residue. The

Figure 7. A schematic diagram of the sample compartment of a spectroelectrochemistry cell containing an optically transparent thin-layer electrode.

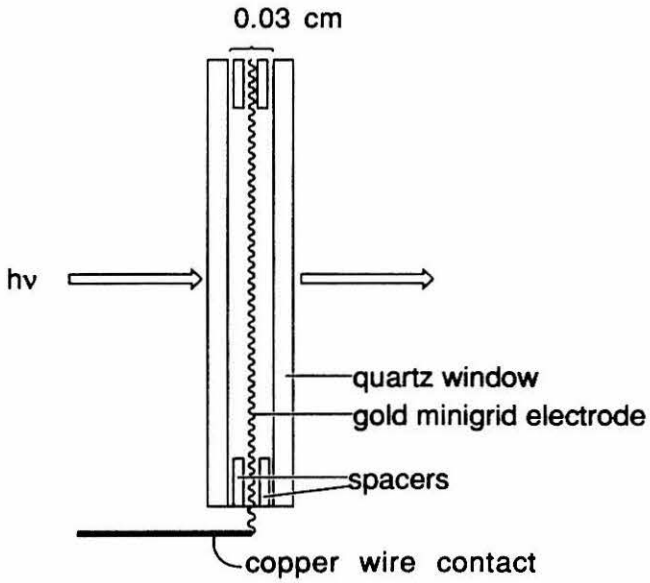
0.03 cm
hν
quartz window
gold minigrid electrode
spacers
copper wire contact

effect of protonation of a nearby residue on the potential of the metal center is illustrated schematically in Scheme 1:[40]

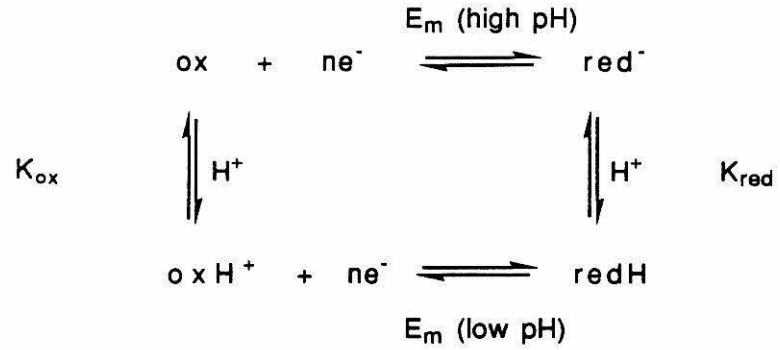

Scheme 1

Here, ox represents the oxidized protein, redH represents the protonated form of the reduced protein, and so on; E_m is the midpoint potential at a given pH. Due to the proximity of a positive charge, the metal center should be more easily reduced in oxH^+ than in ox; thus, the protein will have a higher redox potential at low pH values. In an analogous fashion, the pK_a at which the residue titrates will depend upon the oxidation state of the metal, with the pK_a being lower for the oxidized form. These effects are summarized by Equation 3:

$$E_m(pH) = E_m(\text{low pH}) + \frac{RT}{nF} \ln \frac{K_a^{red} + [H+]}{K_a^{ox} + [H+]} \qquad (3)$$

A plot of $E_m(pH)$ versus pH will have the general form shown in Figure 8. At very low pH values, both the oxidized and the reduced forms of the protein will be protonated; at very high pH values, both forms will be deprotonated. However, at pH values

Figure 8. A theoretical plot of the dependence of the redox potential on pH

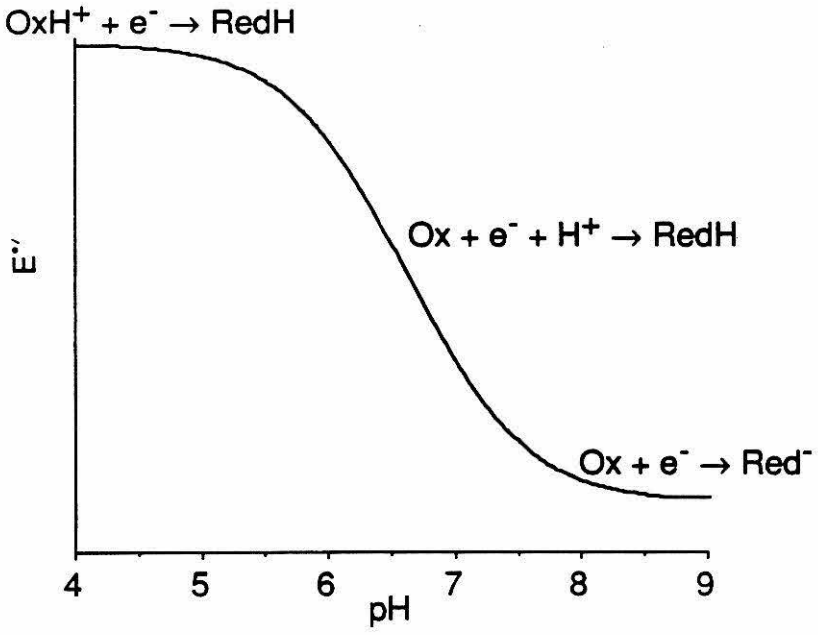
OxH+ + e- → RedH
Ox + e- + H+ → RedH
Ox + e- → Red-
E'
4
5
6
7
8
9
pH

intermediate between K_a^{red} and K_a^{ox}, reduction of the protein will occur with uptake of a proton:

$$ox + e^- + H^+ \rightarrow redH \qquad (4)$$

If more than one nearby residue titrates within the pH range studied, the equation and the plot become more complex.

The extent to which the redox potential of a metal center or the pK_a of a titrating group is affected by a change in a nearby charge will depend on the energy of interaction between the two charges, according to Coulomb's law:

$$E = \frac{q_1 q_2}{4\pi\varepsilon_0\varepsilon_{eff}r} \qquad (5)$$

In this equation, q_1 and q_2 are the charges, ε_0 is the permitivity of free space, ε_{eff} is the effective dielectric constant, and r is the distance between the charges. Thus, the magnitude of the electrostatic contribution to the pH dependence of the redox potential will be a function of several factors, including the distance between the metal center and the titrating residue and the nature of the intervening medium.

Temperature dependence of redox potentials

The entropy and enthalpy of reduction for a redox couple can be determined by measuring the temperature dependence of the redox potential. Two cell configurations are possible for variable temperature electrochemical measurements. In the isothermal configuration,[42] the reference and sample compartments are at the same temperature, and the temperature of the entire electrochemical cell is varied. The temperature dependence of the potential is thus proportional to the entropy change for the overall cell reaction, and Equation 6 yields Equation 7:

$$-nFE^\circ = \Delta G^\circ = \Delta H^\circ - T\Delta S^\circ \qquad (6)$$

$$\left(\frac{dE^\circ}{dT}\right)_{iso} = \left(\frac{\Delta S^\circ cell}{nF}\right) \qquad (7)$$

A problem with variable temperature experiments performed using an isothermal cell configuration is that most common reference electrodes return to equilibrium rather slowly after the temperature is changed. An alternative approach is the non-isothermal arrangement, in which the reference electrode compartment is held at a constant temperature, usually 25°C, while the temperature of the sample compartment is varied.[5,43] Yee et al.[43] have shown that inaccuracies due to temperature gradients are negligible if dE°/dT is at least 0.20 mV per degree. The observed temperature dependence when the redox potential is determined non-isothermally will be proportional to the entropy change for the redox couple of interest, $S^\circ_{red} - S^\circ_{ox}$, or ΔS°_{rc}:

$$\Delta S^\circ_{rc} = S^\circ_{red} - S^\circ_{ox} = nF(dE^\circ/dT)_{non} \qquad (8)$$

ΔS°_{rc} can be related to the entropy change for the complete cell reaction by referring to the overall cell equation, as illustrated for the $Cu^{2+/+}$ and H^+/H_2 couples:

$$Cu^{2+} + \tfrac{1}{2}H_2 \rightarrow Cu^+ + H^+ \qquad (9)$$

$$\Delta S^\circ_{cell} = S^\circ_{Cu^+} + S^\circ_{H^+} - S^\circ_{Cu^{2+}} - \tfrac{1}{2}S^\circ_{H_2} \qquad (10)$$

$$= (S^\circ_{Cu^+} - S^\circ_{Cu^{2+}}) + (S^\circ_{H^+} - \tfrac{1}{2}S^\circ_{H_2}) \qquad (11)$$

The S° terms represent partial molal entropies. According to the convention of the "practical" entropy scale,[44] $S^\circ_{H^+}$ is defined as zero; thus, using the value of 31.2 eu for $S^\circ_{H_2}$, equation (11) yields:

$$\Delta S^\circ_{cell} = \Delta S^\circ_{rc} - 15.6 \text{ eu} \qquad (12)$$

In this way, the entropy change for the overall cell reaction can be obtained from a non-isothermal experiment. If it is assumed that ΔC_p° is negligible (that is, that ΔH° is temperature-independent), then ΔH° can be calculated from ΔS° and ΔG°.

EXPERIMENTAL

Materials and Instrumentation

The culture of *Alcaligenes denitrificans* (NCTC 8582 or ATCC 15173) was obtained from the American Type Culture Collection (ATCC). This bacterium has recently been reclassified as *Alcaligenes faecalis* (not to be confused with NCIB 8156, below). *Alcaligenes faecalis* (ATCC 8750 or NCIB 8156) and *Pseudomonas aeruginosa* (NCTC 6750 or ATCC 19429) were also supplied by ATCC. *Bordetella bronchiseptica* (NCTC 8344) was obtained from the National Collection of Type Cultures (NCTC), London. *Alcaligenes* sp. (NCIB 11015, subspecies *xylosoxidans*) was obtained from NCIB, Torry Research Station, England. This bacterium was originally classified as *"Pseudomonas denitrificans"*,[45] but has been reclassified as a member of the *Alcaligenes* group.[46]

Large-scale bacterial cultures were prepared in a 350 liter fermenter (Stainless and Steel Products, St. Paul, MN) and harvested using a Sharples continuous-flow centrifuge (type AS26).

Chromatographic materials were cleaned and equilibrated as directed by the manufacturer: SP Sephadex C-25 (Pharmacia); CM-52 and DE-52 (Whatman); Sephadex G-75-120 (Sigma). Particulate matter was removed from protein solutions using Millipore 0.22 μm filters. Spectrapor 1 (MW cutoff 6000-8000) dialysis tubing was supplied by Spectrum Medical Industries, Inc.

Absorbance measurements were carried out using a Shimadzu UV-260 or a Varian Cary 219 spectrophotometer. The FPLC (fast protein liquid chromatography) system was supplied by Pharmacia. Analytical isoelectric focusing was performed using LKB PAGplates (pH 3.5-9.5) with an LKB Multiphor (Model 2117).

The gold minigrid used as the working electrode in spectroelectrochemical cells was obtained from Interconics (100 lines per inch, 60% transmittance).

Microthermocouples were supplied by Omega Engineering. Potentials were applied using a Princeton Applied Research polarographic analyzer (Model 174A) and measured with a microvolt digital multimeter (Keithley 177). The reference electrode was a miniature saturated calomel electrode (Sargent-Welch), and the counter electrode was a platinum wire. Sample temperature was monitored during each spectroelectrochemical experiment by a Fluke digital thermometer (2175A) via a microthermocouple (Omega Engineering) placed inside the wall of the working electrode compartment.

Hexaammineruthenium(III) chloride (Strem) was recrystallized from 1 M HCl. All other chemicals were reagent grade and were used without further purification. Water used in the preparation of all aqueous solutions was purified by passage through a Barnstead NANOpure system (Model D2794).

Methods

Protein solutions were concentrated using either Amicon ultrafiltration cells with YM5 membranes or Centricon microconcentrators in a DuPont Sorvall RC-5 centrifuge.

Azurin concentrations were determined by absorbance measurements at 625 nm (ε_{625} = 5700 $M^{-1}cm^{-1}$).[47]

$[Ru(NH_3)_5(py)]Cl_3$ (py=pyridine) was prepared according to literature methods. The crude material was purified by chromatography on SP Sephadex C-25, with elution by stepwise increases in [HCl]; the desired product elutes at 0.3 M HCl.

$[Co(phen)_3]Cl_3$ was prepared by a modification of a previous method.[48] A solution of 1 equivalent $CoCl_2 \cdot 6H_2O$ and 3 equivalents phenanthroline monohydrate in water was refluxed 90 min. The solution was then removed from heat, and chlorine gas was bubbled through the solution for 60 min. After rotary evaporation to dryness, the product was collected and recrystallized from MeOH/ether.

Na[Co(edta)] was prepared according to Kirschner[49] and recrystallized from water.

Spectroelectrochemical experiments were performed as previously described.[50] Optically-transparent thin-layer electrode cells were prepared by modifications of a design by Heineman.[50,51] A single minigrid (gold electroformed mesh, Interconics, St. Paul, MN) was sandwiched between two spacers of 0.1 mm Teflon tape (Dilectrix Corporation, Farmingdale, NY) to give an optical pathlength of ~0.3 mm. Lucite cell bodies were machined as previously described,[50] with the exception that the 7/25 standard taper electrode ports were machined down to within 4 mm of the working cell compartment, in order to reduce the sample volume required.

Sample conditions for spectroelectrochemical measurements were as follows: [azurin] = 0.5 - 1.5 mM; [mediator] = 3[azurin]. At least 6 points were used for each Nernst plot, in addition to the fully reduced and fully oxidized absorbance readings.

Protein isolation and purification

Preparations of azurins from all five species of bacteria were based on modifications of previously described procedures. A general scheme is described below, followed by details specific to each species of bacteria.

Culture media consisted of (per liter) 5.0 g sodium citrate (dihydrate), 5.0 g $NaNO_3$, 1.0 g KH_2PO_4, 0.5 g $MgSO_4 \cdot 7H_2O$, 6.5 g Difco yeast extract, 10 mg $FeCl_3 \cdot 6H_2O$, 10 mg $CuSO_4 \cdot 5H_2O$, and 2 g Bacto Peptone.

Bacterial cultures were prepared by transferring a freeze-dried culture or a single colony from an agar slant into 250 mL of sterile media. The culture was allowed to grow under the conditions described for each species below. A 10 mL aliquot of this culture was then used to inoculate 250 mL of fresh media; this culture was in turn used to inoculate 3 L of media. The 350 L fermenter was then seeded with this 3 L culture.

Cells were harvested at 5-10°C at a flow rate of 60-90 L/h. Cell paste was used immediately or frozen at -50°C.

The cell paste was converted to acetone powder by adding small portions (<1mL) of paste to vigorously stirring technical acetone (5 L acetone per kg cell paste). The acetone was maintained at -20 to -10°C during this process by the addition of powdered dry ice. The mixture was stirred for 1-2 h at -20 to -10°C after the addition of paste was complete. The resulting mixture was filtered on a Buchner funnel; solids were then re-extracted with a similar volume of cold acetone. After filtering, the solids were washed with cold acetone and ether, and allowed to air dry. The powder obtained was then ground in a mortar and pestle and dried in a vacuum desiccator until no further solvent could be removed. Acetone powder was used immediately or stored at -5°C until use.

Acetone powder was extracted by suspending it in 0.1 M ammonium acetate buffer, pH 6.5, which had been preheated to 45°C (1 L buffer per 100 g powder). In some instances, the initial suspension was obtained by blending in a Waring blender (2 x 1 min). The mixture was then stirred at 5°C. Approximately 1 h after the addition of buffer to the acetone powder, a few mg DNase I (Sigma DN-CL) was dissolved in buffer and added to the suspension. Stirring was continued for 12-24 h; this step, and all other steps in the isolation and purification after this point, were carried out at 5°C unless otherwise noted. Solids were removed by centrifugation for 90 min at 11,000 rpm in a GSA rotor (DuPont Sorvall RC-5 centrifuge). The supernatant was dialyzed against three changes of a 10-fold volume excess of 0.05 M ammonium acetate buffer, pH 4.0 (loading buffer). The pH of the dialysate was adjusted to 4.0 if necessary, and the precipitate which forms at low pH was removed by centrifugation as above. Na[Co(edta)] (~1 mg/g acetone powder) was added to the supernatant, followed by cold distilled water to lower the conductivity of the solution to that of the loading buffer. If necessary, the supernatant was filtered through a filter paper mulch or a pad of cell

debris remover (Whatman) to completely clarify it. The resulting brown solution was loaded onto a column of CM-52 cation exchange resin equilibrated with loading buffer; the size of the column was approximately 4.0 cm diameter x 20 cm for a 200 g batch of acetone powder.

A large amount of orange material (cytochromes and other proteins) eluted during loading. When the solution had been completely loaded, the column was washed with loading buffer until the eluent was colorless. The appearance of protein bands on the column varied from species to species; details are described below. Typically, the top of the column was red or brown, and an azurin band appeared below, followed by a red or orange band. Small yellow or green bands were observed with some species of bacteria. Periodically during elution, 20-30 mg portions of Na[Co(edta)] were dissolved in buffer and passed down the column, in order to prevent autoreduction of the proteins. Azurin and other proteins were eluted by stepwise increases in the pH of the 0.05 M ammonium acetate buffer.

At this stage, the azurin preparation contained considerable amounts of cytochromes and other proteins and nucleic acids. Gel filtration chromatography (standard techniques or FPLC) was used as an intermediate step in purification. After gel filtration chromatography, a combination of anion and/or cation exchange chromatography steps was used to purify each azurin to the proper purity ratio ($A_{\sim 620}/A_{280}$).

Chromatographic methods:

Gel filtration chromatography (standard techniques): The protein solution was concentrated to a small volume, and ~2 mL aliquots were loaded onto a 2.5 cm diameter x 90 cm column of Sephadex G-75-150 in 0.1 M sodium phosphate buffer, pH 7.0. A flow

rate of 7.7 mL/h gave baseline separation of an orange band from the azurin band; azurin eluted at ~180 mL.

Gel filtration chromatography (FPLC): The solution of azurin was concentrated and loaded in ≤0.1 mL aliquots on a 25 mL column of Superose 12. Using μ = 0.1 M sodium phosphate, pH 7.0, with a flow rate of 0.5 mL/min, near baseline separation of a cytochrome band from azurin could be achieved; azurin eluted at ~17 mL.

Anion exchange chromatography(standard techniques): The azurin solution was washed into 0.01 M Tris-HCl, pH 8.7 (loading buffer), and concentrated to ~3 mL. The solution was loaded onto a 1.5-2.5 diameter x 20 cm column of DE52 in loading buffer. Protein was eluted with 0.01-0.05 M Tris HCl, pH 8.7.

Cation exchange chromatography (FPLC): Samples were loaded on a Mono S 10/10 column in 0.05 M ammonium acetate buffer, with elution by increasing NaCl concentration. Specific conditions are given below for each bacterial species. Flow rates were 2 mL/min during loading of the sample, and 4 mL/min for the remainder of the run.

Alcaligenes denitrificans: Several changes were made to the general culture medium described above (per liter): Bacto Peptone was increased to 10 g, sodium citrate was replaced by 10 g sodium glutamate, $FeCl_3$ was replaced by 2 mg $FeSO_4$, $MgSO_4$ was replaced by 8 mg $MgCl_2$, and the $NaNO_3$ was deleted. Bacteria were grown without aeration at 34° for 24 h.

A tendency toward autoreduction at low pH, especially during temperature changes, was noted for Ade azurin. Thus, pH 4.5 (rather than 4.0) ammonium acetate was used as the dialysis buffer. The loaded column was washed with pH 4.5 buffer,

followed by pH 4.8 and 5.1. pH 5.5 buffer was used to elute the azurin. If large amounts of cytochromes co-eluted with azurin, the majority of impurities were removed by concentrating the protein to a small volume and passing it down a CM52 column in pH 5.65 ammonium acetate buffer, using isocratic elution conditions. The protein was further purified by gel filtration chromatography (standard techniques or FPLC) as described above. Final purification was by FPLC cation exchange, using pH 4.5 buffer. Gradients were 0 to 0.18 M NaCl in 180 mL. Additional blue material eluted in the 100%B (1 M NaCl) wash; the size of this band varied considerably between batches of azurin. This material absorbs at ~620 nm, and may be azurin which was damaged in some way during the isolation or purification; it was not characterized further. In some cases, an additional chromatographic step was performed to purify the azurin, using FPLC cation exchange on the Mono S 10/10 column with pH 5.2 buffers; the gradient was 0 to 25 mM NaCl in 78 mL. Yields for Ade were far higher than those obtained with the other four species of bacteria, and were typically 2.5 kg cell paste/350 L fermenter run, 800 g acetone powder/2.5 kg cell paste, and 2.4 g azurin/800 g acetone powder. The purity ratio (A_{621}/A_{280}) was ≥0.28; literature values range from 0.25[52] to 0.30.[36,53]

Pseudomonas aeruginosa: Cultures were grown at 37° for 24-48 h, without aeration or agitation. After loading the crude protein solution on the initial CM52 column at pH 4.0, the pH of the eluting buffer was raised stepwise to pH 4.9. The azurin was purified by gel filtration chromatography as described above, and further purified either by anion exchange followed by cation exchange chromatography, or by two cation exchange steps. FPLC cation exchange on a Mono S 10/10 column was performed using pH 4.3 buffer, with a gradient to 0.10 M NaCl in 114 mL. Pae azurin could be further purified by crystallization from 0.10 M sodium acetate buffer, pH 5.5, by bringing a very

concentrated solution of azurin to 65-70% $(NH_4)_2SO_4$ saturation at room temperature over a few hours. When a faint permanent turbidity was apparent, one drop of buffer was added, and the solution was placed in the refrigerator. Within a few days, microcrystallization was evident by the silky appearance of the mixture (Schlerien effect). Yields were typically 2 kg cell paste/350 L fermenter, 500 g acetone powder/2 kg cell paste, and 600 mg azurin/500 g acetone powder; the purity ratio $R(A_{625}/A_{280})$ was ≥0.58. Literature values for R range from 0.46 to 0.56.[47,52-54]

Bordetella bronchiseptica: Bbr azurin showed a tendency toward autoreduction on the CM52 column at pH ≤5.0; thus, Na[Co(edta)] was added to the elution buffer to maintain oxidizing conditions. A small cytochrome band was eluted at pH 4.5, followed by washing at pH 4.8 and elution of azurin (with a second small cytochrome band) at pH 5.0. A minor blue or green band remained bound to the top of the column at pH 5.0, and was not characterized. After gel filtration chromatography as described above, final purification was performed by FPLC cation exchange, using a Mono S 10/10 column with pH 4.4 buffers and [NaCl] increasing from 0 to 0.13 M in 130 min. Azurin elutes at 0.12 M NaCl. The final azurin solution had a purity ratio of ≥0.55.

Alcaligenes faecalis: Cell cultures were allowed to grow for 48 h. The crude protein solution was loaded on the CM52 column at pH 4.0; the column was washed at pH 4.5, then pH 4.7; azurin was eluted at pH 5.0. Typical yields were 850 g cell paste/350 L fermenter; 250 g powder/850 g paste; 300 mg azurin/250 g powder. The purity ratio of the final protein solution was 0.56; literature values range from 0.50 to 0.55.[52,55]

Alcaligenes sp.: The culture medium was as described above, with the deletion of the Bacto Peptone, $FeCl_3$, and $CuSO_4$. Approximately 4.5 mL per liter of 1 N NaOH was added

to the broth to bring the pH to 7. The initial cation exchange column was loaded at pH 4.0, then washed extensively at pH 4.4 and pH 4.7; azurin eluted at pH 5.0. A faint blue band eluted before azurin; this material was not characterized. Final purification was by FPLC cation exchange at pH 4.35; [NaCl] was increased from 0 to 13.5% in 180 mL. Typical yields were 680 g cell paste/200 L fermenter, 170 g powder/680 g cell paste, and 60 mg azurin/170 g acetone powder; the purity ratio was ≥0.58. Literature values for R range from 0.34 to 0.47.[36,56]

RESULTS AND DISCUSSION

Isolation and purification of azurins

The yield of azurin obtained and the stability of the protein were found to vary considerably among different species of bacteria. *Alcaligenes denitrificans* produced a significantly higher (~5x) yield of azurin per liter of culture than the other bacteria, despite the fact that Ade azurin appears to be more easily damaged than the other azurins by the acidic steps in the purification scheme. Ade azurin was observed to bleach slowly at pH 4.5 and room temperature; freezing of the oxidized protein at pH 5 led to irreversible bleaching. Whether the bleaching resulted from irreversible reduction of the copper or from loss of copper from the protein was not determined.

The purity ratio (A_{620}/A_{280}) which could be obtained for Ade azurin was lower than that of the other azurins. The absorbance at 620 nm arises from copper(II), as described above, while the absorbance at 280 nm is due to aromatic amino acid side chains. Of these, tryptophan (Trp) absorbs the most strongly, followed by tyrosine (Tyr); phenylalanine (Phe) also makes a minor contribution. Pae, Afa, and Bbr azurins each contain 1 Trp and 2 Tyr, while Asp contains one extra Tyr; in contrast, Ade contains 2 Trp and 4 Tyr. As a result, Ade azurin absorbs much more strongly at 280 nm than the other azurins do, leading to a lower $A_{\sim 620}/A_{280}$ ratio for Ade. Thus, the variations in purity ratios do not necessarily reflect differences in ε_{625}, which would indicate differences in the copper sites.

Determination of redox potentials

Figure 9 illustrates the results of a typical thin layer spectroelectrochemical experiment with Afa azurin at pH 7.0 and 25°C. The uppermost trace, at E_{app} = 225 mV vs SCE, is the visible spectrum of fully oxidized azurin, and the bottom trace

Figure 9. Overlay spectra from the determination of the Afa azurin redox potential at pH 7.0, 25°C. The applied potentials are relative to SCE.

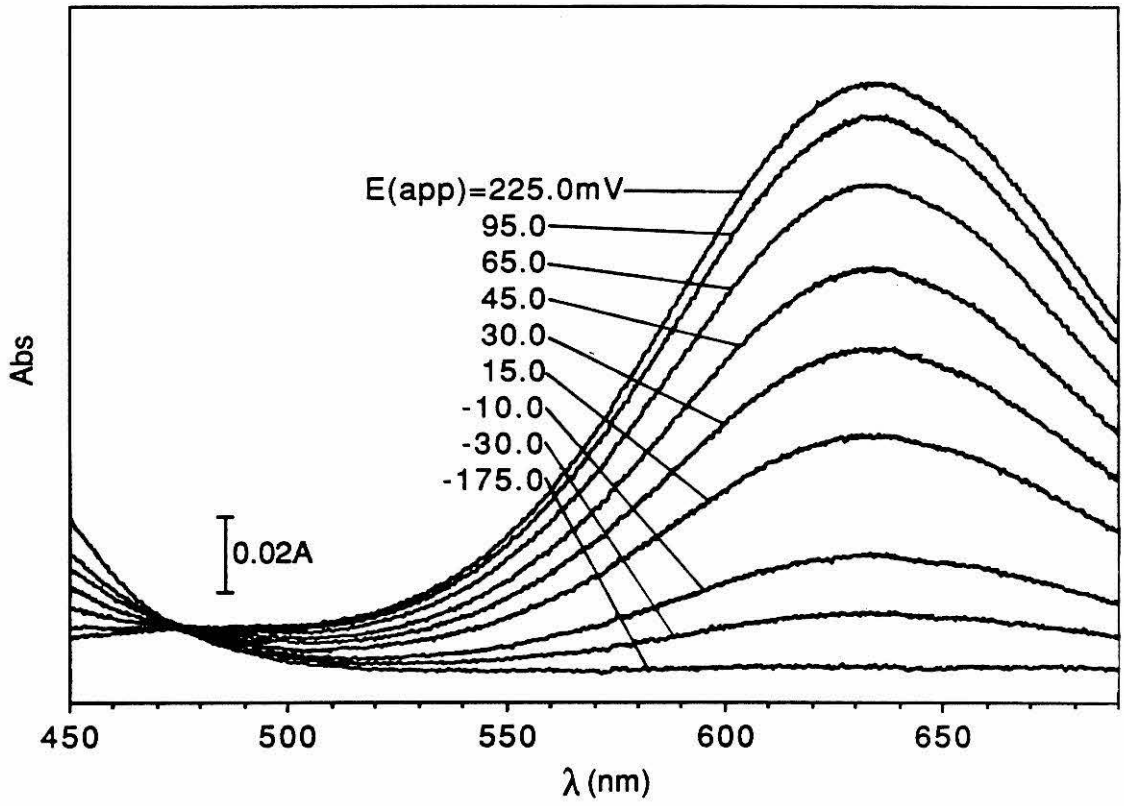
E(app)=225.0mV
95.0
65.0
45.0
30.0
15.0
-10.0
-30.0
-175.0
0.02A
Abs
450
500
550
600
650
λ (nm)

(E_{app} = -175 mV) is that of the fully reduced protein. At each applied potential, the approach to equilibrium between the oxidized and reduced forms of the protein was observed by monitoring the absorbance at 625 nm. Data points were collected in both the reducing and oxidizing directions, and the absorbance of the fully oxidized protein was rechecked at the end of the experiment in order to detect possible decomposition of the protein. The mediators used in this study, $[Ru(NH_3)_5(py)]Cl_3$ and $[Co(phen)_3]Cl_3$, are essentially transparent in both redox states at 625 nm; thus, the recorded A_{625} values could be analyzed directly to determine the amounts of oxidized and reduced azurin present at each potential. The Nernst plot obtained from these data is shown in Figure 10; a least squares analysis of the data yields $E^{o'}$ = 25.4 mV vs SCE and n = 1.03.

Redox potentials at pH 8, 25°C

The potentials of the five species of azurin at pH 8 and 25°C are listed in Table 3. To facilitate an analysis of redox potential differences among species in terms of copper site geometry alone, the potentials are compared at pH 8 rather than pH 7. At pH 7, electrostatic interactions between the copper and ionizable histidine residues in the protein may contribute to differences in potentials among the proteins; this point is discussed in more detail below. At pH 8, it is expected that all accessible histidine residues will be in the deprotonated form. Thus, interspecies potential differences due to histidine titrations will be essentially eliminated, and an analysis in terms of the copper site geometry becomes more feasible.

Ade and Pae are the two species of azurin which have been the most extensively studied. The copper-ligand bond lengths for both species (Table 4) are known from the crystal structures and supported by spectroscopic evidence. The copper sites of the two azurins are quite similar; each includes three relatively short bonds to two histidine imidazoles and a cysteine thiolate, and two longer bonds to a methionine thioether and a

Figure 10. Nernst plot of the data in Figure 9. A least squares fit to the data yields $E^{\circ\prime}$ = 25.4 mV vs SCE.

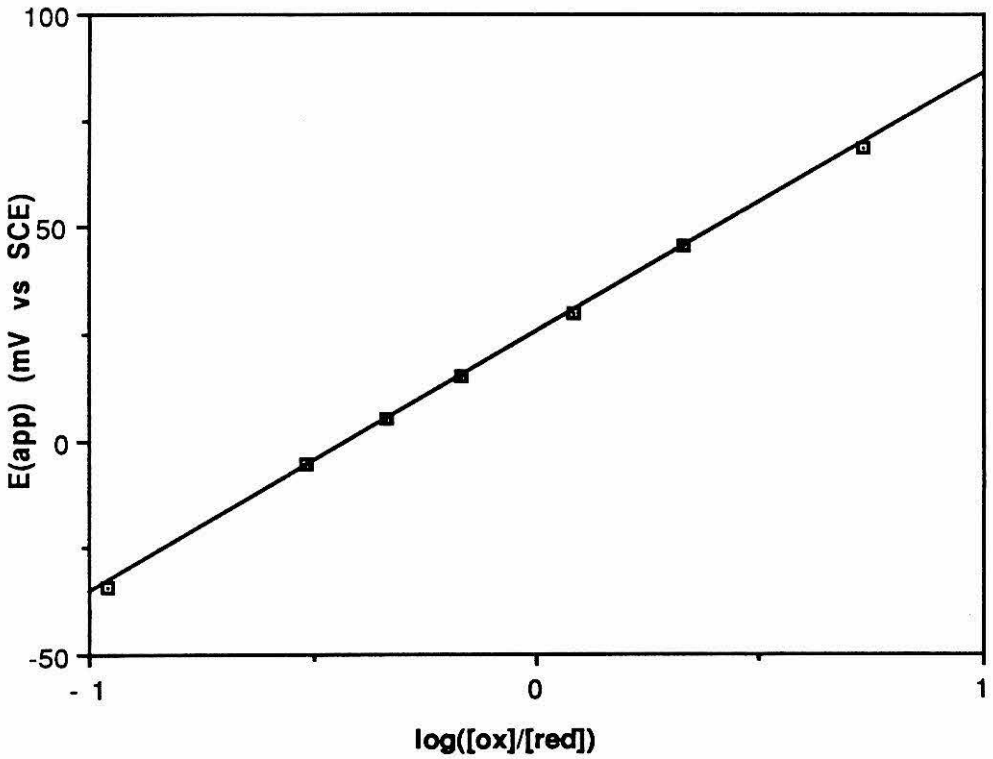
100
50
0
-50
E(app) (mV vs SCE)
- 1
0
1
log([ox]/[red])

Table 3. Redox potentials at pH 8, 25° for azurins from five species of bacteria

Azurin source	E_{m8} (mV vs NHE)[a]
Ade	266.9
Pae	291.9
Afa	251.5
Asp	278.1
Bbr	250.3

[a] pH 8.0, μ = 0.10 M. See reference 40 for an explanation of the notation used to denote redox potentials under other than standard conditions.

Table 4. Copper-ligand bond distances in Å. The data for Ade and the first line of data for Pae were obtained from crystal structure determinations; the remaining data were obtained from EXAFS studies.

Azurin source	Redox state	pH	r(Cu-L) (Å)					Ref
			N His	N His	S Cys 112	S Met 121	O Gly 45	
Ade[a]	Cu(II)	6.0	2.08(4)	2.01(4)	2.12(4)	3.12(4)	3.16(4)	16
			2.09(4)	1.99(4)	2.17(4)	3.10(4)	3.09(4)	16
Pae	Cu(II)	6.0	2.11(6)	2.11(11)	2.20(12)	2.79(8)	b	c
	Cu(II)	9.1	1.95(3)	1.95(3)	2.23(3)	d	e	57
	Cu(II)	4.1	1.95(3)	1.95(3)	2.19(3)	d	e	57
	Cu(I)	9.2	2.05(3)	1.89(3)	2.21(3)	2.74(5)	e	57
	Cu(I)	5.5	2.04(3)	1.89(3)	2.24(3)	2.70(4)	e	57

a The two sets of distances correspond to the two molecules in the unit cell.
b An accurate distance is not available.
c Personal communication from E. T. Adman in ref 57.
d The Cu-S(Met) distance in oxidized azurin could not be determined accurately.
e Not detected.

main-chain carbonyl. In Pae azurin, however, the Cu-S(Met) bond appears to be shorter than in Ade azurin, while the Cu-O(carbonyl) bond is longer. In terms of the hard/soft acid/base model, the "soft" methionine sulfur ligand would be expected to stabilize the soft copper(I) oxidation state, while the "hard" carbonyl oxygen ligand should preferentially stabilize the copper(II) state. Thus, the Pae copper site is expected to be more favorable for Cu(I) coordination, leading, as observed, to a higher redox potential for Pae than for Ade. Baker[58] has used a similar analysis to explain the difference in potential at pH 7 between Ade azurin and plastocyanin. In *Phaseolus vulgaris* plastocyanin, the Cu-S(Met) bond is shorter (2.7-2.9 Å) than in either of the azurins, and the carbonyl oxygen ligand is not present at all;[21,59] accordingly, the potential of plastocyanin is ~80 mV higher than that of Ade azurin at pH 7.[5] Baker also notes that selenomethionine-containing azurin from Pae exhibits a significantly higher potential at pH 7 (333 mV vs NHE)[60] than native Pae azurin; such a change would be expected on substitution of the softer Se for S at the copper site. Thus, taken together with these previous results, the observed potentials of Pae and Ade azurins at pH 8 seem to follow the trend expected on the basis of the hard/soft model.

It is likely that the variations in redox potentials among species of azurin at pH 8 represent the sum of the effects of several differences among the proteins. These differences might include small variations among the proteins in copper-ligand bond lengths and angles, differences in nearby charged residues, and differences in solvation changes on reduction. Thus it is not apparent to what extent the bond length differences discussed above are controlling the potentials, and to what extent other factors are involved. If it is assumed that differences in copper site geometry alone cause the variation in redox potentials at pH 8, it is predicted that Bbr and Afa azurins will have sites more like Ade, while the copper site of Asp will be intermediate between those of Pae and Ade. As more data become available on the copper site geometries of these three

species of azurin, it should be possible to test these predictions and further define the factors controlling the potentials.

pH dependences of the azurin redox potentials

Tables 5 - 9 and Figures 11 - 15 give the pH dependence of the redox potentials for the five azurins in this study. In each case, data were collected over as wide a pH range as possible. At pH values above or below those for which data are given, an accurate potential could not be determined, either because the absorbance of the protein decayed at constant applied potential, or because the Nernst plots had low correlation coefficients or slopes outside the range of ±5%.

The data for each of the five azurins show the trend of decreasing E_m with increasing pH, as expected based on the model of electrostatic interaction between the copper site and a titrating residue described above. The residues in each protein which may titrate in the pH range studied are listed in Table 10. Also included in Table 10 are pK_a values for the titrating residues of the azurins from Pae, Ade, and Afa; this information has been obtained from published NMR studies.[20,29,61,62] The distances from the copper to each of the titratable histidines were obtained from the crystal structure of Ade azurin.[14,15] Since the resolution of the Pae azurin structure is 2.7 Å[34] while the Ade structure has been refined to 1.8 Å, the Pae copper-proton distances are known less accurately, but they fall within the range listed for the Ade structure.

Analysis of the pH dependence of the potentials will focus on the non-ligand histidine residues, since histidine pK_a values typically fall within the pH range examined in this study. Aspartic acid (pK_a = 3.9)[63], glutamic acid (4.3), cysteine (10.78), and other ionizable amino acid side chains will not be expected to titrate except, in some cases, at the high- or low-pH limits of this work. Histidines which are

Table 5. The pH dependence of the redox potential of Pae azurin.

pH	E_m
4.49	352.2
4.98	348.6
5.28	348.2
5.43	345.4
5.97	339.5
6.25	332.6
6.49	326.7
6.81	317.0
6.99	314.0
7.29	304.5
7.33	301.5
7.50	298.9
7.69	295.8
8.03	291.9
8.48	287.6

Table 6. The pH dependence of the redox potential of Ade azurin.

pH	E_m
4.88	287.2
5.42	283.7
5.94	282.9
6.12	281.0
6.30	280.9
6.46	279.6
6.49	278.5
6.61	278.2
6.71	276.2
6.83	274.3
6.99	273.9
7.09	270.3
7.21	271.0
7.49	267.6
7.75	268.2
8.03	266.9
8.32	263.7
8.48	260.5

Table 7. The pH dependence of the redox potential of Afa azurin.

pH	E_m
3.96	317.6
4.33	304.6
4.63	301.7
4.96	299.4
5.43	292.8
5.94	290.2
6.30	286.5
6.46	283.3
6.82	273.1
6.99	270.0
7.33	259.5
7.50	257.4
7.96	251.5
8.48	250.6

Table 8. The pH dependence of the redox potential of Asp azurin.

pH	E_m
3.96	358.7
4.63	349.4
4.96	338.9
5.43	323.5
5.94	308.3
6.30	300.4
6.46	291.1
6.70	288.1
6.99	279.3
7.50	278.9
7.96	278.1

Table 9. The pH dependence of the redox potential of Bbr azurin.

pH	E_m
3.96	343.7
4.29	332.0
4.96	317.7
5.43	306.4
5.94	293.7
6.46	279.9
6.99	261.1
7.50	253.3
8.03	250.3
8.48	243.1
9.06	240.1

Figure 11. The pH dependence of the redox potential of Pae azurin. The curve represents a fit of the data to Equation 3.

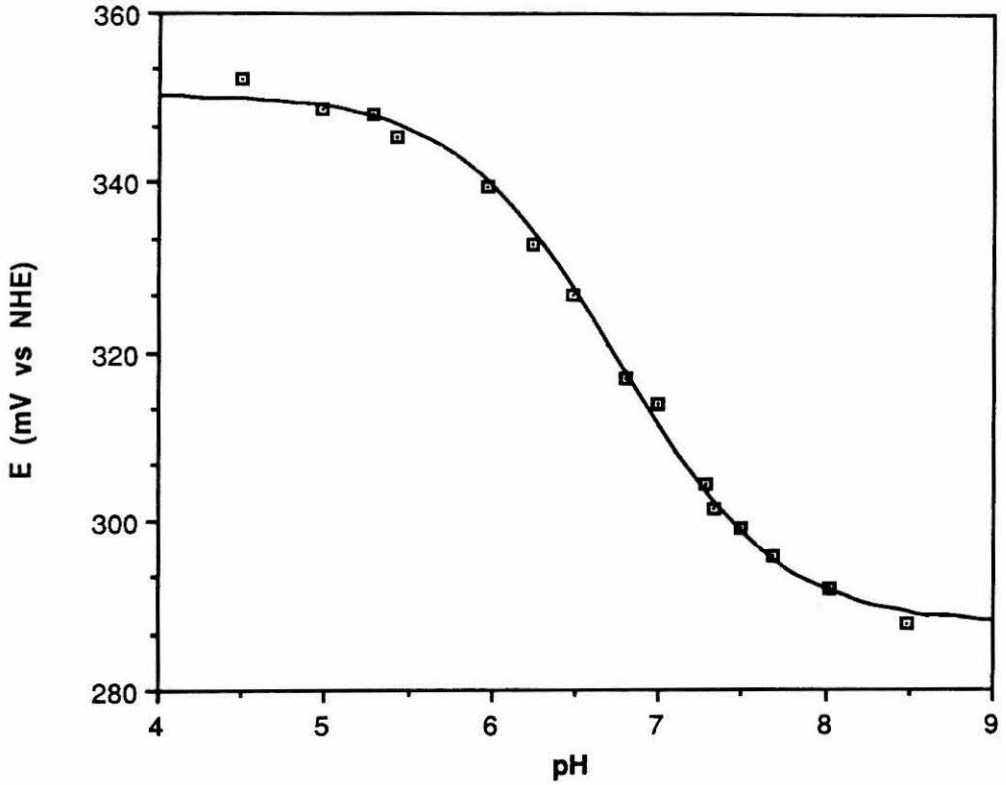
360
340
320
300
280
E (mV vs NHE)
4
5
6
7
8
9
pH

Figure 12. The pH dependence of the redox potential of Ade azurin. The points at pH 4.8, 8.3, and 8.5 were excluded from the fit.

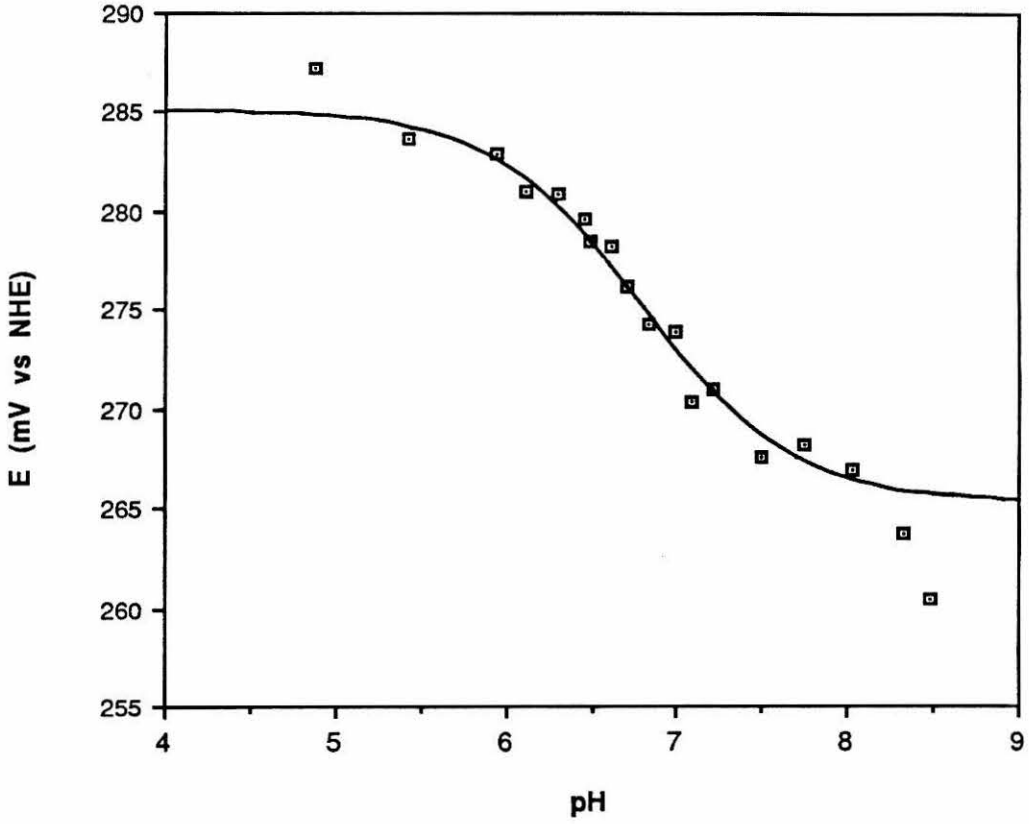
290
285
280
275
270
265
260
255
E (mV vs NHE)
4
5
6
7
8
9
pH

Figure 13. The pH dependence of the redox potential of Afa azurin. The point at pH 4.0 was excluded from the fit.

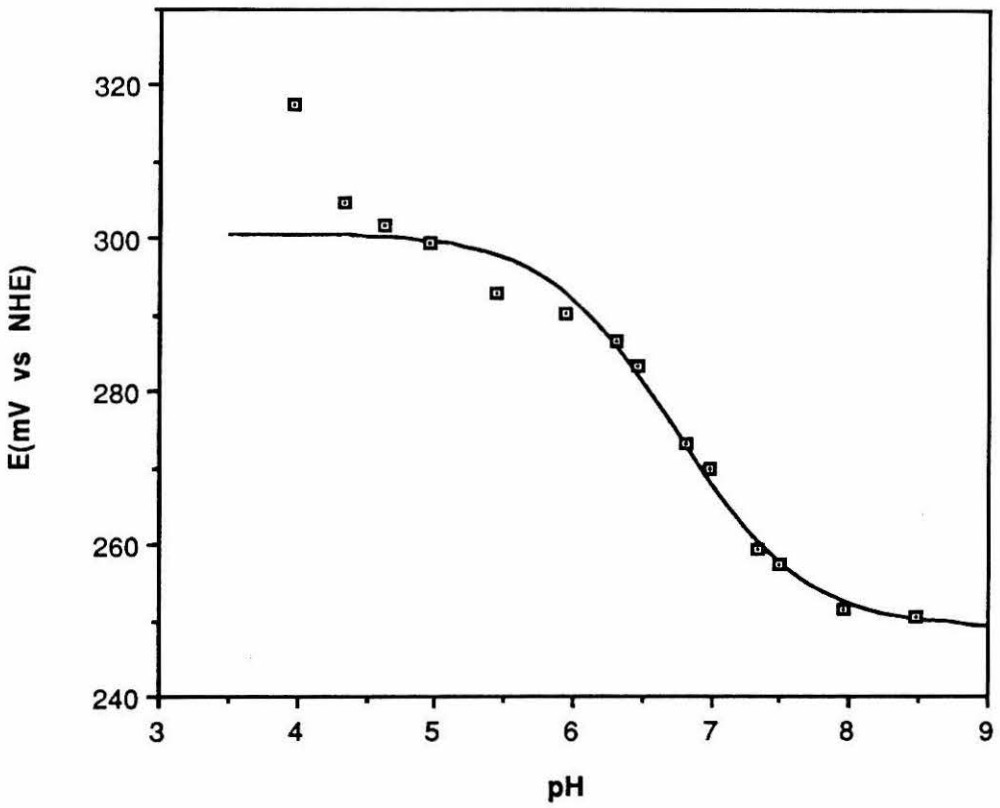
320
300
280
260
240
E(mV vs NHE)
3
4
5
6
7
8
9
pH

Figure 14. The pH dependence of the redox potential of Asp azurin.

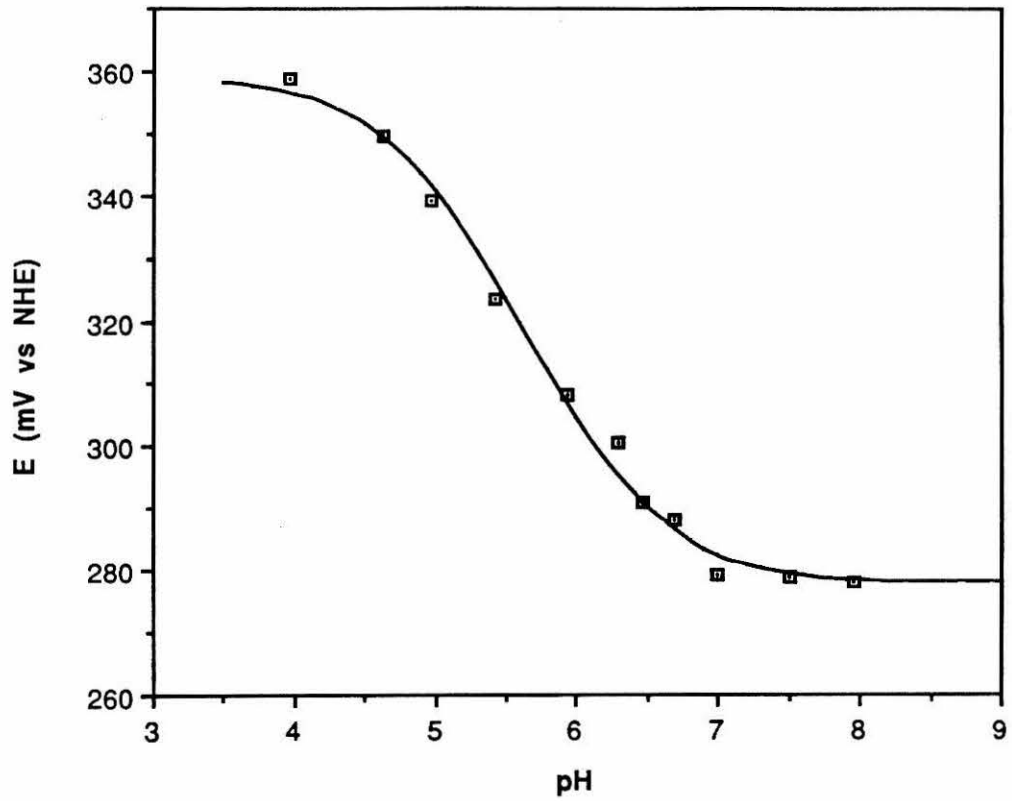
E (mV vs NHE)
360
340
320
300
280
260
3
4
5
6
7
8
9
pH

Figure 15. The pH dependence of the redox potential of Bbr azurin. The two lowest pH and two highest pH points were excluded from the fit.

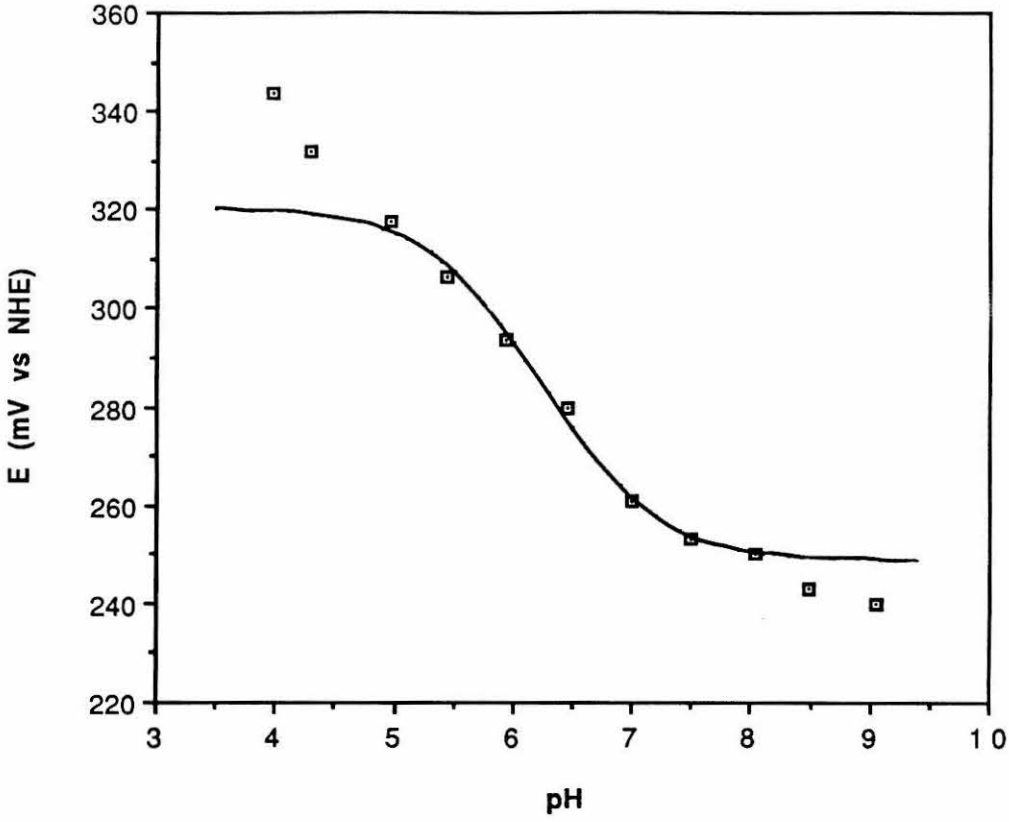
360
340
320
300
280
260
240
220
E (mV vs NHE)
3
4
5
6
7
8
9
10
pH

Table 10. Previously reported pK_a values for histidines of Ade, Pae, and Afa azurins

	His 32		His 35		His 83	
	pK^{red}	pK^{ox}	pK^{red}	pK^{ox}	pK^{red}	pK^{ox}
Ade[a]	6.24	6.17	(4.8)[b]		7.05	6.80
Pae			6.9-7.3[c]		7.57[c]	7.35[c]
			6.9-7.3[d]		7.6[d]	
			6.8-7.8[e]		7.5[e]	
			~7.7[f]	5.5-6.3[f]		
Afa[g]			<4	<4	6.8	6.8
r(Cu-H^+)[h]	18-19		7-8		12-15	

a Ref. 29; 36°C.
b Tentative.
c Ref. 61; 24°C.
d Ref. 64; 37°C.
e Ref. 20; 31°C.
f Ref. 54; 25°C.
g Ref. 62; 35°C.
h Copper-histidine(H^+) distances (in Å) were obtained from coordinates of the Ade azurin crystal structure,[14,15] as deposited in the Brookhaven Protein Data Bank.

coordinated to the copper (His 46 and His 117) will not be considered, as their pK_a values are shifted to ≤ 4.[20].

In Pae azurin, both non-ligand histidine residues have been shown by ^{1}H-NMR to titrate in the pH range considered in this study. In addition, the pK_a of each histidine titration is known to be affected by the oxidation state of the copper. This implies that the potential of the copper should be affected to some degree by the state of protonation of each of the histidines. In order to assess the impact of the histidine titrations on the copper potential, the potentials were fit to Equation 3, yielding the curve shown in Figure 11. The apparent pK_a values obtained are shown in Table 11: for Pae, pK_a^{red} = 7.31 and pK_a^{ox} = 6.26. These values are intermediate between the pK_a values of His 35 and His 83 determined by NMR (Table 10), as would be expected if both histidines are influencing the potential.

A more quantitative comparison between the observed pH dependence of the Pae potential and the pK_a values obtained by ^{1}H-NMR can be made using a modification of Equation 3. At pH values where both histidines are in the deprotonated state, $[H^+]$ in the equation will be negligible relative to K_a^{red} and K_a^{ox}. Thus, Equation 3 becomes

$$E_m(\text{low pH}) - E_m(\text{high pH}) = \frac{RT}{nF} \ln \frac{K_a^{ox}}{K_a^{red}} \qquad (13)$$

Using Equation 13 and the pK_a values obtained by NMR (Table 10), it is possible to calculate the change in redox potential from low to high pH which could be attributed to the titration of the two histidines. Thus, the deprotonation of His 83 is predicted to cause a 13 mV shift in the potential, while the shift in potential due to His 35 will be approximately 70 mV, giving a total effect for the two histidines of 83 mV. As indicated in Figure 11, the observed change in potential over the pH range in which the histidines titrate is about 60 mV. This result is in reasonable agreement with the prediction based

Table 11. Apparent pKa values derived from the pH dependence of the redox potentials

Azurin source	pK_a^{ox}	pK_a^{red}
Pae	6.26	7.31
Ade	6.63	6.97
Afa	6.31	7.17
Asp	4.95	6.32
Bbr	5.65	6.85

on the pK_a values, particularly in light of the uncertainty (±0.4) in the pK_a^{ox} value of 5.9 for His 35.[54]

These electrostatic interactions may only partially account for the observed pH dependence of the azurin redox potentials; that is, there may be slight pH-dependent variations in the copper site geometry and other features of the protein which contribute to the pH dependence of the potential. In fact, several lines of evidence indicate that slight but detectable changes do occur as the pH is changed. In reduced Pae azurin, ^{1}H-NMR line-broadening studies indicate that a shift in pH from 4.6 to 8.2 induces a change in the position of histidine 35 relative to the copper, resulting in a change in copper-His 35 distance of about 1 Å.[22,65] The position of the C4 proton of His 46 relative to the His 35 ring also changes by 0.5 - 0.9 Å.[66] These changes occur with a pK_a of 7.3, approximately the same as the pK_a of His 35 in Cu(I) azurin. Based on these and other observations, it has been concluded that the protonation of His 35 is accompanied by a slight movement of the residue. The crystal structure of Pae azurin[34] indicates that the imidazole ring of His 46, a copper ligand, lies parallel to and adjacent to the ring of His 35; thus, His 46 may relay the effects of the movement of His 35 to the copper site. ^{1}H-NMR spectra of the reduced protein also indicate pH-dependent behavior for the ligand methionine (Met 121) methyl resonance, which is reduced in intensity and shifts slightly between pH 4.6 and 8.2.[65-67] This shift has been interpreted as a change of ≥0.15 Å in the position of the methyl group with respect to the aromatic ring of a nearby phenylalanine (Phe 15) and/or His 46.[65] In addition, ^{13}C-NMR results[20] indicate that the Gly 45 carbonyl ligand resonance titrates with pH, indicating either that the carbonyl moves slightly, and thus the copper-oxygen bond length probably changes, or that a nearby residue (perhaps His 46) moves with respect to the carbonyl. These changes also occur at the same pK_a as the titration of histidine 35, implying that the motion of His 35 is transmitted to the copper site. Corroborating

these results, a recent EPR study of oxidized Pae azurin at 40 K reveals that the copper-ligand geometry does change slightly between pH 5.2 and 9.2; the change in the EPR spectrum can be fitted by a 0.035 Å displacement of ligand atoms.[53]

EXAFS (extended x-ray absorption fine structure) experiments at 30 K[57,68] indicate that the copper-ligand bond lengths for the four closest ligands are unaffected by pH, within the error of 0.03 Å for the histidines and cysteine and 0.05 Å for the methionine; the carbonyl ligand was not observed. The pH range studied was 4.1 to 9.1 for Cu(II), and 5.5 to 9.2 for Cu(I). An increase in the Debye-Waller factor for the methionine ligand was observed at high and low pH values in the reduced protein, which may indicate increased motion or a slight lengthening of the bond at extremes of pH. Thus, it appears that the conformational change induced by shifts in pH has a very minor effect on the copper site of the protein, probably involving rotation of a ligand rather than changes in copper-ligand bond lengths. These minor changes may, however, have an effect on the redox potential.

Thus, the observed pH dependence of the Pae azurin potential must arise from a combination of electrostatic and other effects. By comparing the pH dependence of the potentials of a series of azurins, it may be possible to separate the contribution due to electrostatic interactions from actual changes in geometry resulting from the pH change. Further, it may be possible to correlate these variations among proteins to subtle structural differences.

The pH dependence of the Ade azurin redox potentials, shown in Figure 12, provides a sharp contrast with the Pae data. Over the range of pH 5.0 to 8.0, Ade exhibits only an 18 mV change in potential, compared to the 60 mV change for Pae. Pae has two non-ligand histidines with pK_a values in the range of 5 to 8, as described above and listed in Table 10: His 35, at 7-8 Å from the copper, and His 83, at ~13 Å. Ade azurin contains those same two histidines plus a third not found in Pae, His 32. The

distance from the copper to the His 32 protons is approximately 18 Å. However, in Ade, it is known from ^{1}H-NMR results[29] that His 35 titrates with a pK_a of about 4.8, well below the normal range for histidine. According to Coulomb's law (Equation 5), the energy of interaction between two charges decreases as r, the distance between the charges, increases. The His 35 titration would therefore be expected to make a much greater contribution to the pH dependence of the potential than would His 83 or His 32. Thus, the pH dependence of the redox potentials should be much less dramatic in Ade than in Pae, at least over the pH range 5 to 8. In addition, NMR evidence indicates that protonation of His 35 of Ade azurin does not result in a conformational change, as it does in Pae. The results of a recent EPR study at 40 K support this conclusion: the EPR spectrum of Ade azurin was found to be invariant between pH 5.2 and 9.2 at 40K. In contrast, the Pae copper site undergoes a slight change over the same pH range, as described above. Thus, any contribution to the pH dependence of the redox potential in Pae due to a change in copper site geometry with pH should not be a factor in Ade.

The pK_a values of the Ade azurin histidines obtained from NMR measurements (Table 10) can be inserted in Equation 13 to predict the effect on the potential of the deprotonations of the two more distant histidines. Thus, the protonations of His 32 and His 83 are expected to raise the potential by 4 and 15 mV, respectively, for a total of 19 mV. This calculated ΔE_m is in excellent agreement with the observed change of 18 mV, implying that the pH dependence of the potential can be explained entirely on the basis of electrostatic interactions. This result provides further evidence that the Ade copper site does not undergo a change in geometry with pH.

A model proposed by Adman[1] to explain the difference in titration behavior of His 35 between Pae and Ade azurins based on differences in amino acid sequences can be used to compare the five species examined in this report. The positions of His 35 and the other non-ligand histidine residues in Ade azurin are shown in Figure 16; His 35 is seen

Figure 16. Diagram of the Ade azurin structure. Copper ligands are shown in pink, and histidine side chains are in green. His 32 and His 83 are solvent exposed, while His 35 is somewhat buried in the protein.

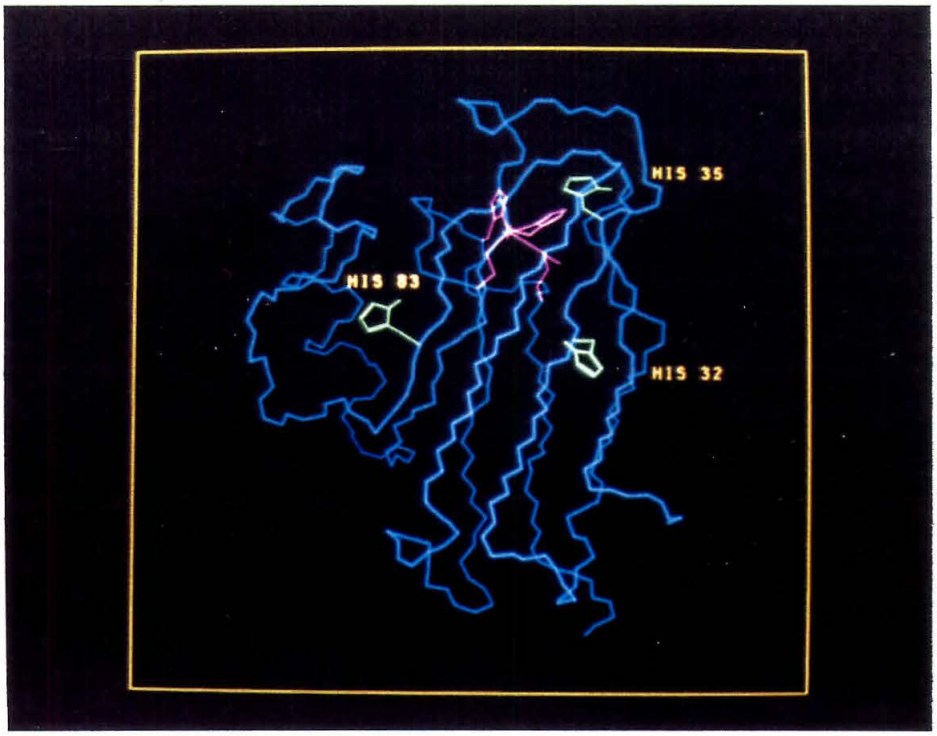
HIS 35
HIS 83
HIS 32

to be shielded from the solvent by the surrounding residues. A schematic diagram of the region of the protein surrounding His 35 is given in Figure 17. In Adman's model, a comparison is made between Ade and Pae azurins in terms of the residues of the strands of β-sheet which shield His 35 from the solvent; these strands are highlighted in color and are labelled F, C, and A in Figure 17. In Ade, several hydrogen bonds and a salt bridge between Lys 34 and Glu 8 appear to hold strands C and A together, and may help to shield His 35 from the solvent and inhibit its protonation. In Pae, the residues involved in the salt bridge are replaced by neutral residues, thus eliminating an important link between the two chains; in addition, one of the hydrogen bonds between chains C and A is eliminated and a new hydrogen bond is present between chain C (Gly 37) and neighboring chain F (Ser 89). Adman suggests that the effect of these amino acid substitutions is to pull chains C and A apart slightly in Pae relative to Ade, making His 35 more solvent-accessible and thus available for protonation. This proposal gains support from the observation that His 35 of Pae is known from NMR evidence to titrate slowly,[61,64] suggesting that the residue is somewhat buried or restricted. His 35 of Ade, by comparison, cannot be protonated except at very low pH, perhaps after the salt bridge holding strands C and A together is broken. Results from a recent refinement of the Ade azurin crystal structure[16] indicate that residues 34 and 8 do not form a salt bridge, thus calling this model into question. However, considering the high mobility of the side chains of residues 34 and 8 and other solvent-exposed residues, it seems plausible that a salt bridge may be present in the solution structure.

Based on Adman's model and the known amino acid sequences of Afa, Asp, and Bbr azurins, predictions can be made as to whether or not His 35 will titrate in each of these three azurins. In Afa azurin, the residues involved in the salt bridge and hydrogen bonding interactions between strands C and A are conserved relative to Ade. Thus, the

Figure 17. The region of the azurin structure near His 35. His 35 (viewed from the side) is shown in yellow near the center of the diagram, behind chain C. The region of the β-sheet which shields His 35 from the solvent is shown in color: chain F in blue, chain C in red, and chain A in green.

a. Ade azurin. A salt bridge between Lys 34 (chain C) and Glu 8 (chain A) holds chains C and A together.

b. Pae azurin. The residues involved in the salt bridge in the Ade structure are replaced by neutral residues. A hydrogen bond between Ser 89 (chain F) and Gly 37 (chain C) appears to pull chain C toward chain F.

a.

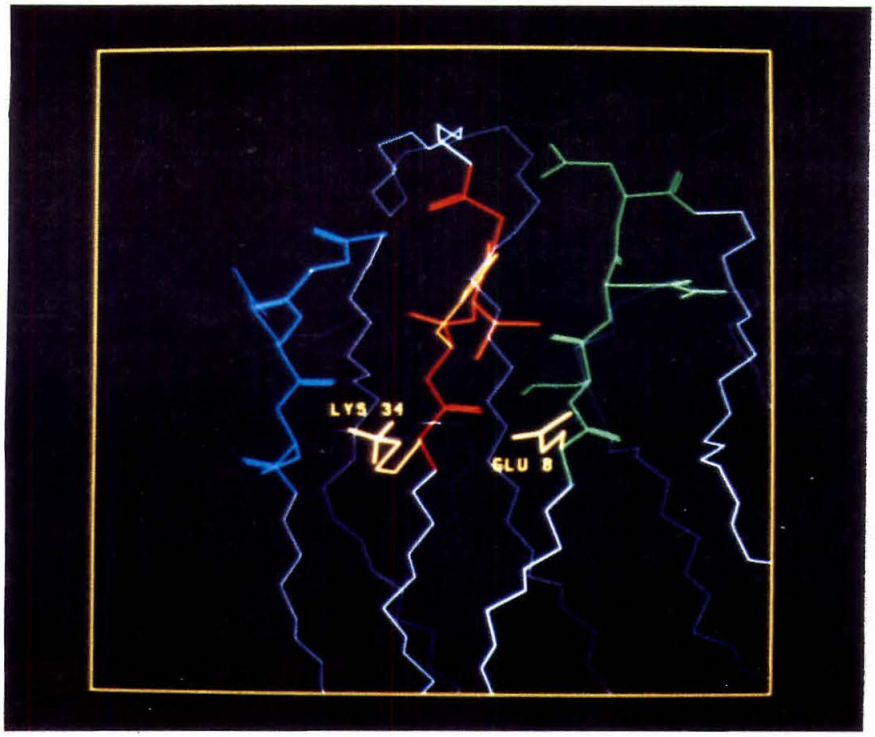

F C A

b.

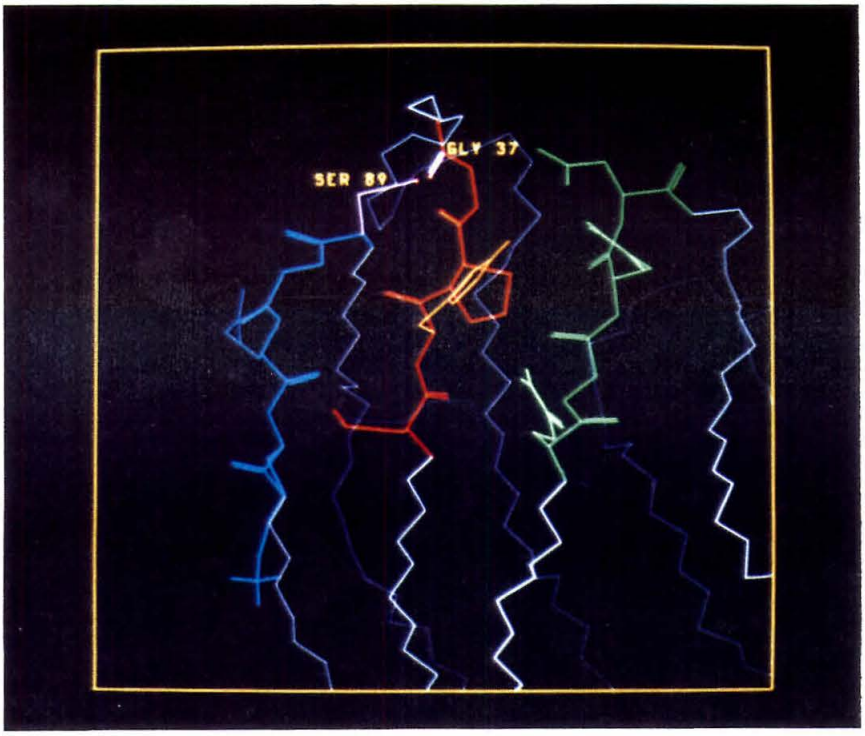

F C A

pK_a of His 35 should be shifted to very low pH, as in Ade. Indeed, ^{1}H-NMR results indicate that His 35 does not titrate over the range of pH 4 to 9.5.[62] In addition, a ^{1}H-NMR study of the titration of the His 83 protons of Afa indicates that the pK_a of His 83 (6.8) is not affected by the oxidation state of the copper.[62] This implies that the redox potential of the copper will not be affected by the state of protonation of His 83. However, the redox potential of Afa azurin shows a strong pH dependence (Figure 13), including a clearly sigmoidal curve in the pH range at which a histidine would be expected to titrate. A fit of this portion of the curve to Equation 1 yields $pK_a^{red} = 7.17$ and $pK_a^{ox} = 6.31$. The change in potential over the same range of pH is about 50 mV, intermediate between the change observed for Pae and Ade.

The discrepancy between the observed change in the Afa redox potential with pH and the predicted lack of a pH dependence in the redox potential is puzzling. One possible explanation is that a residue other than histidine has a pK_a within the pH range studied. For example, the pK_a of a glutamic acid side chain carboxylate could be shifted up by hydrogen bonding to another side chain. It seems unlikely, however, that a pK_a near 7 would result. Another possibility is that the His 35 resonances were incorrectly assigned in the ^{1}H-NMR spectrum, and His 35 does in fact titrate in the pH range studied. Alternatively, it may be that the observed pH dependence is entirely due to factors other than electrostatic interactions between the copper and titrating residues. Although the inability of His 35 to titrate implies that the type of pH-dependent change in the copper site that is observed for Pae does not occur for Afa, other possibilities exist. A pH-dependent structural change may occur which is not linked to the state of protonation of His 35. ESR, EXAFS, and other types of spectroscopic data at low and high pH values are needed in order to assess this possibility. Finally, the sharp increase in redox potential observed at pH values below 4.5 is probably due to the protonation of

aspartic acid or glutamic acid residues (pK_a = 3.9-4.3[63]) and the resulting changes in electrostatic interactions with the copper.

The pH dependences of the Asp and Bbr azurin redox potentials are shown in Figures 14 and 15. These data can be fit according to Equation 3, yielding the pK_a values listed in Table 11. The Asp azurin data fit a sigmoidal curve, but the apparent pK_a values obtained (pK_a^{ox} = 4.95, pK_a^{red} = 6.32) are not within the normal range for histidine titrations. The relatively large change in potential (80 mV) over the pH range observed may indicate that His 35 (the closest non-ligand histidine to the copper) titrates in Asp azurin. If so, the apparent pKa values indicate that protonation of the histidine is somewhat hindered, perhaps by shielding of the histidine from solvent as observed in Ade azurin. Alternatively, the shift in the copper potential with pH may result from a pH-dependent conformational change in the protein.

Bbr azurin exhibits a very dramatic change in redox potential with pH: 104 mV over the pH range of 4 to 9. Unlike the potentials of the other four azurins, the data for Bbr do not level off at low pH. This may be due to overlap between the pK_a values of carboxylic acid and histidine side chains. If, however, the shift in potential with pH reflects a pH-dependent conformational change, the potential would not be expected to fit a sigmoidal curve. Further analysis of the redox potentials of Asp and Bbr azurins will require the determination of histidine pK_a values and spectroscopic properties of the proteins at low and high pH values.

Implications concerning the redox activity of Pae azurin

The data presented here for Pae azurin provide insight into proposals that the protein exists in a redox-active and a redox-inactive form. These proposals have derived from temperature-jump kinetic studies of the redox reaction between azurin and cytochrome c_{551}, in which two distinct relaxation processes were observed.[69,70]

On the basis of several lines of evidence, the slow relaxation process was attributed to a pH-dependent interconversion between two forms of azurin, only one of which is redox active; the reactive form has been proposed by different authors to be the low-pH or the high-pH form of the protein.[55,71] The observation that the interconversion occurs on approximately the same time scale as protonation of a slowly titrating histidine (His 35) led to the proposal that the protonation of His 35 provides the trigger for the conformational change. However, more recent work by Corin et al.[54] casts doubt on this interpretation, and suggests that the kinetics of the azurin/cytochrome c_{551} reaction can be adequately explained without invoking a significant change in azurin's redox activity with pH. The pH dependence of the Pae azurin redox potential, as presented in this report, indicates that the rates of intermolecular electron transfer reactions involving azurin should vary with pH, but that the low- or high-pH form of Pae azurin cannot be termed a "redox-inactive" form. The magnitude of the variation in the rate of electron transfer is expected to depend on the driving force for the reaction. At zero driving force, as in the self-exchange reaction of azurin, the rate should be pH-independent. Recent measurements of the azurin self-exchange rate[72-74] support this conclusion.

pH dependence: Conclusions

The pH dependences of the azurin redox potentials observed in this study demonstrate the potential for controlling the redox reactivity of a metalloprotein through fluctuations in pH. This may represent one mechanism by which a bacterium can manipulate the rate of electron transfer between the azurins and their biological electron transfer partners. At low driving forces, as are typically found in biological systems, the electron transfer rate is markedly dependent on the reaction exothermicity.

Thus, the relatively small change in potential which can be induced by a protonation or deprotonation may effectively correspond to an on/off switch for electron transfer.

These results are also relevant to studies involving binding of a transition metal complex or other modifying agent to the surface of a protein. Such experiments have been important in mapping out sites for intermolecular electron transfer on protein surfaces, and have been used extensively with azurin and other blue copper proteins. If a metal complex binds to the surface of the protein, and the binding is found to decrease the rate of electron transfer between the modified protein and a redox partner, then it can be inferred that the binding site of the metal complex represents an important pathway for electron transfer between the redox partner and the copper site. However, just as binding of a proton has been shown to influence the redox potential of the copper, binding of a charged complex to the surface of the protein would be expected to have some effect on the potential. Thus, the possible change in copper redox potential and the effect of that change on the observed intermolecular electron transfer rates must be borne in mind when interpreting the observations.

Temperature dependences of the azurin redox potentials

In an effort to determine the relative importance of electrostatic interactions and conformational changes in the pH dependences of the azurin redox potentials, the temperature dependences of the potentials of four of the azurins were measured at low and high pH values. From temperature-dependence data, the entropic and enthalpic contributions to the redox potential can be extracted. It was anticipated that a comparison of the thermodynamic parameters for a single protein at low and high pH would aid in determining the extent to which structural changes contribute to the pH dependence of the potential. In addition, a comparison between the thermodynamic parameters for two azurins at similar points on their titration curves might provide

insight into the factors which result in different redox potentials for different species of azurin.

Tables 12 - 19 and Figures 18 - 25 give the temperature dependences of the redox potentials of Pae, Ade, Afa, and Bbr azurins at low and high pH. The thermodynamic parameters extracted from these plots are presented in Table 20. $\Delta H^{\circ\prime}$ and $\Delta S^{\circ\prime}$ are reported for the complete cell reaction, referenced to NHE. For each species, the temperature dependence data were obtained at the lowest and highest pH values possible.

The enthalpies of reduction all fall within the range of approximately -13 to -16 kcal/mol. These values are comparable to previously reported ΔH° values for blue copper proteins (Table 21) and other metalloproteins. The negative enthalpies of reduction for blue copper proteins have been interpreted as indicating enhanced copper-methionine back-bonding in the reduced form. The strong similarity in ΔH° among the four different species of azurin implies that the bonding interactions at copper are very similar in both the reduced and oxidized states for the four species. A comparison of ΔH° for each protein at low and high pH, including previously reported ΔH° values for Pae and Ade azurins at pH 7, indicates that ΔH° remains essentially constant over a wide pH range. Afa azurin appears to be an exception: the enthalpy of reduction is -15.1 ± 0.4 at pH 5.0 and -12.6 ± 0.9 at pH 8.5. Thus, the enthalpic component is the primary contributor to the observed pH dependence of the potential for Afa azurin.

In small transition metal complexes, the entropies of reduction tend to correlate with the overall charge on the complex. This effect can be understood in terms of the orienting effect of the complex on the structure of the surrounding water. Reduction of a positively charged complex will result in some relaxation in the water structure, and thus an increase in the entropy. In contrast, a negatively charged complex will exhibit a negative entropy of reduction, due to increased ordering of the water molecules. Bulky

Table 12. The temperature dependence of the redox potential of Ade azurin at pH 5.4.

T(°C)	$E_{m5.4}$
5.6	290.9
12.0	288.1
14.6	286.6
21.4	287.3
24.8	284.2
35.5	279.9
39.8	277.1

Table 13. The temperature dependence of the redox potential of Ade azurin at pH 8.0.

T(°C)	$E_{m8.0}$
4.8	273.2
9.4	272.2
15.6	271.0
15.6	272.2
18.2	268.5
20.0	268.5
24.9	265.7
25.0	267.6
30.4	265.8
35.0	262.6

Table 14. The temperature dependence of the redox potential of Pae azurin at pH 5.0.

T(°C)	$E_{m5.0}$
7.2	357.7
11.0	355.1
12.4	355.5
16.0	353.5
19.2	351.1
23.2	349.6
25.0	348.2
30.1	345.5
33.6	345.1

Table 15. The temperature dependence of the redox potential of Pae azurin at pH 8.0.

T(°C)	$E_{m8.0}$
10.4	300.8
13.6	299.2
17.2	295.9
21.6	293.5
25.6	291.7
30.5	289.0

Table 16. The temperature dependence of the redox potential of Afa azurin at pH 5.0.

T(°C)	$E_{m5.0}$
4.0	309.9
10.8	306.9
15.0	305.0
20.0	301.6
25.0	298.7
30.0	296.6
34.0	295.3

Table 17. The temperature dependence of the redox potential of Afa azurin at pH 8.5.

T(°C)	$E_{m8.5}$
4.6	256.0
7.6	257.8
12.8	253.4
16.2	255.1
19.4	250.0
20.0	252.8
21.2	252.7
25.0	250.6
27.7	248.7
32.4	248.9

Table 18. The temperature dependence of the redox potential of Bbr azurin at pH 4.0.

T(°C)	$E_{m4.0}$
5.0	352.7
9.7	349.4
13.2	349.3
15.6	346.5
15.7	346.7
18.6	344.5
20.2	345.0
21.2	344.8
22.2	345.5
25.0	342.5
27.6	342.5
29.8	343.2
30.0	343.0

Table 19. The temperature dependence of the redox potential of Bbr azurin at pH 8.0.

T(°C)	$E_{m8.0}$
5.6	265.2
10.0	265.0
12.2	263.5
16.8	257.4
20.2	253.5
25.0	248.0
25.2	250.5
30.6	246.8

Figure 18. Plot of the temperature dependence of the redox potential of Ade azurin at pH 5.4

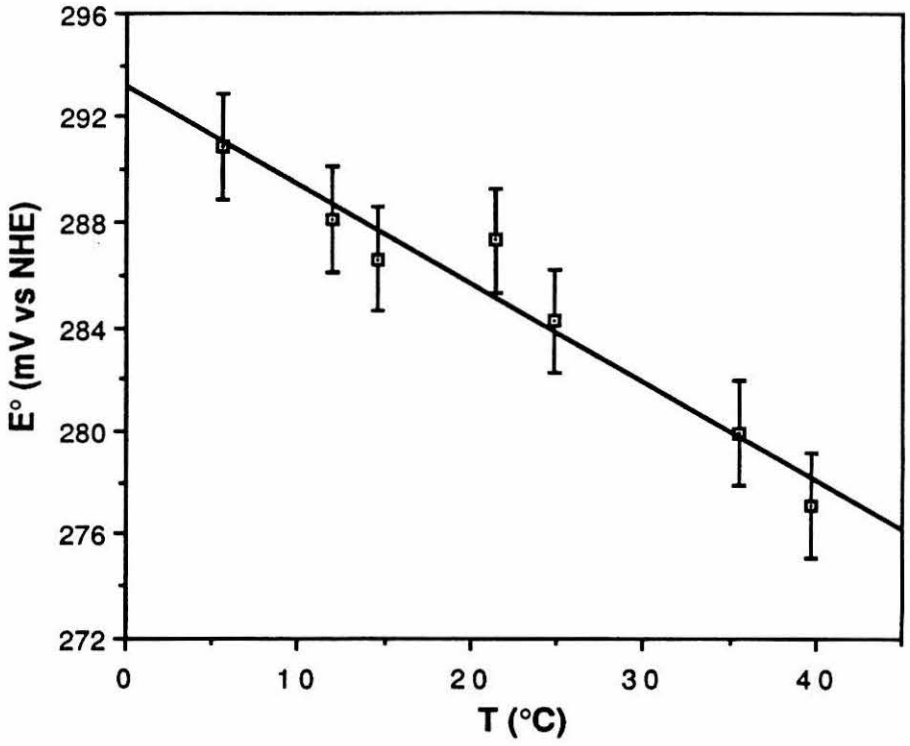
296
292
288
284
280
276
272
E° (mV vs NHE)
0
10
20
30
40
T (°C)

Figure 19. Plot of the temperature dependence of the Ade azurin redox potential at pH 8.0

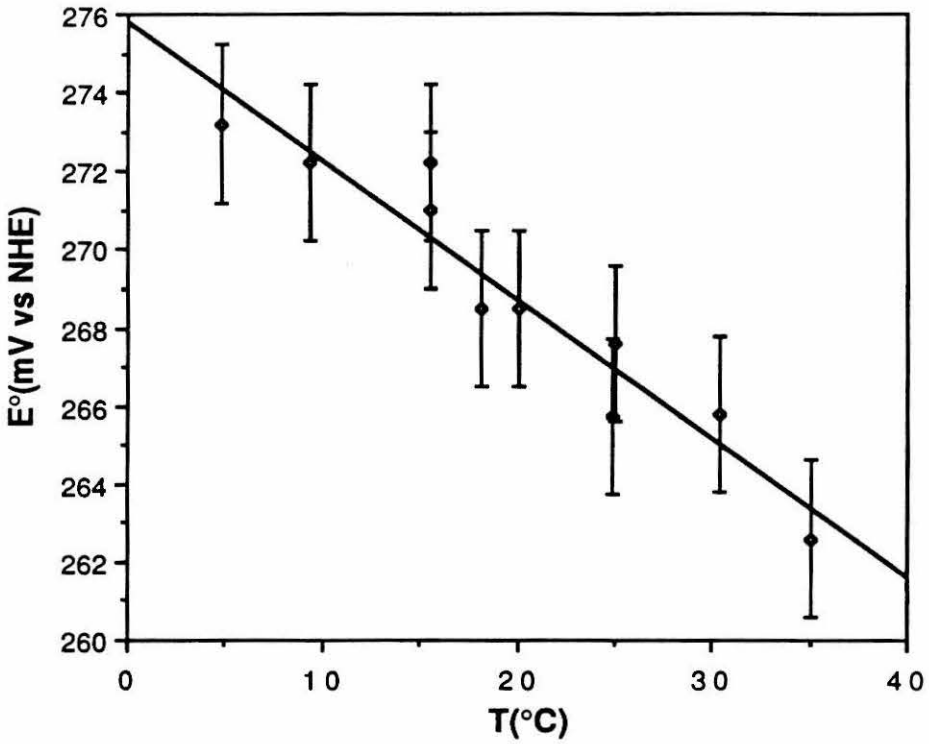
276
274
272
270
268
266
264
262
260
E°(mV vs NHE)
0
10
20
30
40
T(°C)

Figure 20. Plot of the temperature dependence of the Pae azurin redox potential at pH 5.0

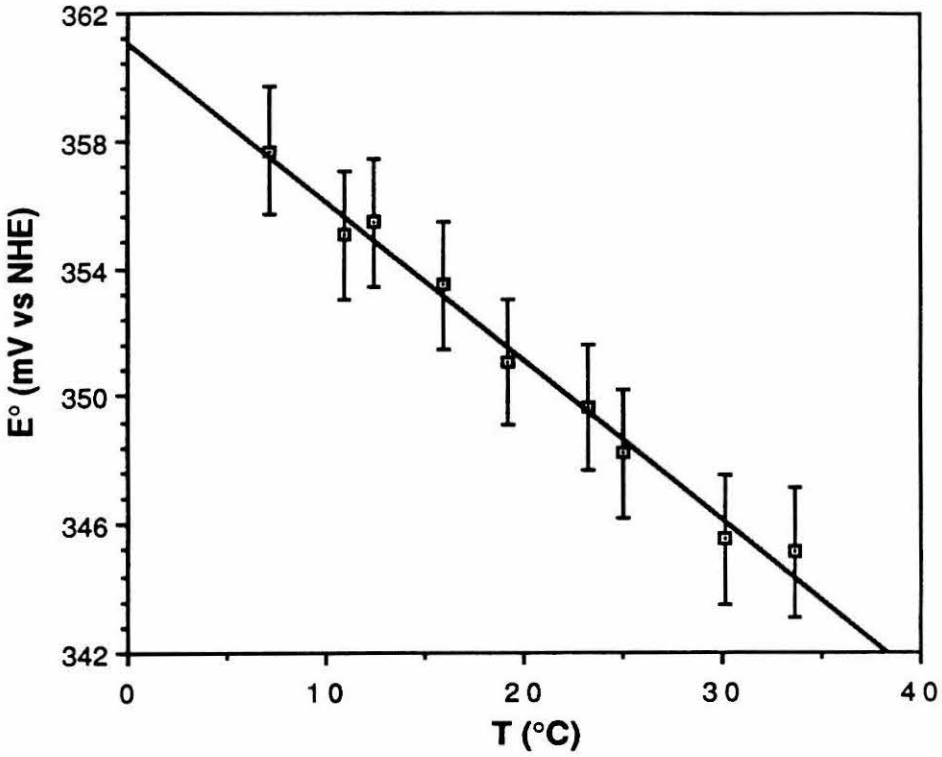
362
358
354
350
346
342
E° (mV vs NHE)
0
10
20
30
40
T (°C)

Figure 21. Plot of the temperature dependence of the Pae azurin redox potential at pH 8.0

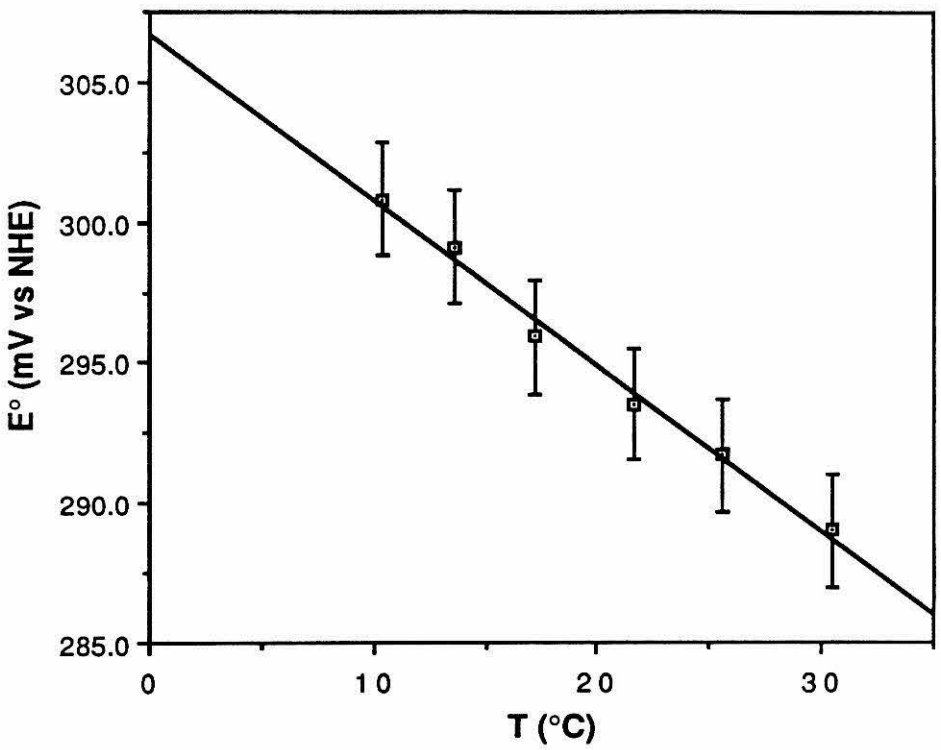
305.0
300.0
295.0
290.0
285.0
E° (mV vs NHE)
0
10
20
30
T (°C)

Figure 22. Plot of the temperature dependence of the Afa azurin redox potential at pH 5.0

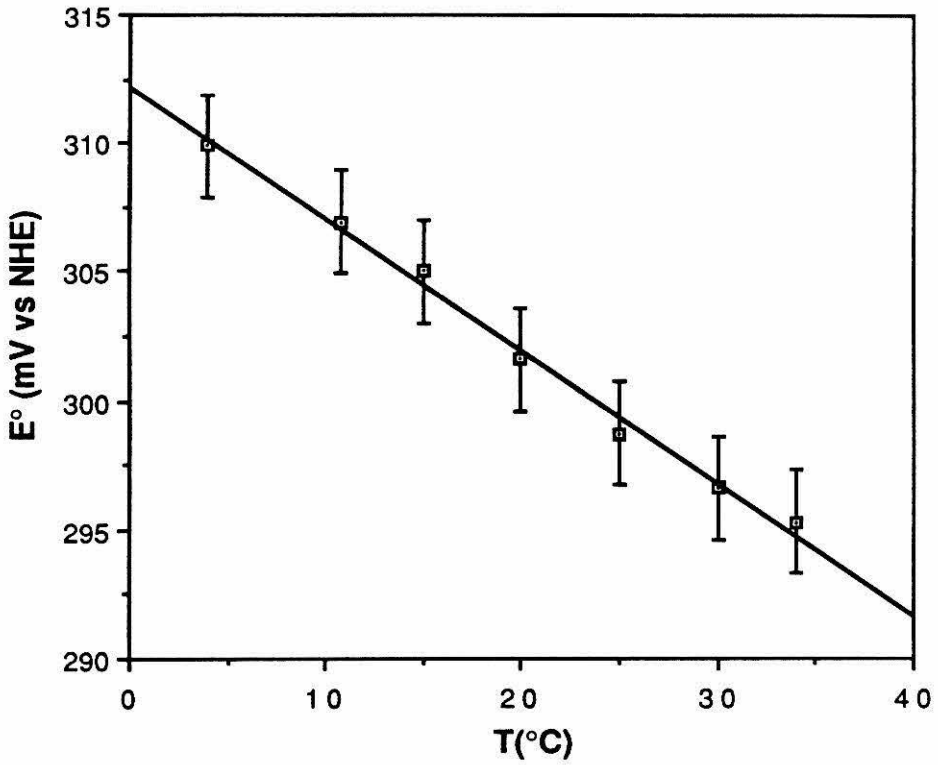
315
310
305
300
295
290
E° (mV vs NHE)
0
10
20
30
40
T(°C)

Figure 23. Plot of the temperature dependence of the Afa azurin redox potential at pH 8.5

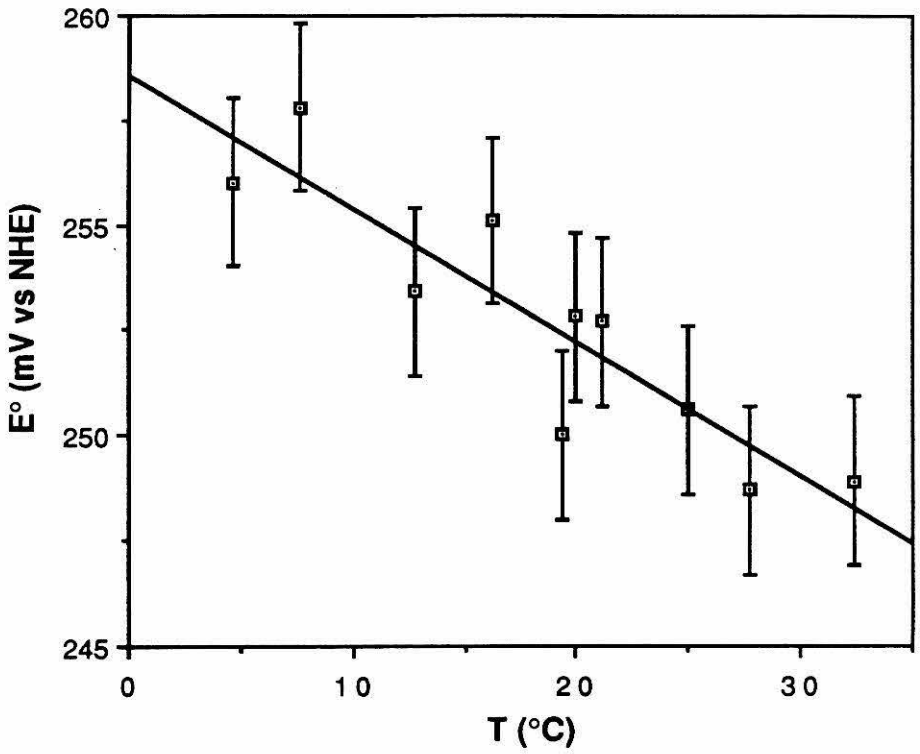
260
255
250
245
E° (mV vs NHE)
0
10
20
30
T (°C)

Figure 24. Plot of the temperature dependence of the Bbr azurin redox potential at pH 4.0

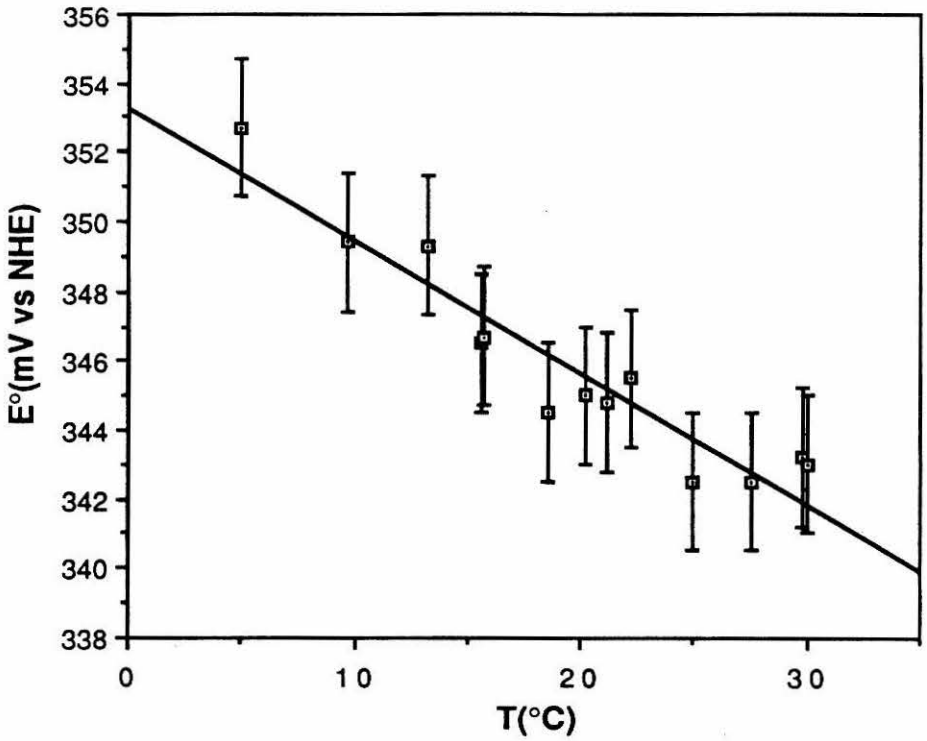
356
354
352
350
348
346
344
342
340
338
E°(mV vs NHE)
0
10
20
30
T(°C)

Figure 25. Plot of the temperature dependence of the redox potential of Bbr azurin at pH 8.0

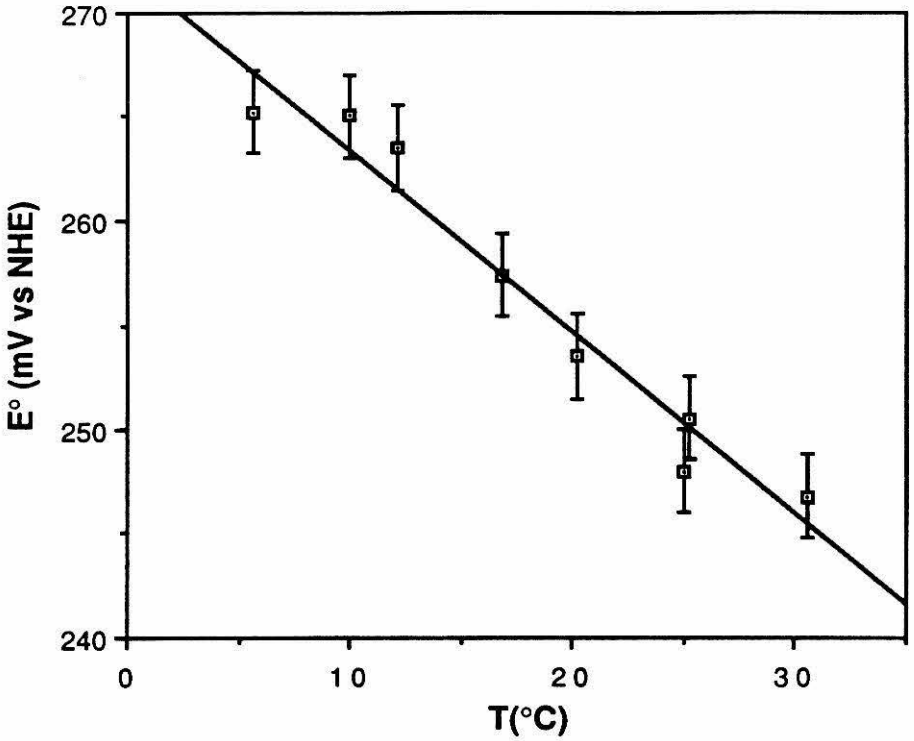
270
260
250
240
E° (mV vs NHE)
0
10
20
30
T(°C)

Table 20. Thermodynamic parameters for the reduction of azurin at 25°C

	pH	E_m (mV vs NHE)[a]	$\Delta S°'$ (eu)	$\Delta H°'$ (kcal/mol)	$\Delta G°'$ (kcal/mol)[b]
Ade	5.4	283.7	-24.4 (±2.3)	-13.8 (±0.7)	-6.5
	8.0	267.0	-23.7 (±2.1)	-13.2 (±0.7)	-6.2
Pae	5.0	348.6	-27.1 (±1.2)	-16.1 (±0.4)	-8.0
	8.0	291.9	-29.2 (±1.9)	-15.4 (±0.6)	-6.7
Afa	5.0	299.4	-27.4 (±1.2)	-15.1 (±0.4)	-6.9
	8.5	250.6	-22.9 (±2.9)	-12.6 (±0.9)	-5.7
Bbr	4.0	343.7	-24.4 (±1.9)	-15.2 (±0.6)	-7.9
	8.0	250.3	-35.6 (±4.4)	-16.4 (±1.4)	-5.8

a ±2 mV
b ±0.1 kcal/mol

Table 21. Previously reported thermodynamic parameters for blue copper proteins at pH 7

	E_m (mV vs. NHE)[a]	$\Delta S°'$ (eu)	$\Delta H°'$ (kcal/mol)	$\Delta G°'$ (kcal/mol)	Ref.
Pae azurin	308	-31.7±1.2	-16.6±0.4	-7.10±0.05	5
Ade azurin	276	-23.2±1.2	-13.3±0.4	-6.4±0.05	50
Plastocyanin[b]	360	-18.0±1.2	-13.7±0.4	-8.3±0.05	5
Stellacyanin[c]	191	-19.8±1.2	-10.3±0.4	-4.4±0.05	5

a At 25°C.
b From *Phaseolus vulgaris.*
c From *Rhus vernicifera.*

ligands tend to shield the effect of the charged complex on the solvent. Metalloproteins in which the metal center is buried below the surface of the protein represent an extreme example of shielding the metal from the water; thus, entropies of reduction for metalloproteins are found to be essentially independent of overall charge,[5,50,75,76] and instead reflect changes in protein conformation and solvent structure on reduction.

With the exception of Bbr azurin at pH 8, the $\Delta S°$ terms for the four azurins are all between -23 and -29 eu. When the data obtained for Pae and Ade azurins are compared with previously reported entropies of reduction at pH 7, it is apparent that $\Delta S°$ is essentially independent of pH. The pH dependences of the Pae and Ade potentials (Figures 11 and 12) suggest that reduction of either protein at pH 7 will occur with uptake of a proton, while reduction at high or low pH will not. Binding of a proton should contribute a negative component to the $\Delta S°$ term, resulting in a more negative $\Delta S°$ at neutral pH than at low or high pH. Since such an effect was not observed for Pae or Ade azurin in this study, other effects must be dominant in determining the entropies of reduction.

In Bbr azurin, $\Delta S°$ decreases substantially when the pH is increased from 4.0 to 8.0. This result implies that a significant reorganization of the protein structure and/or the solvent occurs on reduction at high pH. Of the five azurins for which the pH dependence of the redox potential was determined, Bbr exhibits the largest change in potential with pH. The thermodynamic results indicate that the entropic term is clearly the dominant contributor to the observed pH dependence. It would be of interest to determine the self-exchange rate of Bbr azurin at low and high pH, to see if the rates reflect the implied reorganization of Bbr azurin on reduction at high pH.

REFERENCES

1. Adman, E. T. In "Topics in Molecular and Structural Biology"; Harrison, P., Ed.; VCH Verlagsgesellschaft: Weinheim, BRD, 1984; Vol. 1, Chapter 1.

2. Farver, O.; Pecht, I. In "Copper Proteins and Copper Enzymes"; Lontie, R., Ed.; CRC Press, Inc.: Boca Raton, Florida, 1984; Vol. I, Chapter 7.

3. Adman, E. T.; Turley, S.; Bramson, R.; Petratos, K.; Banner, D.; Tsernoglou, D.; Beppu, T.; Watanabe, B. *J. Biol. Chem.* **1989,** *264,* 87-99.

4. Tobari, J.; Harada, Y. *Biochem. Biophys. Res. Comm.* **1981,** *101,* 502-508.

5. Taniguchi, V. T.; Sailasuta-Scott, N.; Anson, F. C.; Gray, H. B. *Pure Appl. Chem.* **1980,** *52,* 2275-2281.

6. Ambler, R. P. In "Recent Developments in the Chemical Study of Protein Structures"; Previero, A. Pechere, J. F.; Coletti-Previero, M. A., Eds.; Inserm: Paris, 1971; pp. 289-305.

7. Omura, T. *J. Biochem.* **1961,** *50,* 394.

8. Ingledew, W. J.; Cobley, J. C. *Biochim. Biophys. Acta* **1980,** *590,* 14.

9. (a) Cobley, J. G.; Haddock, B. A. *FEBS Lett.* **1975,** *60,* 29; (b) Cox, J. D.; Boxer, D. H. *Biochem. J.* **1978,** *174,* 497.

10. Colman, P. M.; Freeman, H. C.; Guss, J. M.; Murata, M.; Norris, V. A.; Ramshaw, J. A. M.; Benkatappa, M. P.; Vickery, L.E. *J. Mol. Biol.* **1977,** *112,* 649.

11. Murata, M.; Begg, G. S.; Lambrou, F.; Leslie, B.; Simpson, R. J.; Freeman, H. C.; Morgan, F. J. *Proc. Natl. Acad. Sci. U.S.A.* **1982,** *79,* 6434.

12. Kakutani, T.; Watanabe, H.; Arima, K.; Beppu, T. *J. Biochem.* **1981,** *89,* 463-472.

13. Lehninger, A. L. "Bioenergetics"; Benjamin: Menlo Park, CA, 1971; p. 84.

14. Norris, G. E.; Anderson, B. F.; Baker, E. N. *J. Mol. Biol.* **1983,** *165,* 501-521.

15. Norris, G. E.; Anderson, B. F.; Baker, E. N. *J. Am. Chem. Soc.* **1986,** *108,* 2784-2785.

16. Baker, E. N. *J. Mol. Biol.* **1988,** *203,* 1071-1095.

17. van Rijn, J.; Driessen, W. L.; Reedijk, J.; Lehn, J.-M. *Inorg. Chem.* **1984,** *23,* 3584-3588.

18. Agnus, Y.; Louis, R.; Weiss, R. *J. Am. Chem. Soc.* **1979,** *101,* 3381-3384.

19. Gazo, J.; Bersuker, I. B.; Garaj, J.; Kabesova, M.; Kohout, J.; Lanfelderova, H.; Melnik, M.; Serator, M.; Valach, F. *Coord. Chem. Rev.* **1976,** *19,* 253-297.

20. Ugurbil, K.; Norton, R. S.; Allerhand, A.; Bersohn, R. *Biochemistry* **1977,** *16,* 886-894.

21. Guss, J. M.; Harrowell, P. R.; Murata, M.; Norris, V. A.; Freeman, H. C. *J. Mol. Biol.* **1986,** *192,* 361-375.

22. Groeneveld, C. M.; Canters, G. W. *J. Biol. Chem.* **1988,** *263,* 167-173.

23. Peisach, J.; Levine, W. G.; Blumberg, W. E. *J. Biol. Chem.* **1967,** *242,* 2847.

24. Bergman, C.; Grandvik, E.; Nyman, P. O.; Strid, L. *Biochem. Biophys. Res. Commun.* **1977,** *77,* 1052.

26. (a) Brill, E. *Mol. Biol. Biochem. Biophys.* **1977,** *26,* 40; (b) Malmstrom, B.; Vanngard, M. *J. Mol. Biol.* **1960,** *2,* 118.

27. Gray, H. B.; Malmstrom, B. G. *Comments Inorg. Chem.* **1983,** *2,* 203-209.

28. Garrett, T. P. J.; Clingeleffer, D. J.; Guss, J. M.; Rogers, S. J.; Greeman, H. C. *J. Biol. Chem.* **1984,** *259,* 2822-2825.

29. Groeneveld, C. M.; Ouwerling, M. C.; Erkelens, C.; Canters, G. W. *J. Mol. Biol.* **1988,** *200,* 189-199.

30. Groeneveld, C. M.; van Rijn, J.; Reedijk, J.; Canters, G. W. *J. Am. Chem. Soc.* **1988,** *110,* 4893-4900.

31. Mino, Y.; Loehr, T. M.; Wada, K.; Matsubara, H.; Sanders-Loehr, J. *Biochemistry* **1987,** *26,* 8059-8065.

32. (a) Szabo, A. G.; Stepanik, T. M.; Wayner, D. M.; Young, N. M.*PNAS* **1968,** *58,* 498; (b) Williams, R. J. P. *J. Mol. Catal.* **1985,** *30,* 1.

33. Bacteria will be designated by the first letter of the genus name followed by the first two letters of the species name; thus, *Pseudomonas aeruginosa* becomes Pae, etc.

34. Adman, E. T.; Jensen, L. H. *Isr. J. Chem.* **1981,** *21,* 8-12.

35. Adman, E. T.; Stenkamp, R. E.; Sieker, L. C.; Jensen, L. H. *J. Mol. Biol.* **1978,** *123,* 35-47.

36. Norris, G. E.; Anderson, B. F.; Baker, E. N.; Rumball, S. V. *J. Mol. Biol.* **1979,** *135,* 309-312.

37. Korszun, Z. R. *J. Mol. Biol.* **1987,** *196,* 413-419.

38. For example, see: Armstrong, F. A.; Cox, P. A.; Hill, H. A. O.; Lowe, V. J.; Oliver, B. N. *J. Electroanal. Chem.* **1987,** *217,* 331-366; Eddowes, M. J.; Hill, H. A. O. *Biosci. Reports* **1981,** *1,* 521-532.

39. Dutton, P. L. *Meth. Enzymol.* **1978,** *54,* 411-433.

40. In this report, the convention (Ref. 41) of using E_{mx} to represent redox potential values measured under other than standard conditions will be used, where m indicates midpoint and x is the pH.

41. Clark, W. M. "Oxidation-Reduction Potentials of Organic Systems"; Waverly Press: Baltimore, 1960.

42. Armstrong, F. A.; Cox, P. A.; Hill, H. A. O.; Lowe, V. J.; Oliver, B. N. *J. Electrochem. Soc.* **1959,** *106,* 616.

43. Yee, E. L.; Cave, R. J.; Guyer, K. J.; Tyma, P. D.; Weaver, M. J *J. Am. Chem. Soc.* **1979,** *101,* 1131-1137.

44. (a) Hanania, G. I. H.; Irvine, D. H.; Eaton, W. A.; George, P. *J. Phys Chem.* **1967,** *71,* 2022; (b) Latimer, W. M. In "Oxidation Potentials", 2nd ed.; Prentice-Hall: New York, 1952; p. 30; (c) Latimer, W. M.; Pitzer, K. S.; Smith, W. V. *J. Am. Chem. Soc.* **1938,** *60,* 1831-1833.

45. Iwasaki, H.; Shidara, S.; Suzuki, H.; Mori, T. *J. Biochem.* **1963,** *53,* 299-303.

46. Ambler, R. P. *Biochem. J.* **1973,** *135,* 751-758.

47. Rosen, P.; Pecht, I. *Biochemistry* **1976,** *15,* 775-786.

48. Schilt, A. A.; Taylor, R. C. *J. Inorg. Nucl. Chem.* **1959,** *9,* 211.

49. Kirschner, S. *Inorg. Synth.* **1957,** *5,* 186-190.

50. Ellis, W. R., Ph.D. dissertation, California Institute of Technology, Pasadena, California, 1986.

51. Heineman, W. R.; Meckstroth, M. L.; Norris, B. J.; Su, C.-H. *J. Electroanal. Chem.* **1979,** *104,* 577.

52. Petrich, J. W.; Longworth, J. W.; Flemin, G. R. *Biochemistry* **1987,** *26,* 2711-2722.

53. Groeneveld, C. M.; Aasa, R.; Reinhammar, B.; Canters, G. W. *J. Inorg. Biochem.* **1987,***31,* 143-154.

54. Corin, A. F.; Bersohn, R.; Cole, P. E. *Biochemistry* **1983,** *22,* 2032-2038.

55. Rosen, P.; Segal, M.; Pecht, I. *Eur. J. Biochem.* **1981,** *120,* 339-344.

56. Wherland, S.; Pecht, I. *Biochemistry* **1978,** *17,* 2585-2591.

57. Groeneveld, C. M.; Feiters, M. C.; Hasnain, S. S.; van Rijn, J.; Reedijk, J.; Canters, G. W. *Biochim. Biopys. Acta* **1986,** *873,* 214-227.

58. Ainscough, E. W.; Bingham, A. G.; Brodie, A. M.; Ellis, W. R.; Gray, H. B.; Loehr, T. M.; Plowman, J. E.; Norris, G. E.; Baker, E. N. *Biochemistry* **1987,** *26,* 71-82.

59. Collman, P. M.; Freeman, H. C.; Guss, J. M.; Murata, M.; Norris, V. A.; Ramshaw, J. A. M.; Venkatappa, M. P. *Nature* **1978,** *272,* 319.

60. Frank, P.; Licht, A.; Tullius, T. D.; Hodgson, K. O.; Pecht, I. *J. Biol. Chem.* **1985,** *260,* 5518-5525.

61. Ugurbil, K.; Bersohn, R. *Biochemistry* **1977,** *16,* 3016-3023.

62. Mitra, S.; Bersohn, R. *PNAS* **1982,** *79,* 6807-6811.

63. Schulz, G. E.; Schirmer, R. H. In "Principles of Protein Structure"; Cantor, C. R., Ed.; Springer-Verlag: New York, 1978.

64. Hill, H. A. O.; Smith, B. E. *J. Inorg. Biochem.* **1979,** *11,* 79-93.

65. Adman, E. T.; Canters, G. W.; Hill, H. A. O.; Kitchen, N. A. *Inorg. Chim. Acta.* **1983,** *79,* 127-128.

66. Canters, G. W.; Hill, H. A. O.; Kitchen, N. A.; Adman, E. T. *Eur. J. Biochem.* **1984,** *138,* 141-152.

67. Adman, E. T.; Canters, G. W.; Hill, H. A. O.; Kitchen, N. A. *FEBS Lett.* **1982,** *143,* 287-292.

68. Feiters, M. C.; Hasnain, S. S.; Groeneveld, Cm M.; Canters, G. W.; van Rijn, J.; Reedijk, J.; Dahlin, S.; Reinhammar, B. *J. Phys., Colloq.* **1986,** *2,* C8/1173-C8/1176.

69. Wilson, M. T.; Greenwood, C.; Brunori, M.; Antonini, E. *Biochem. J.* **1975,** *145,* 449-457.

71. Silvestrini, M. C.; Brunori, M.; Wilson, T.; Darley-Usmar, V. *J. Inorg. Biochem.* **1981,** *14,* 327-338.

72. Groeneveld, C. M.; Canters, G. W. *Eur. J. Biochem.* **1985,** *153,* 559-564.

73. Ugurbil, K.; Mitra, S. *Proc. Natl. Acad. Sci. USA* ***1985***, *82,* 2039-2043.

74. Groeneveld, C. M.; Dahlin, S.; Reinhammar, B.; Canters, G. W. *J. Am. Chem. Soc.* **1987,** *109,* 3247-3250.

75. Taniguchi, V. T.; Malmstrom, B. G.; Anson, F. C.; Gray, H. B. *Proc. Natl. Acad. Sci. U.S.A.* **1982,** *79,* 3387.

76. Crutchley, R. J.; Ellis, W. R.; Gray, H. B. *J. Am. Chem. Soc.* **1985,** *107,* 5002.

CHAPTER 3

SPECTROELECTROCHEMISTRY OF CU/ZN SUPEROXIDE DISMUTASE

INTRODUCTION

The superoxide radical is generated in biological systems as a by-product of oxidative metabolism. The toxicity of superoxide and the utility of a protective mechanism against superoxide in the cell have been topics of considerable controversy.[1,2] It appears, however, that certain metalloproteins are particularly suited to catalyze the dismutation of superoxide, according to Equation 1:

$$2O_2^- + 2H^+ \rightarrow O_2 + H_2O_2 \qquad (1)$$

These enzymes, known as superoxide dismutases, utilize manganese, iron, or copper and zinc in the catalytic role.

In bovine erythrocytes, superoxide dismutase (SOD) is a dimeric enzyme of molecular weight 31,200 Da, containing one copper and one zinc per monomer. The metal binding sites, shown in Figure 1, share a common ligand, a deprotonated imidazole ring from histidine 61.[3-5] In addition to the bridging histidine, three other histidine side chains and an axial water molecule are coordinated to copper, forming an approximately square pyramidal ligand geometry. The zinc ion is bound by an aspartic acid oxygen, two histidine side chains, and the His 61 imidazolate in a distorted tetrahedral arrangement.

An x-ray crystal structure of bovine Cu/Zn SOD has been reported at 2 Å resolution.[3,6] The structure of the protein backbone derived from the coordinates is shown in Figure 2. The metal binding site in each monomer is located at the bottom of a channel approximately 12 Å deep. Several charged residues on the surface of the protein and in the active site channel appear to be important for directing the superoxide ion toward the active site.[7,8] Dismutation occurs at the copper ion, which is accessible to solvent; zinc is shielded from solvent by copper and the copper ligands, and appears to

Figure 1. The metal-binding sites of Cu/Zn SOD. The geometry about copper is approximately square pyramidal, while the zinc ligands form a distorted tetrahedral arrangement.

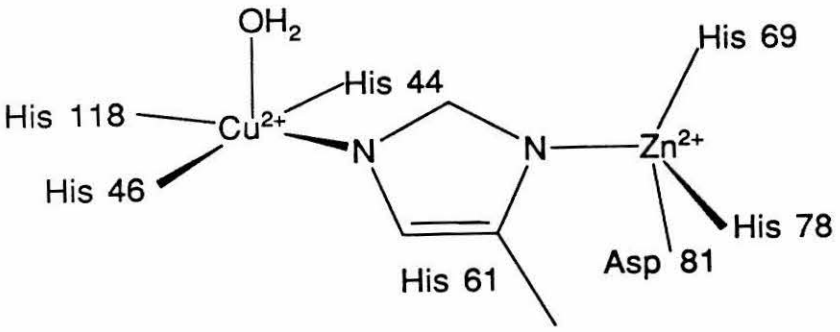
OH2
His 69
His 44
His 118
Cu2+
N
N
Zn2+
His 46
His 78
Asp 81
His 61

Figure 2. The structure of bovine erythrocyte SOD, as described by the crystal structure coordinates.[3,6] In the lower left corner, the main chain of one monomer is shown in blue. The monomer is oriented with the active site channel in view; ligands to the copper are shown in green, zinc ligands in red, and the bridging histidine imidazolate in yellow. The extensive β-sheet structure is evident in the view of the second monomer (white) in the upper right corner.

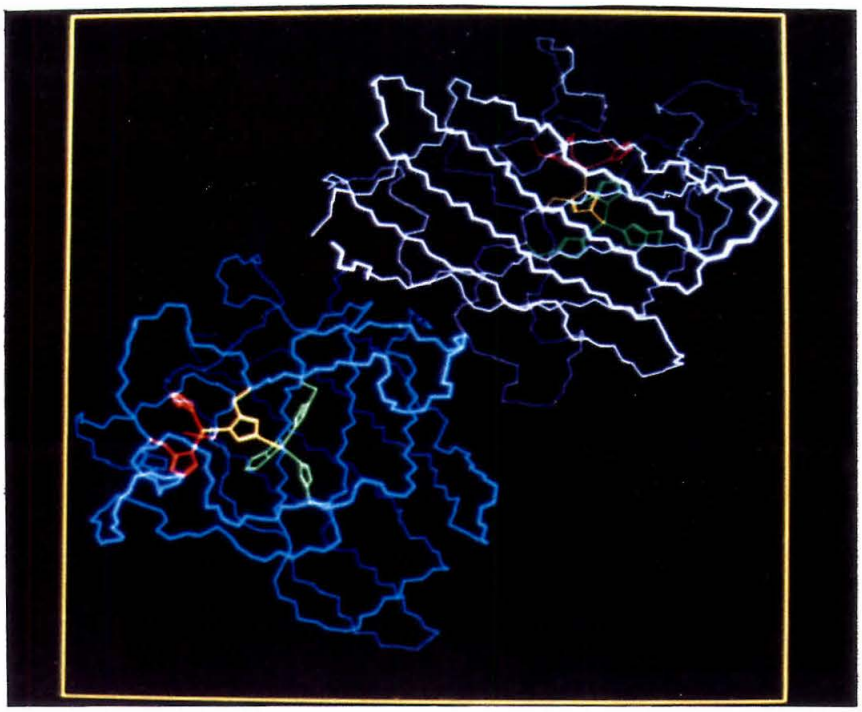

play a primarily structural role.[9] The copper ions in the two peptide chains are separated by about 34 Å,[6] and are thought to function independently rather than in a cooperative fashion.

A proposed mechanism for the dismutation of superoxide to form H_2O_2 and O_2 is shown schematically in Scheme 1.[6,10] Superoxide binds to copper(II) by

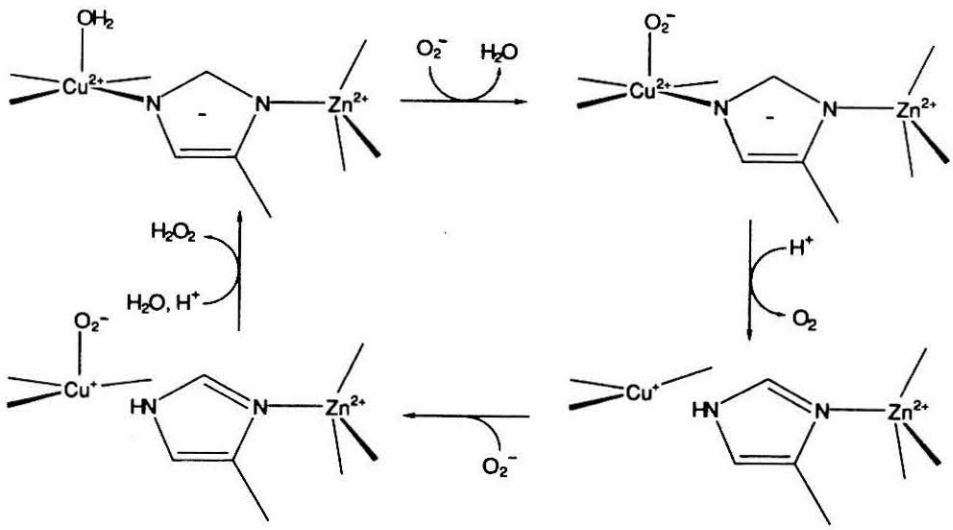

Scheme 1

displacing the axial water molecule. Copper is then reduced by the bound superoxide, which leaves as O_2. On reduction of the copper, His 61 is displaced and protonated, breaking the Cu-Zn bridge.[11-14] A second O_2^- ion then binds and is reduced by copper to form H_2O_2, and the copper-His 61 bond is restored.

An alternative mechanism has recently been proposed, in which superoxide binds to copper(II), but does not reduce it. This intermediate complex is stabilized by an arginine side chain (Arg 141) in the active site channel, which forms a hydrogen bond to the bound superoxide. A second superoxide ion then reduces the copper to Cu(I), and leaves as O_2. Next, Arg 141 transfers a proton to the bound O_2^-, forming HO_2^- or H_2O_2. This mechanism is based primarily on theoretical studies.[15,16]

Both proposed mechanisms for superoxide dismutation involve cycling the copper between reduced and oxidized states. Thus, the redox potential of copper is relevant to an understanding of the enzymatic mechanism. The potential has previously been reported to be in the range of 280 to 420 mV vs NHE.[11,12] A more accurate determination of the redox potential of SOD was undertaken, using the technique of visible spectroelectrochemistry.

In addition, the temperature dependence of the SOD potential was measured, in order to determine the enthalpy and entropy of reduction.[17] Evaluation of these thermodynamic parameters can provide insight into the factors which control the redox potential and the redox activity of the protein. Qualitative observations indicate that SOD exchanges electrons very slowly with redox reagents such as ascorbate and $Fe(CN)_6^{4-/3-}$. In contrast, the reaction of SOD with superoxide occurs extremely rapidly, with a rate constant near the diffusion limit.[18] Knowledge of the enthalpy and entropy of reduction may contribute to an understanding of the reorganization of the copper site on reduction or other factors which cause SOD to be relatively redox-inactive.

EXPERIMENTAL

Materials

Bovine erythrocyte superoxide dismutase was obtained from Diagnostic Data, Inc., Mountain View, California, through Professor J. S. Valentine of the University of California at Los Angeles. The protein did not require further purification.

$[Ru(NH_3)_5(py)]Cl_3$, $[Co(phen)_3]Cl_3$, and Na[Co(edta)] were prepared as described in Chapter 2. Cacodylic acid was recrystallized from water. (Note: cacodylic acid is extremely carcinogenic.) All other materials were purified as described in Chapter 2, or used as supplied.

Methods and Instrumentation

Long-path spectroelectrochemical measurements were performed using 2-cm optical path length cells, prepared by minor modifications of a previously reported design.[19] The working electrode was a piece of gold foil which lines three walls of the sample compartment; the foil is connected by conducting epoxy to a gold wire, which acts as the external contact. The dimensions of the working electrode compartment were altered as follows: the height was increased to 16.0 mm, to avoid clipping the spectrophotometer beam, and the width was narrowed to 7.2 mm, to reduce the sample volume required. Potentials were applied using a Princeton Applied Research polarographic analyzer (Model 174A) and measured with a microvolt digital multimeter (Keithley 177). The reference electrode was a miniature SCE (Sargent-Welch), and the counter electrode was a platinum wire. Sample solutions were stirred during electrochemical equilibration via a pneumatic stirrer contained in the shroud holder, which was mounted in the spectrophotometer sample compartment. Sample temperature was monitored during each experiment by a Fluke digital thermometer (2175A) via a microthermocouple (Omega Engineering) placed inside the wall of the sample

compartment. The digital thermometer readout was calibrated in a separate experiment by measuring the actual temperature of the solution in the cell using a second thermocouple probe.

The spectroelectrochemical runs were performed under anaerobic conditions, in order to avoid producing hydrogen peroxide during the experiments. H_2O_2 has been shown to inactivate Cu/Zn SOD.[18,20] Samples were rigorously degassed and transferred to an inert atmosphere (Ar) box (Vacuum Atmospheres), where they were loaded into the cell and mounted in a gas-tight stainless steel shroud. The shroud was then removed from the glove box and placed in the spectrophotometer for the electrochemical experiment. The shroud and spectrophotometer mount have been described previously.[19]

Sample solutions were prepared to give a three-fold excess of ferricyanide over SOD copper, with a total ΔA_{680} of 0.10 - 0.20 AU. Typical concentrations were [SOD] = 0.32 mM and $[K_3Fe(CN)_6]$ = 1.9 mM. The redox potential at each temperature was determined by varying the potential applied across the cell and allowing the mediator and protein to come to redox equilibrium at each potential. The approach to equilibrium and the ratio of oxidized to reduced SOD at each applied potential were determined by monitoring the absorbance at 680 nm. Data points were fit to the Nernst equation to obtain the redox potential, as described in Chapter 2. At least 5 points were obtained for each plot, in addition to the fully oxidized and fully reduced absorbance readings.

Enclosing the sample cell and reference electrode compartment in the shroud to maintain anaerobic conditions results in partial thermostating of the SCE. Thus, the temperature of the SCE at each cell temperature was determined in control experiments, and the observed SOD potentials were corrected for the variation in SCE potential with temperature before the thermodynamics calculations were performed.

RESULTS AND DISCUSSION

The results of a typical experiment are shown in Figure 3. At each applied potential(E_{app}), the approach to electrochemical equilibrium was monitored by observing the absorbance at 680 nm; at that wavelength, the oxidized form of SOD absorbs, but the reduced form does not. The ratio of the concentrations of oxidized and reduced SOD was plotted according to the Nernst equation (Equation 2), to obtain

$$E_{app} = E^{\circ} - \left(\frac{RT}{nF}\right) \ln \frac{[red]}{[ox]} \qquad (2)$$

Figure 4. A least squares analysis of the data yields $E^{\circ\prime}$ = 403 mV vs. NHE (pH 7.0, 25°C, μ = 0.10M); the error is estimated to be ±5mV. This potential is at the high end of the 280 to 420 mV range of previously reported values for $E^{\circ\prime}$.[11,12]

The mediator used in these experiments was potassium ferricyanide. Previous investigators have reported that the ferricyanide ion binds to SOD near the active site;[12,21] thus, the possibility of perturbation of the SOD redox potential by ferricyanide must be considered. Differential scanning calorimetry studies show that ferricyanide decreases the melting temperature of SOD, indicating that the stability of the enzyme is affected.[21] On the basis of coulometric titrations, Lawrence and Sawyer[12] suggested that ferricyanide binds to one copper ion per protein dimer, causing the copper to be nontitratable. However, the protein used in that study was heterogeneous, and exhibited anomalous behavior during coulometric titration with methylviologen as well as with ferricyanide. Other observations indicate that the perturbation of the copper redox potential by ferricyanide is minimal. The active site channel is ~4Å wide;[3,6] thus, $Fe(CN)_6^{3-}$ should not be able to approach the copper ion. In this study, no change in the visible spectrum of the protein occurred which could be attributed to perturbation of the copper site by ferricyanide, either on addition of ferricyanide to the

Figure 3. Overlay spectra obtained in the determination of the redox potential of SOD at pH 7, 25°C. The applied potentials are relative to SCE. The feature near 640 nm was apparent in the baseline spectrum.

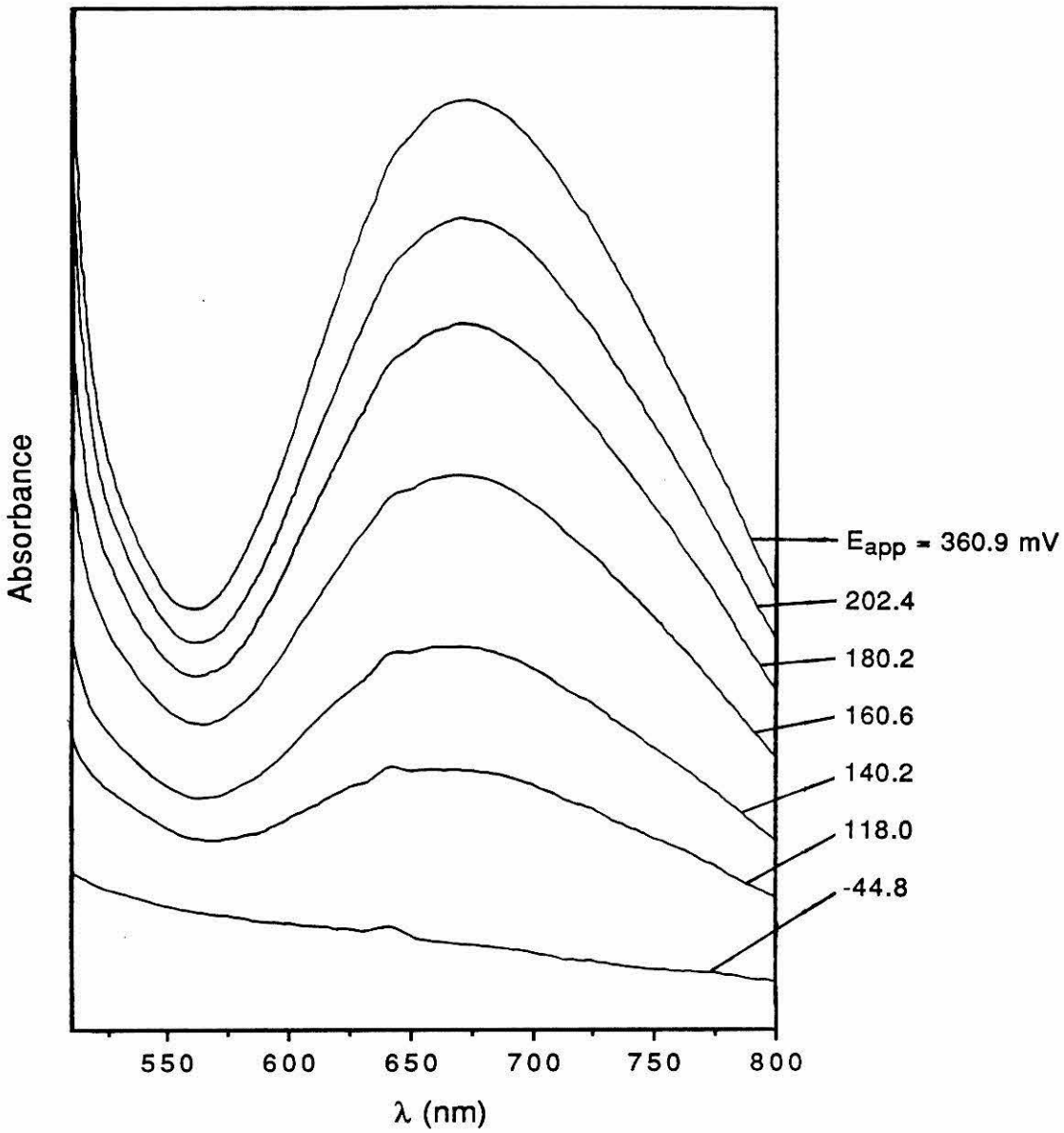
Absorbance
550
600
650
700
750
800
λ (nm)
E_{app} = 360.9 mV
202.4
180.2
160.6
140.2
118.0
-44.8

Figure 4. Nernst plot of the data in Figure 3. A value of $E^{o'}$ = 159 mV vs SCE was obtained from a least squares fit of the data.

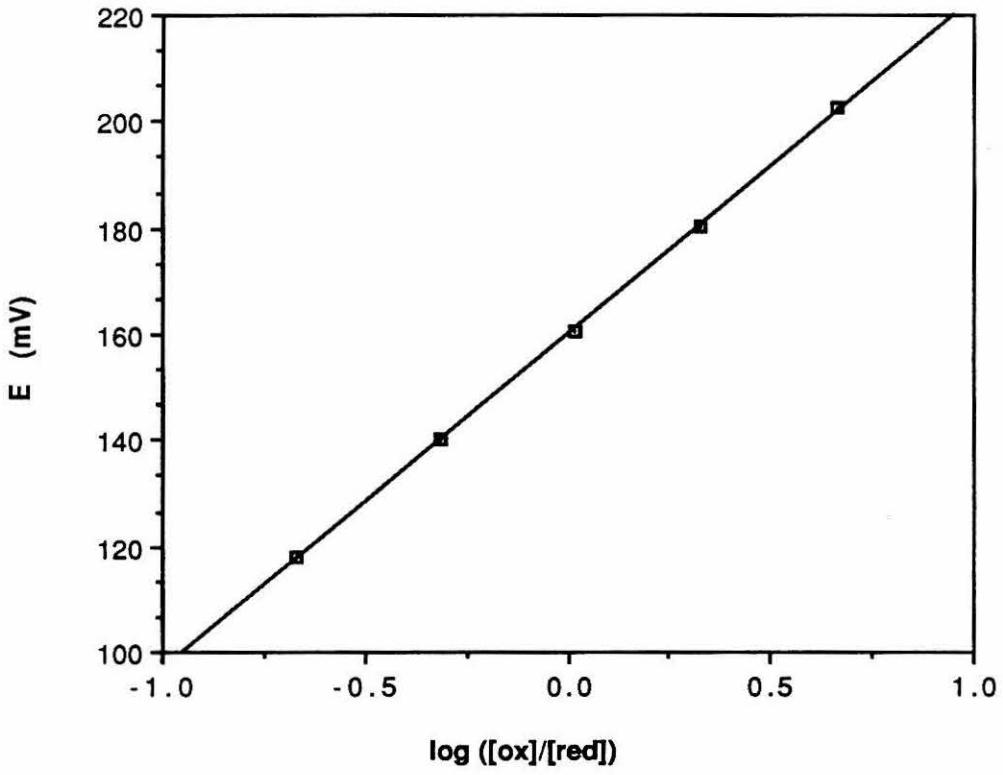
220
200
180
160
140
120
100
E (mV)
-1.0
-0.5
0.0
0.5
1.0
log ([ox]/[red])

solution or during the electrochemical experiments.

Several attempts were made to determine the SOD potential using mediators other than ferricyanide. A wide variety of mediators and combinations of mediators were tried, but each one failed to meet one or more criteria as a mediator, in either the reduced or the oxidized state. These criteria include (a) the ability to exchange electrons readily with the protein, (b) stability over the temperature range desired, and (c) lack of substantial absorbance at the wavelength used to monitor the redox state of the protein. Mediators such as $[Ru(NH_3)_6]Cl_3$, $[(Ru(NH_3)_5(py)]Cl_3$ (py = pyridine), and $[Co(phen)_3]Cl_3$ (phen = phenanthroline) did not meet the first criterion; establishing equilibrium between the oxidized and reduced forms of the protein at each applied potential required more than 4 hours, making a complete spectroelectrochemical experiment infeasible in terms of the stability of the protein and mediators over the temperature range desired. Other mediators were unsuitable due to significant absorbance at 680 nm in one or both redox states. Since the copper(II) chromophore of SOD absorbs only weakly[22] (ε_{680} = 155$M^{-1}cm^{-1}$), a mediator which absorbs even slightly at that wavelength can interfere with the determination of the SOD potential.

Although an accurate measurement of the SOD potential in the absence of ferricyanide was not possible using visible spectroelectrochemistry, two observations indicate that ferricyanide does not cause a significant perturbation of the potential. Qualitative redox kinetics experiments were performed, with SOD in the oxidized state and $Ru(NH_3)_6^{2+}$ (E° = 60mV[23]) and $Ru(NH_3)_5(py)^{2+}$ (E° = 260mV[23]) as reductants. SOD was completely reduced by both complexes, and reduction by $Ru(NH_3)_6^{2+}$ was faster than by $Ru(NH_3)_5(py)^{2+}$. According to the Nernst equation (Equation 2), this result places the SOD potential at ≥350mV. Reduction of SOD by $Fe(CN)_6^{4-}$ occurred more rapidly than reduction by either ruthenium complex, but the protein was not

reduced completely, indicating that an equilibrium between reduced and oxidized forms of mediator and protein was produced. In addition, although spectroelectrochemical experiments using $[Ru(NH_3)_6]Cl_3$, $[(Ru(NH_3)_5(py)]Cl_3$, and $[Co(phen)_3]Cl_3$ as mediators equilibrated too slowly to be practical, they did indicate that the SOD potential was in the approximate range of 400 mV vs NHE.

The possibility of phosphate buffer ions binding to the protein and perturbing the potential was also of concern. Phosphate buffer has been reported to bind to and inhibit Cu/Zn SOD.[24,25] The proposed binding site is Arg 141, which is located very near the copper in the active site channel.[3,6] Thus, phosphate binding could conceivably influence the SOD potential. Inhibition of SOD by phosphate has recently been disputed;[26] however, as a precaution, the SOD potential at 25°C was measured with cacodylic acid (dimethylarsenic acid) as buffer. An $E^{\circ\prime}$ of 400 ±5 mV vs NHE was determined, which is within the error of the result in phosphate buffer.

Temperature dependence of the redox potential of SOD

Table 1 lists the results of redox potential measurements at eight temperatures. A fresh protein sample was used for each experiment, due to the long equilibration time required at each applied potential. A plot of the data in Table 1 is shown in Figure 5; from the fit of the data to the line shown, thermodynamic parameters can be extracted, as described in Chapter 2. The results are as follows, calculated for T = 25°C: $\Delta G^{\circ\prime}$ = -9.31 kcal/mol, $\Delta H^{\circ\prime}$ = -21.4 kcal/mol, $\Delta S^{\circ\prime}$ = -40.7 eu; $\Delta S^{\circ\prime}_{rc}$ = -25.1 eu.

The thermodynamic parameters obtained can be interpreted in terms of changes in the copper site which accompany reduction. Substantial reorganization of the copper site is known to occur on reduction, including protonation of the bridging imidazole ligand and breaking of the copper-imidazole bond. In addition, the aquo ligand at copper may be lost on reduction, although the evidence for this change is less conclusive.[27]

Table 1. Temperature dependence of the redox potential of bovine superoxide dismutase

T(°C)	E(mV vs NHE)	n	r^2
0.7	432.5	0.99	0.9955
5.4	423.9	1.05	0.9992
11.4	417.2	1.03	1.0000
17.9	411.5	1.00	0.9991
24.8	404.5	1.07	0.9998
30.7	395.0	1.00	0.9997
31.3	397.6	1.07	1.0000
37.2	390.6	1.15	0.9900

Figure 5. Plot of the temperature dependence of the redox potential of SOD

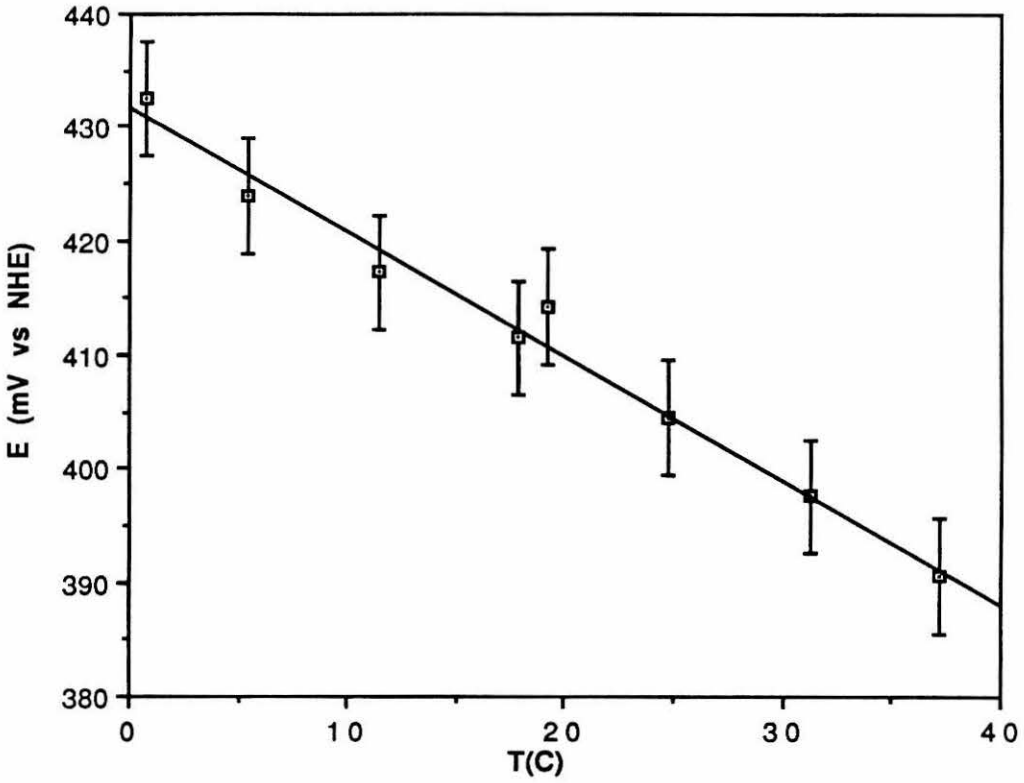
440
430
420
410
400
390
380
E (mV vs NHE)
0
10
20
30
40
T(C)

According to EXAFS results,[27] the three remaining histidine ligands move in slightly (~0.05Å) when the copper is reduced. In Table 2, the thermodynamic parameters obtained for SOD are compared with those for other metalloproteins, and the entropy of reduction of SOD is found to be comparable to that observed in *Pseudomonas aeruginosa* azurin or sperm whale myoglobin. In azurin, no appreciable structural reorganization occurs on reduction of the copper, while in myoglobin, reduction of iron is accompanied by dissociation of an aquo ligand. Binding of a proton on reduction of SOD should contribute a negative term to the entropy of reduction, while breaking the Cu-His 61 and Cu-OH_2 bonds will contribute positive terms. However, previous results indicate that the proton taken up by His 61 comes not from the solution but from another amino acid side chain, perhaps Arg 141.[6,10] Thus, the protonation of His 61 should not correspond to a decrease in entropy. The large negative entropy of reduction observed for SOD may instead reflect greater ordering of water near the active site in the reduced form of the enzyme.

On reduction of copper, the loss of bonding interactions due to the breaking of the Cu-His 61 bond and possibly the Cu-OH_2 bond is expected to result in a positive enthalpy change. Interestingly, however, the enthalpy of reduction for SOD is observed to be very negative (-21.4 kcal/mol). In azurin and plastocyanin, the negative enthalpy of reduction (Table 2) can be partly attributed to a back-bonding interaction between copper(I) and a thioether ligand.[28] Imidazole ligands are not expected to participate significantly in back bonding; thus, the large negative enthalpy of reduction observed for SOD is particularly striking. The negative $\Delta H^{\circ\prime}$ must be due in part to the shortening of the three remaining copper-imidazole bonds and from the protonation of His 61 which accompanies reduction. Also, a contribution to the negative enthalpy change will come from a decrease in electrostatic repulsion between the copper and zinc ions as the charge on the copper decreases from +2 to +1. Although the relative importance of each of

Table 2. Thermodynamic parameters for several metalloproteins at pH 7, 25°C.

	$E^{o\prime}$ (mV vs. NHE)	$\Delta S^{o\prime}$ (eu)	$\Delta S^{o\prime}_{rc}$ (eu)	$\Delta H^{o\prime}$ (kcal/mol)	ΔG^{o} (kcal/mol)	Ref.
Azurin[a]	308	-31.7±1.2	-16.1±1.2	-16.6±0.4	-7.10±0.05	28
Plastocyanin[b]	360	-18.0±1.2	-2.4±1.2	-13.7±0.4	-8.3±0.05	28
Myoglobin[c]	60	-39.2±1.2	-23.6±1.2	-13.0±0.4	-1.36±0.05	19
Cytochrome c[d]	270	-30.5±1.2	-14.9±1.2	-15.3±0.4	-6.23±0.05	28
Superoxide dismutase[e]	403	-40.7±4.4	-25.1±4.4	-21.4±1.4	-9.31±0.1	f

a *Pseudomonas aeruginosa*
b *Phaseolus vulgaris*
c Sperm whale
d Horse heart
e Bovine
f This work

these contributions to the enthalpy of reduction cannot be deduced from these experiments, it is clear that $\Delta H^{\circ\prime}$, rather than $\Delta S^{\circ\prime}$, is the dominant factor in establishing the high redox potential of SOD.

The slow rates of reduction and oxidation of SOD by transition metal complexes can be partially attributed to the reorganization at the copper site which accompanies electron transfer. Another major reason for the slow rate may be that, while superoxide can diffuse into the narrow (~4 Å wide) active site channel, most redox reagents cannot; thus, an electron must be transferred over several angstroms. Negatively charged reagents such as ferricyanide may bind to positively charged residues near the active site channel, but the electron will still need to travel through several angstroms of water in the channel.

Metalloproteins such as cytochrome c (iron(III))[29] and laccase (copper(II))[30] react very rapidly with one superoxide ion, but are then reoxidized by H_2O_2 or O_2 much faster than by O_2^-. In contrast, reduced SOD is rapidly reoxidized by O_2^-, as shown in Scheme 1. According to the proposed mechanism, this specificity of SOD toward the superoxide ion is a crucial aspect of the protein's role as a superoxide dismutase.[31] Thus, the low redox activity of SOD toward most redox reagents may reflect an important functional adaptation of the enzyme. Further study will be required in order to fully understand the mechanisms by which SOD achieves this specificity toward superoxide.

REFERENCES AND NOTES

1. Fee, J. A.; Lees, A. C.; Bloch, P. L.; Neidhardt, F. C. In "Biochemical and Clinical Aspects of Oxygen"; Caughey, W. S., Ed.; Academic Press: New York, 1979; pp. 635-658.

2. Fridovich, I. *Adv. Inorg. Biochem.* **1979,** *1,* 67-90.

3. Tainer, J. A.; Getzoff, E. D.; Beem, K. M.; Richardson, J. S.; Richardson, D. C. *J. Mol. Biol.* **1982,** *160,* 181-217.

4. Gaber, B. P.; Brown, R. D.; Koenig, S. H.; Fee, J. A. *Biochim. Biophys. Acta* **1972,** *271,* 1.

5. Boden, N.; Holmes, M. C.; Knowles, P. F. *Biochem. J.* **1979,** *177,* 303-309.

6. Tainer, J. A.; Getzoff, E. D.; Richardson, J. S.; Richardson, D. C. *Nature* **1983,** *306,* 284-287.

7. Getzoff, E. D.; Tainer, J. A.; Weiner, P. K.; Kollman, P. A.; Richardson, J. S.; Richardson, D. C. *Nature* **1983,** *306,* 287-290.

8. Cudd, A.; Fridovich, I. *J. Biol. Chem.* **1982,** *257,* 11443-11447.

9. Valentine, J. S.; Pantoliano, M. W. In "Metal Ions in Biology"; Spiro, T. G., Ed; Wiley: New York, 1981; Vol. 3, pp. 291-358.

10. Klug, D.; Rabani, J.; Fridovich, I. *J. Biol. Chem.* **1972,** *247,* 4839-4842.

11. Fee, J. A.; DiCorleto, P. E. *Biochemistry* **1973,** *12,* 4893-4899.

12. Lawrence, G. D.; Sawyer, D. T. *Biochemistry* **1979,** *18,* 3045-3050.

13. Bertini, I.; Luchinat, C.; Monnanni, R. *J. Am. Chem. Soc.* **1985,** *107,* 2178-2179.

14. Fee, J. A. In "Metal Ions in Biological Systems"; Sigel, H., Ed.; Marcel Dekker: New York, 1981; Vol. 13, Chapter 8.

15. Osman, R.; Basch, H. *J. Am. Chem. Soc.* **1984,** *106,* 5710-5714.

16. Rosi, M.; Sgamellotti, A.; Tarantelli, F.; Bertini, I.; Luchinat, C. *Inorg. Chem.* **1986,** *25,* 1005-1008.

17. See Chapter 2 for a discussion of the temperature dependence of metalloprotein redox potentials.

18. Rotilio, G.; Bray, R. C.; Fielden, E. M. *Biochim. Biophys. Acta* **1972,** *268,* 605-609.

19. Ellis, W. R., Ph.D. dissertation, California Institute of Technology, Pasadena, California, 1986.

20. Bray, R. C.; Cockle, S. A.; Rielden, E. M.; Roberts, P. B.; Rotilio, G.; Calabrese, L. *Biochem. J.* **1974,** *139,* 43-48.

21. Personal communication from J. A. Roe, University of California, Los Angeles.

22. McCord, J. M.; Fridovich, I. *J. Biol. Chem.* **1969,** *244,* 6049-6055.

23. Matsubara, T.; Ford, P. C. *Inorg. Chem.* **1976,** *15,* 1107.

24. Mota de Freitas, D. M.; Valentine, J. S. *Biochemistry* **1984,** *23,* 2079-2082.

25. Valentine, J. S.; Roe, J. A.; Butler, A.; Mota de Freitas, D. M. In "Biological and Inorganic Copper Chemistry"; Karlin, K. D. and Zubieta, J., Eds.; Adenine Press: New York, 1985; pp. 53-60.

26. Beyer, W. F.; Wang, Y.; Fridovich, I. *Biochemistry* **1986,** *25,* 6084-6088.

27. Blackburn, N. J.; Hasnain, S. S.; Binsted, N.; Diakun, G. P.; Garner, C. D.; Knowles, P. F. *Biochem. J.* **1984,** *219,* 985-990.

28. Taniguchi, V. T.; Sailasuta-Scott, N.; Anson, F. C.; Gray, H. B. *Pure Appl. Chem.* **1980,** *52,* 2275-2281.

29. Koppenol, W. H.; Van Buuren, K. J. H.; Butler, J.; Braams, R. *Biochim. Biophys. Acta.* **1976,** *449,* 157.

30. Farver, O.; Pecht, I. In "Metal Ions in Biology"; Spiro, T. G., Ed.; Wiley-Interscience: New York, 1981; Vol. 3, Chapter 4.

31. (a) Fielden, E. M.; Rotilio, G. In "Copper Proteins and Copper Enzymes"; Lontie, R., Ed.; CRC Press: Boca Raton, Florida, 1984; Vol. 2, Chapter 2; (b) Rigo, A.; Rotilio, G. In"Chemical and Biochemical Aspects of Superoxide and Superoxide Dismutase"; Bannister, J. V.; Hill, H. A. O., Eds.; Elsevier: New York, 1980; p. 56.

CHAPTER 4

RUTHENIUM MODIFICATION OF AZURINS

INTRODUCTION

Electron transfers between metal sites in proteins form the basis of the processes of respiration and photosynthesis. An understanding of the factors which affect the rate at which an electron is transferred through a protein medium is a goal of current theoretical and experimental research. According to theory,[1,2] the effects of a number of factors on the rate constant for electron transfer can be expressed by Equation 1:

$$k_{et} = \nu \ \exp(-\beta(d - d_0)) \ \exp(-\Delta G^*/RT) \qquad (1)$$

Equation 1 is composed of three terms: the nuclear frequency factor (ν), an electronic term ($\exp(-\beta(d-d_0))$, and a free energy term ($\exp(-\Delta G^*/RT)$). The second term indicates that the rate will decrease as the distance, d, between donor and acceptor is increased. The van der Waals contact distance, d_0, is typically taken to be 3 Å. β describes the rate of decrease in electronic coupling with distance, and is expected to vary with the protein medium; for example, intervening aromatic amino acid residues may enhance the coupling between the sites, and thus enhance the electron-transfer rate.[3-5] The third component describes the dependence of the rate constant on the free energy of activation (ΔG^*). ΔG^* can be expressed as

$$\Delta G^* = \frac{(\Delta G^\circ + \lambda)^2}{4\lambda} \qquad (2)$$

where ΔG° and λ represent the free energy of the reaction and the nuclear reorganization energy, respectively. The reorganization energy includes both inner sphere and outer sphere contributions.

Recent experimental studies by several investigators have provided data which are useful in evaluating and refining theoretical predictions. Evaluations of the distance dependence of electron-transfer rates have provided estimates of β, and have shown that

electron transfer proceeds through the protein matrix in a relatively direct path from donor to acceptor, rather than along the protein backbone.[5,6] Investigations of the dependence of the electron-transfer rate on thermodynamic driving force and temperature have established estimates of λ.[6-9] These experiments require a system in which one variable can be systematically varied while the remaining variables are held constant.

One approach which has been used successfully in the study of intramolecular electron transfer is the surface modification of metalloproteins using substitutionally-inert metal complexes.[5-14] Semi-synthetic metalloproteins have been prepared in which a ruthenium ammine complex is bound to a surface histidine residue of a protein, and the rate of electron transfer between the native metal and the ruthenium site is determined. The thermodynamic driving force for electron transfer can be determined by measuring the redox potentials of the two sites, and the electron transfer distance can be obtained from the crystal structure coordinates. This report describes experiments with ruthenium modification of the blue copper protein azurin which are designed to probe both the driving force dependence and the medium dependence of the electron-transfer rate.

The driving force for electron transfer can be modulated by varying the ligand environment of the ruthenium site. In previous work, *Pseudomonas aeruginosa* (Pae) azurin was modified with pentaammine ruthenium (a_5Ru), and the rate of electron transfer from ruthenium to copper was determined;[11,12] the driving force for this reaction is ~270 mV. Replacement of one ammine ligand at ruthenium with a π-acceptor ligand such as pyridine will stabilize Ru(II) relative to Ru(III),[15,16] raising the redox potential of the ruthenium site. Thus, the driving force for electron transfer in Pae azurin can be varied, while the distance and medium between donor and acceptor are held constant.

Pae azurin contains four histidine residues, two of which (His 46 and His 117) are copper ligands.[17,18] Of the other two histidines, His 83 is solvent accessible, while His 35 is shielded from the solvent by surrounding residues. The results of previous work[11,12] in which azurin was modified with $[a_5Ru]^{3+}$ indicate that His 83 is the primary site of ruthenium labeling. The distance for electron transfer from the copper site to His 83 is approximately 12 Å.[17,18]

The second part of this chapter describes the modification of *Alcaligenes denitrificans* (Ade) azurin with pentaammineruthenium. Ade azurin contains the four histidine residues found in Pae azurin, as well as a fifth histidine, His 32.[19-21] Figure 1 shows the backbone of Ade azurin as determined by x-ray crystallography.[19-21] The main chain of the protein is shown in blue, with the copper ligands in pink; non-ligand histidine residues are shown in green. Like His 83, His 32 is located on the surface of the protein and titrates freely; thus, both of these residues should be accessible to the ruthenium reagent. His 35 of Ade azurin is even more rigidly buried in the protein than His 35 of Pae azurin[22] and thus is not expected to label. Both His 83 and His 32 are located about 12 Å from the copper site. A comparison of the intramolecular electron-transfer rates in Ade azurin modified at His 83 with that modified at His 32 will provide information on how β varies with the specific pathway through the protein.

Figure 1. The main chain of Ade azurin, constructed from the crystal structure coordinates.[19-21]

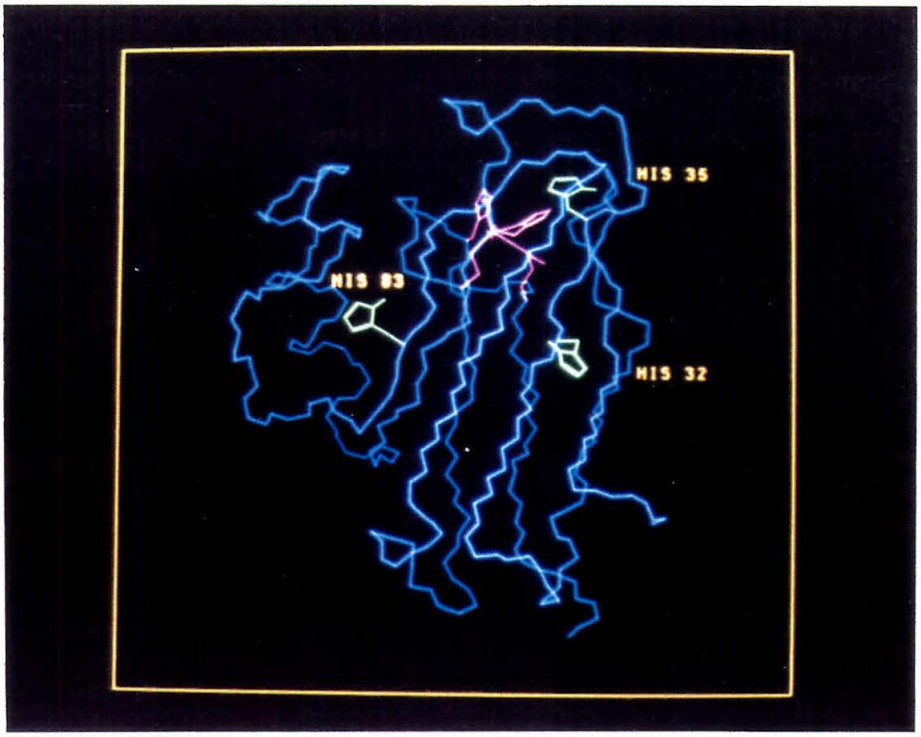
HIS 35
HIS 83
HIS 32

EXPERIMENTAL

Materials

Hexaammineruthenium(III) chloride and pentaammineruthenium(III) chloride were used as supplied by Strem Chemicals. Imidazole (Aldrich) was recrystallized from toluene. All other materials were purified as described in Chapter 2, or used as supplied.

Methods and Instrumentation

Preparation of cell cultures and isolation and purification of Ade azurin were performed as described in Chapter 2. Pae azurin was isolated by the method described in Chapter 2; purification was by standard chromatographic techniques rather than by FPLC. After elution from the CM52 column, the azurin was purified by anion exchange and gel filtration chromatography, as described in Chapter 2.

Electrochemical measurements were performed at a 2 mm gold disk electrode (Bioanalytical Systems, Inc.) using a Princeton Applied Research polarographic analyzer (Model 174A) with a Keithley 177 microvolt digital multimeter. The reference electrode was an SSCE (NaCl); E° = +0.2360 V vs. NHE. Sample concentration was 2.0 mM in a mixed buffer solution of 0.05 M sodium acetate, 0.05 M MES(2[N-Morpholino]ethanesulfonic acid), and 0.10 M Tris-HCl, μ=0.10 M. Cyclic voltammograms were recorded at 1.0 pH unit increments over a pH range of 4.0 to 9.0. Scan rates were varied from 20 to 500 mV/sec.

Analytical isoelectric focusing (IEF) gels (pH 3.5-9.5) were supplied by Pharmacia. Electrophoresis gels were prepared using 7.5% acrylamide (w/w), with 2.6% crosslinker, in ammonium acetate buffer, pH 4.5. Isoelectric focusing and electrophoresis were performed using an LKB 2117 Multiphor with a Model #2197

power supply. Protein isoelectric points were assigned relative to IEF standards provided by Pharmacia.

Concentrations of azurin solutions were determined by measuring the absorbance at the maximum of the blue band, near 625 nm; an ε_{625} value of $5700 M^{-1}cm^{-1}$ was used for both species of azurin.[23]

NMR spectra were recorded on a Bruker AM-500 spectrometer. The sample concentration was 0.5 - 2.0 mM in azurin. NMR samples were prepared by exchanging the protein into D_2O via several cycles of washing in an ultrafiltration cell. The protein was then lyophilized to dryness, dissolved in D_2O, and lyophilized a second time. The sample was redissolved in D_2O, and a small amount of concentrated buffer solution (sodium acetate-d_3 or sodium phosphate-d_2) was added to obtain the desired pH. pH values reported are uncorrected for the deuterium isotope effect.[24] NMR spectra were referenced to DSS (sodium 2,2-dimethyl-2-silapentane-5-sulfonate).

Flash photolysis experiments were performed using an instrument constructed at Caltech.[14c,25] A ~5 μs flash was produced by a flash lamp (Xenon Corp. N851D) fired by a Model 457A micropulser. Sample concentrations were as follows: 10 μM azurin, 70 μM $[Ru(bpy)_3]Cl_2$, 5 mM Na_2(edta). The sample was placed in a cylindrical cell with an optical path length of 15 cm. The change in absorbance was monitored at 625 nm. Data were hand digitized.

$[Ru(NH_3)_5Cl]Cl_2$, *trans*-$[Ru(NH_3)_4(HSO_3)_2]$, *trans*-$[Ru(NH_3)_4(SO_2)Cl]Cl$, and *trans*-$[Ru(NH_3)_4(SO_4)(py)]Cl$ (py = pyridine) were prepared according to literature methods.[26,27] Attempts to purify $[Ru(NH_3)_4(SO_4)(py)]Cl$ by ion-exchange chromatography resulted in very low recovery; the complex appears to decompose on the cationic resin used (SP Sephadex G-25). *trans*-$[Ru(NH_3)_4(py)Cl]Cl_2$ was prepared according to Meyer et al.[27] and recrystallized from 0.01 M HCl.

*Preparation of trans-[Ru(NH$_3$)$_4$(py)(imz)]Cl$_3$ (**1**):*

A solution of 100 mg *trans*-[Ru(NH$_3$)$_4$(SO$_4$)(py)]Cl in 5 mL H$_2$O was deaerated and transferred to ~1 g freshly prepared Zn/Hg amalgam. Reduction was allowed to proceed 30 min with constant Ar bubbling. The reduced ruthenium solution was added to a deaerated solution of 22 mg (1.2 equivalent) imidazole (imz) in 10 mL H$_2$O. Reaction proceeded 6 h with continuous agitation via Ar bubbling. The solution was then exposed to air, oxidized by the dropwise addition of a 1:1 mixture of 2 M HCl and 30% H$_2$O$_2$, and precipitated from solution by the addition of 200 mL acetone. The solid was collected by filtration, dried, and dissolved in 0.1 M HCl. The solution was loaded on a column of SP Sephadex G-25 or Biorad AG50W-X4. Stepwise elution with increasing [HCl] separated the desired product from unreacted [Ru(NH$_3$)$_4$(SO$_4$)(py)]$^+$, which decomposes on the column. Rechromatography followed by recrystallization from 0.1 M HCl produced red crystals of **1**; overall yield, 27%. Anal. Calcd. for C$_8$H$_{21}$Cl$_3$N$_7$Ru·H$_2$O: C, 21.80; H, 5.26; N, 22.25. Found: C, 21.78; H, 5.33; N, 22.31.

Modification of Pae azurin

Reaction of [Ru(NH$_3$)$_4$(SO$_4$)(py)]Cl or [Ru(NH$_3$)$_4$(py)Cl]Cl$_2$ with azurin was performed as described for the reaction with imidazole to yield **1**. Typical reaction conditions were [Az] = 0.10 mM, [Ru] = 5.0 mM in 0.05 M Tris, pH 7.2; T ~25°C; length of reaction, 5 h. Initial optimization of the reaction conditions was performed by removing aliquots of the reaction mixture at time intervals and monitoring the progress of the reaction by isoelectric focusing. All steps following reaction with the ruthenium reagent were performed at 5°C. The excess ruthenium reagent was removed from the protein solution either by repeated washings with buffer in an ultrafiltration cell, or by passing the solution over a column of Sephadex G-25-80. A 15-fold excess per metal ion of Na[Co(edta)] or [Co(phen)$_3$]Cl$_3$ was added, and the solution was stirred 5-10 h to

oxidize the modified protein. Excess oxidant was removed by several cycles of ultrafiltration and dilution by H_2O or buffer.

The modified azurin was separated into components on a cation exchange column (Whatman CM52). Starting buffers were 0.05 M ammonium acetate, pH 4.5, with elution by increasing ionic strength ([NaCl]).

The pentaammineruthenium modification of Pae azurin was also performed, in order to compare the ^{1}H-NMR spectrum of the product with that of a_4Ru(py)-azurin. Preparation was as previously described.[12] The modified products were separated by cation-exchange chromatography as described above for the a_4Ru(py)-azurin modification, with 0.05 M ammonium acetate, pH 4.5, as the starting buffer, and a linear gradient to 0.05 M ammonium acetate with 0.15 M NaCl.

Modification of Ade azurin

9.6 mg $[a_5RuCl]Cl_2$ was dissolved in 27.5 mL of 0.05 M Tris-HCl buffer, pH 7.2, and degassed by several cycles of evacuation and flushing with argon. In a separate flask, 46 mg Ade azurin in 5.4 mL buffer was degassed; the two flasks were then transferred to an inert atmosphere (argon) glove box. The ruthenium solution was added to ~1 g Zn/Hg amalgam, and reduction was allowed to proceed 30 min. The ruthenium solution was then transferred to the azurin solution. The final concentrations in the reaction mixture were thus [azurin] = 10^{-4} M, [Ru] = 10^{-3} M, yielding a Ru(II):azurin ratio of 9, since one equivalent of Ru(II) will be consumed in the initial oxidation of azurin. Reaction was allowed to proceed 45 min at room temperature. The solution was then removed from the glove box and oxidized by the addition of Na[Co(edta)]. The reaction solution was washed several times in an ultrafiltration cell to remove the excess ruthenium reagent. Additional Na[Co(edta)] was then added, and the solution was left at 5°C overnight.

The modified products were separated by FPLC, using a Mono S 10/10 column. The protein was loaded in 0.05 M ammonium acetate buffer, pH 5.2, and eluted with a gradient to 0.12 M NaCl in 192 mL.

RESULTS AND DISCUSSION

Modification of Pae azurin

Synthesis and characterization of trans-[Ru(NH$_3$)$_4$(py)(imz)]Cl$_3$

Prior to the synthesis of trans-Ru(NH$_3$)$_4$(py)-azurin, the preparation of the model complex was necessary in order to gain information concerning the ease of formation of the complex and its relative stability in aqueous solution. Characterization of this complex was essential for the later identification of modified azurin products.

UV-Visible absorption data for the model complex are as follows: λ_{max} = 249 nm ($\varepsilon = 6.4 \times 10^3$ $M^{-1}cm^{-1}$); 311 (3.6×10^3). By analogy to spectroscopic assignments of similar ruthenium(III) ammine complexes, it is likely that the 249 nm band corresponds to an internal transition ($\pi \rightarrow \pi^*$) of the pyridine ligand,[28] while the absorption at 311 nm is due to a imidazole (π^2) to Ru(III) charge transfer transition.[29]

The reduction potential of the model complex was determined in aqueous solution as 317 mV vs NHE. Reduction was quasi-reversible ($\Delta E°$ = 63 mV) at scan rates of 100 mV/sec or less. $E°$ is constant over a pH range of 4.0 - 7.0; at pH 8.0, the complex decomposes in aqueous solution.

Certain observations concerning the synthesis of the model complex are pertinent to the modification of azurin. The reaction of $[a_4Ru(py)(OH_2)]^{2+}$ (a = NH_3) with imidazole proceeds more slowly than the analogous reaction[30,31] of $[a_5Ru(OH_2)]^{2+}$. This problem was anticipated, based on the available kinetic data for ruthenium ammine complexes.[32-34] Apparently, removal of electron density from Ru(II) by back-bonding to pyridine increases the strength of the Ru-OH_2 bond, thereby decreasing the rate of the initial dissociative step.[15,16] Thus, preparation of a_4Ru(py)-modified proteins will require higher reactant concentrations and/or longer reaction times than modification with a_5Ru.

Preparation of a_4Ru(py)-azurin

Modification of azurin with the a_4Ru(py) complex led to several protein products. A typical elution profile for separation of the products by cation exchange chromatography on CM52 resin is shown in Figure 2. Native Pae azurin exhibits a slight tendency toward autoreduction during chromatography; this problem was exacerbated on modification with ruthenium. Autoreduction resulted in loss of resolution of some of the bands as they moved down the column. Addition of ~1 mM Na[Co(edta)] to the elution buffers prevented this problem by keeping the protein in the oxidized state.

Longer retention on the CM52 cation exchange column is expected for ruthenium-labeled azurin, since binding of the ruthenium(III) complex to the protein will increase the overall charge on the protein by 3. Thus, the first band eluted is native azurin, and evidence presented below indicates that bands 2a-2d are singly modified species, while bands 3a-3c are multiply modified. Although all of the modified products were not clearly resolved on the CM52 column, polyacrylamide gel electrophoresis allowed clear separation of a total of seven modified bands. The partial characterization of the individual products is discussed below.

Characterization of Band 2c

Band 2c was obtained in ~10% yield; after repurification on a second CM52 column, an overall yield of ~7% was obtained. The UV-Visible spectrum of Band 2c is shown in Figure 3a. Both the pyridine $\pi \rightarrow \pi^*$ (λ = 249 nm) and the imidazole to ruthenium charge transfer (λ = 311 nm) bands are evident in the spectra of these products, indicating ligation of the a_4Ru(py) complex to the imidazole ring of histidine. The native spectrum was subtracted from the spectrum of the modified protein until a spectrum resembling that of the model imidazole complex (Figure 3b) was obtained; the

Figure 2. An elution profile of the separation of modified Pae azurin on a CM52 column. Buffer A is 0.05 M NH_4OAc; buffer B is 0.05 M NH_4OAc + 0.15 M NaCl.

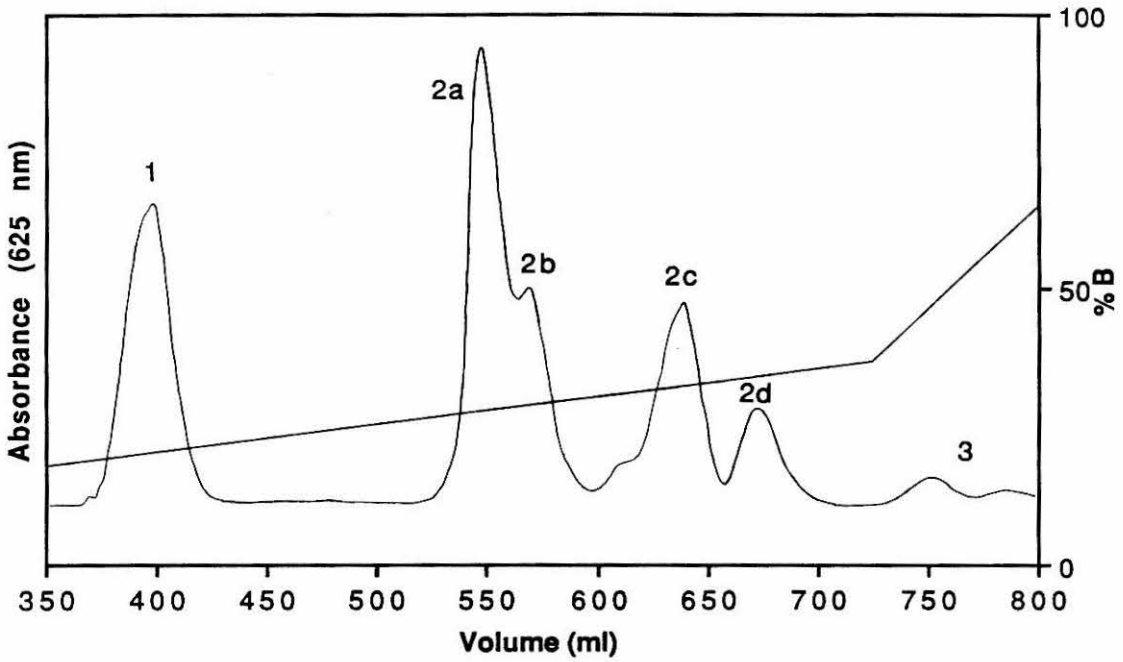
Absorbance (625 nm)
100
50
0
%B
1
2a
2b
2c
2d
3
350
400
450
500
550
600
650
700
750
800
Volume (ml)

Figure 3. UV-Visible spectra of Pae azurin and the model complex

a. Band 2c from the modification of Pae azurin with $a_4Ru(py)$

b. $[a_4Ru(py)(imz)]Cl_3$

c. Difference spectrum (modified azurin - native azurin). See text.

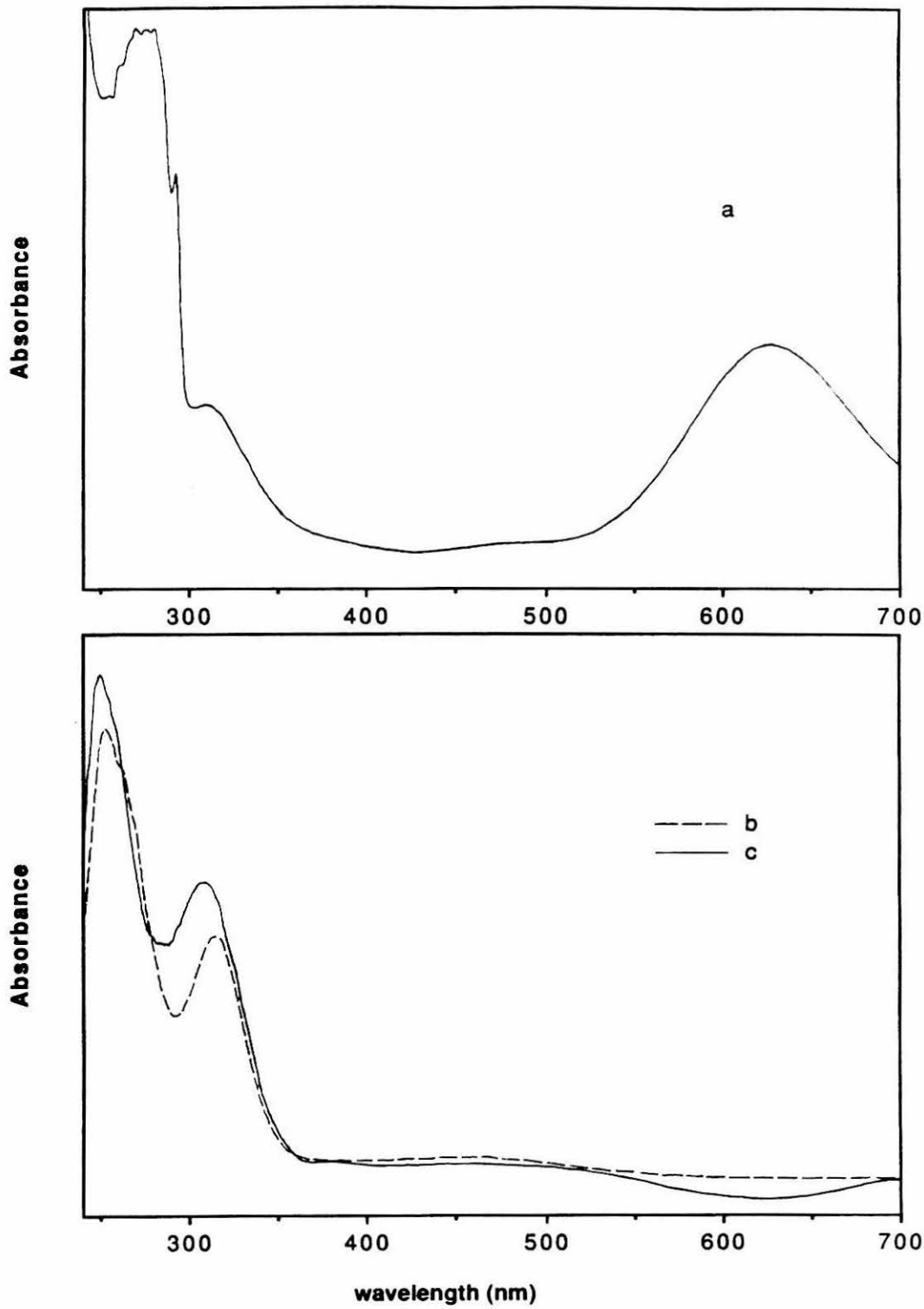
Absorbance
a
300
400
500
600
700
Absorbance
b
c
300
400
500
600
700
wavelength (nm)

result is shown in Figure 3c. The strong similarity between the difference spectrum and the model complex spectrum provides compelling evidence that the protein contains an $[a_4Ru(py)]^{3+}$ label at a histidine imidazole. Using the values of ε_{249} and ε_{311} for the model complex, the concentration of $[a_4Ru(py)(imz)]^{3+}$ to which this difference spectrum corresponds was determined. Similarly, the azurin concentration of the modified sample was determined by the absorbance at 625 nm of the (subtracted) native spectrum. An estimated Ru:azurin ratio of 0.94 was obtained. The native azurin absorption band at 625 nm is due to a sulfur(Cys) to copper charge transfer transition;[35] a decrease in the intensity of this band relative to the 280 nm band is an indication of either denaturation of the protein or autoreduction of the copper site. Thus, the weak negative absorption band at 625 nm in the difference spectrum reflects the Ru:azurin ratio of less than 1, and indicates a small amount of damage to the protein or autoreduction of copper.

In previous work[11,12] in which Pae azurin was modified with pentaammine-ruthenium, His 83 was the major site of modification. Examination of the solvent accessibility of the two non-ligand histidines in Pae azurin by computer graphics also indicates that His 83 will be the primary site of modification. The solvent accessibility of each non-ligand histidine was evaluated by determining the area of the side chain which is accessible to a probe of 1.4 Å radius, based on the x-ray crystal structure of the protein. The surface area of the His 83 side chain was found to be 70.4 $Å^2$, while that of His 35 is zero.

^{1}H-NMR spectra of oxidized native azurin and band 2c were recorded. Resonances due to the C2 and C4 protons of the imidazole ring of His 83 were identified in the native spectrum according to the assignments in the literature;[36] these resonances are labeled in Figure 4a. Pentaammineruthenium azurin was also prepared, for comparison of its NMR spectrum (Figure 4c) with that of the tetraamminepyridine

Figure 4. NMR spectra of native and modified Pae azurins

a. Native azurin

b. Band 2c

c. a_5Ru-(His 83)azurin

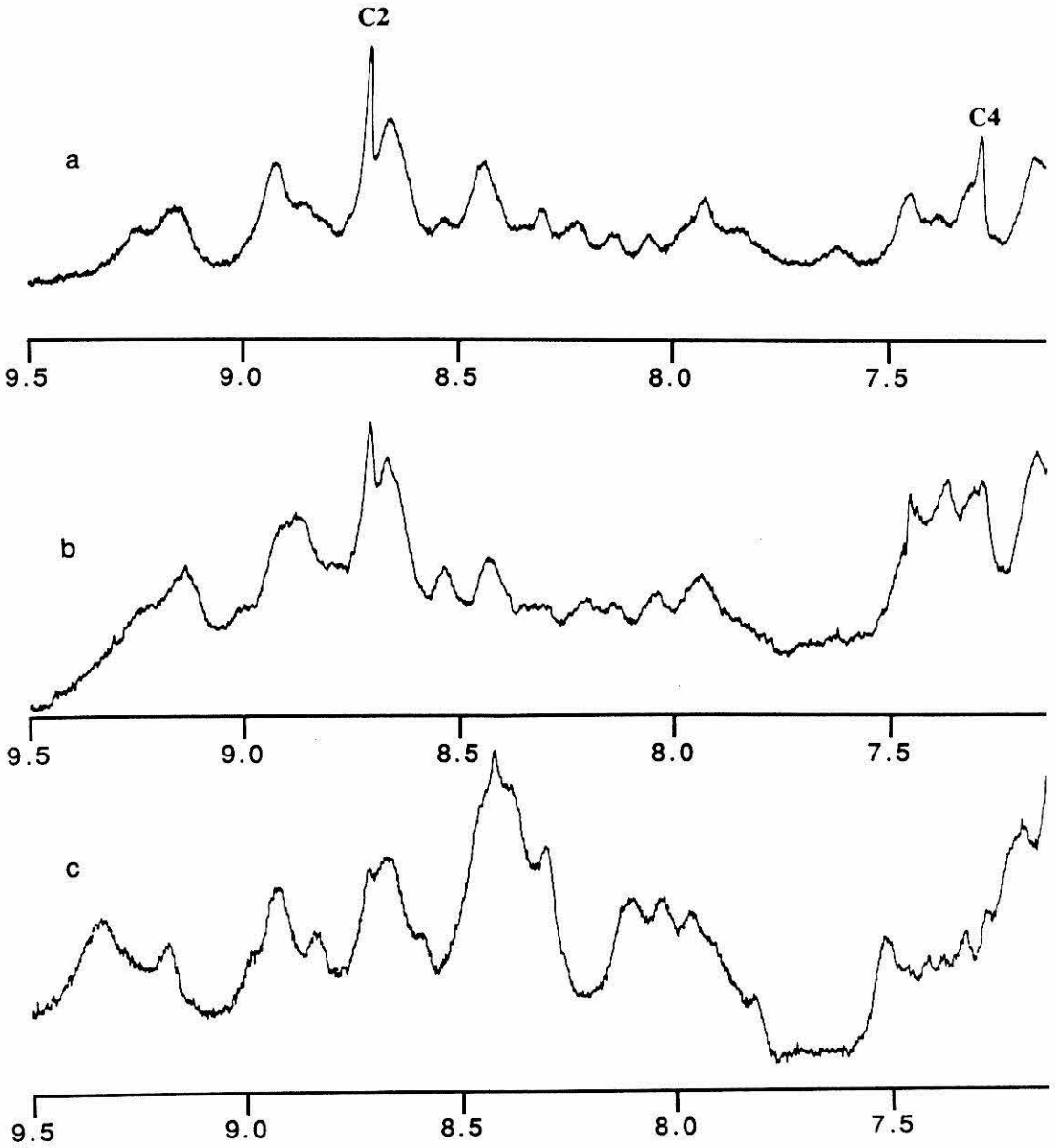
C2
C4
a
9.5
9.0
8.5
8.0
7.5
b
9.5
9.0
8.5
8.0
7.5
c
9.5
9.0
8.5
8.0
7.5

derivative. Previous peptide mapping experiments have identified the site of modification in a_5Ru-azurin as His 83. In the ^{1}H-NMR spectrum of a_5Ru-azurin, the C2 and C4 protons of His 83 are clearly broadened or shifted relative to the native spectrum. However, in the spectrum of a_4Ru(py)-azurin (Figure 4b), the protons due to His 83 are not completely broadened. Other changes relative to the native spectrum are also much less apparent in the a_4Ru(py)-azurin spectrum than in the a_5Ru-azurin spectrum. Thus, the ^{1}H-NMR spectrum of the a_4Ru(py) protein does not support ruthenium modification at His 83. Proton resonances due to His 35, the other histidine residue potentially available for modification, are broadened beyond detection in all three spectra, due to their proximity (6.3, 9.4 Å) to Cu(II).[36]

The possibility that the ruthenium label was lost from the protein during preparation of the NMR samples or accumulation of the spectra was considered. The stability of band 2c was determined by monitoring the UV-visible absorption spectrum of a dilute solution of the protein in pH 4.5 buffer over a period of two weeks. Loss of the ruthenium label from the protein would be indicated by loss of the band at ~310 nm, while loss of pyridine from the complex will cause a decrease in absorbance at ~250 nm. No decrease in intensity of either absorbance was observed over two weeks at 5°C. UV-visible spectra of the NMR samples were also recorded; the spectra indicated a loss of no more than 8% of the ruthenium label during preparation of the NMR samples and recording of the spectra.

In previous work with a_5Ru-azurin, the site of ruthenium modification was identified by peptide mapping.[12] In this procedure, the native and modified proteins are digested with trypsin, a sequence-specific protease. The peptides produced in the tryptic digests are separated by HPLC, and the tryptic maps for the native and modified proteins are compared. A peptide of the modified protein which contains the ruthenium label will move in the chromatogram relative to its position in the chromatogram from

the native digest. Peptides identified as being modified are then hydrolyzed and analyzed for amino acid content; comparison of the amino acid content of the modified peptide with the amino acid sequence of the protein allows the site of modification to be determined. Hydrolysis by trypsin is optimal near pH 8.[37] However, at pH 8 or above, $[a_4Ru(py)]^{3+}$ complexes undergo disproportionation to Ru(II) and Ru(IV).[38] Thus, tryptic mapping of the protein could not be performed. Digestion by trypsin at a lower pH was attempted, but resulted in a wide variety of peptides and incomplete digestion of the protein core. Since trypsin cleaves after positively-charged lysine and arginine residues, lowering of the pH probably affects the specificity of the enzyme both by reducing the efficiency of cleavage at Lys and Arg and by increasing the extent of non-specific cleavage at other protonated residues. Other methods of cleaving the protein were tried, including o-iodosobenzoic acid and pepsin, but satisfactory peptides were not obtained.

Characterization of other products

Band 2a was the major product of the modification reaction, and represented about 25% of the reaction mixture. The UV-visible spectrum of this band (Figure 5) exhibits a broad absorption centered near 360 nm. This band may result from loss of an ammine ligand from the ruthenium complex; however, the spectrum does not correspond to that expected for an $a_4Ru(H_2O)$-histidine product.[39] The spectrum also eliminates the possibility of a C-bound histidine-ruthenium complex.[30,31]

Alternatively, band 2a may represent azurin modified with ruthenium at a site other than histidine. Cysteine and methionine are the most likely candidates for labeling by the ruthenium reagent, after histidine. Azurin contains three cysteines; one of these is coordinated to copper, while the other two form a cysteine bridge. Five methionine residues are located on the surface of the protein. The work of Taube et al.[40,41]

Figure 5. UV-visible spectrum of band 2a from the modification of Pae azurin with $a_4Ru(py)$

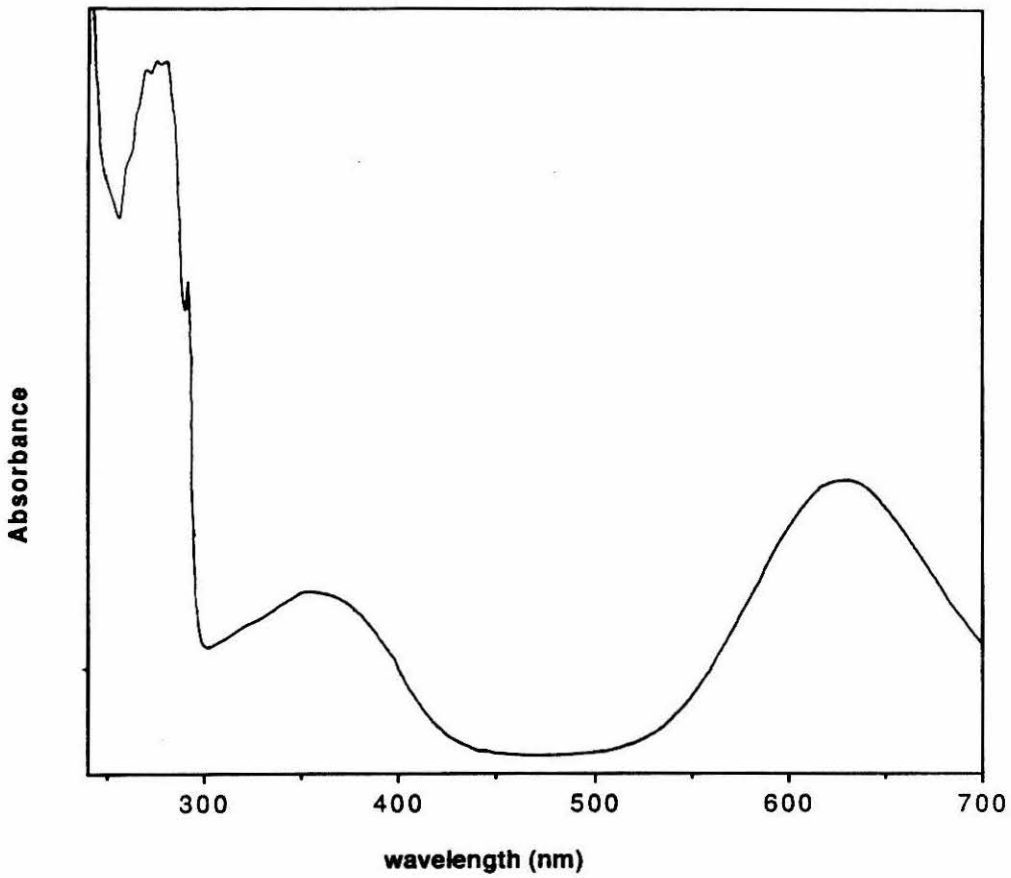
Absorbance
300
400
500
600
700
wavelength (nm)

provides relevant formation and stability constants for ruthenium ammine complexes of SMe_2, a model for methionine. Formation of $[a_5Ru(SMe_2)]^{2+}$ from $[a_5Ru(OH_2)]^{2+}$ proceeds at roughly the same rate as formation of $[a_5Ru(imz)]^{2+}$, and the stability constants for the two complexes are comparable (10^5 - 10^6). Once oxidized to the Ru(III) state, however, the SMe_2 complex will dissociate, while the imidazole complex is stable. The dissociation of $[a_5Ru(SMe_2)]^{3+}$ is very slow ($k = 2.6 \times 10^{-7}$ s^{-1} in 0.2M HCl at 25°C); thus, the oxidized thioether complex persists in solution for a period of weeks.[41] However, in the preparation of modified azurin, the reagents used to oxidize Ru(II) and Cu(I) to Ru(III) and Cu(II) are not capable of oxidizing a Ru(II)-thioether complex. The redox potential of $[Co(edta)]^{0/-}$ is 380 mV vs NHE,[42] while that of $[a_5Ru(Met)]^{3+/2+}$ is 530 mV.[40] The reduction potential of the $[a_4Ru(py)(Met)]^{3+/2+}$ complex is predicted to be even more positive than that of $[a_5Ru(Met)]^{3+/2+}$, due to back-bonding to the pyridine by Ru(II). Thus, all but a small fraction of the methionine complex will remain in the Ru(II) state, and will therefore be stable indefinitely ($K_{eq} \geq 10^5$).[40] The UV-visible spectrum of band 2a shows the presence of the pyridine $\pi \rightarrow \pi^*$ transitions, but at higher energy (~245 nm) than in band 2c (250 nm). The pyridine absorptions are expected to appear near 245 nm in complexes of ruthenium(II),[28,34] perhaps indicating that band 2a corresponds to a methionine modification. However, the UV-Visible spectrum of $a_5Ru(SMe_2)$ exhibits relatively intense absorptions ($\varepsilon = 2 \times 10^3$ $M^{-1}cm^{-1}$) at 235 nm and 258 nm, but only a very weak absorption in the visible region ($\varepsilon_{358} = 64$ $M^{-1}cm^{-1}$); thus, methionine modification would not explain the strong absorption in the visible region observed for band 2a.

The ^{1}H-NMR spectrum of band 2a (data not shown) was different from the native spectrum, but did not clearly indicate modification at His 83. The product was not further characterized.

Recently, Jackman et al. reported the a_5Ru modification of the blue copper protein plastocyanin.[43] The modification products included a band (band 3) which travelled ahead of the a_5Ru-histidine product on a cation exchange column, and which exhibited a UV-visible spectrum similar to that of band 2a in this work. Jackman et al. suggested that their band 3 contained ruthenium bound at histidine, but the product was not further characterized. The observation in the plastocyanin modification of an apparently singly-modified product other than the desired a_5Ru-histidine product, together with the results of this work, demonstrate the importance of obtaining conclusive UV-visible difference spectra as part of the characterization of ruthenium-modified proteins.

The UV-visible spectrum of band 2b is similar to that of band 2a. Band 2b was obtained in significantly lower yields than band 2a (~8%), and was not further characterized.

Band 2d exhibits a UV-visible spectrum identical to that of band 2c, and travels with band 2c on a polyacrylamide electrophoresis gel. If band 2c is $a_4Ru(py)$-(His 83)azurin, then a possible assignment for band 2d would be $a_4Ru(py)$-(His 35)azurin. As discussed above, His 35 is not accessible to the solvent, according to a simulation of solvent accessibility based on the crystal structure. However, His 35 of Pae azurin can be protonated;[44] the protonation is slow, indicating some inhibition of the protonation by the surrounding protein structure. One possibility is that the solution conformation of the protein allows substantial mobility in the region near His 35, and thus His 35 can be modified by the ruthenium reagent. Pae azurin is known to undergo a small conformational change, involving the region of the protein near His 35. His 35 is very close to the copper site (~6 Å); the imidazole ring of His 35 lies adjacent to His 46, a copper ligand.[17,18] Thus it seems likely that ruthenium modification of His 35 would

perturb the copper site. No evidence of a change at the copper site was found in the UV-Vis spectrum of the modified protein.

Evidence that His 35 of Pae azurin can be modified is found in the UV-visible spectrum of band 3. Figure 6a shows the spectrum of band 3; the difference spectrum obtained by subtracting the native spectrum is shown in Figure 6c. The similarity between the difference spectrum and the spectrum of $[a_4Ru(py)(imz)]Cl_3$ (Figure 6b) indicates that $[a_4Ru(py)]^{3+}$ is bound to histidine residues in the protein. From the difference spectrum and the spectrum of the model complex, a Ru:azurin ratio of 1.8 is obtained. Since the only two histidines which are not ligands to copper are His 83 and His 35, the spectrum of band 3 provides compelling evidence that His 35 in Pae azurin can be modified.

Electron transfer kinetics

An approximate rate of electron transfer between the copper and ruthenium sites in band 2c was measured by a flash photolysis method. The reaction sequence is shown in Scheme 1. A ~5 μs flash from a xenon lamp produces the strongly reducing excited state

$$Ru(bpy)_3^{2+} \xrightarrow{h\nu} Ru(bpy)_3^{2+*}$$

$$Ru(bpy)_3^{2+*} + Ru^{3+}\text{-}Cu^{2+} \rightarrow Ru(bpy)_3^{3+} + Ru^{2+}\text{-}Cu^{2+} + Ru^{3+}\text{-}Cu^{+}$$

$$\downarrow \text{EDTA}$$

$$Ru(bpy)_3^{2+}$$

$$Ru^{2+}\text{-}Cu^{2+} \xrightarrow{k_{et}} Ru^{3+}\text{-}Cu^{+}$$

Scheme 1

of $Ru(bpy)_3^{2+}$ ($E°(Ru^{3+/2+*})$ = -0.84 V vs NHE[45]), which transfers an electron to the fully oxidized modified protein (Ru(III)-Cu(II)). Both Ru(II)-Cu(II) and

Figure 6. UV-visible spectra of Pae azurin and the model complex

a. Band 3 from the modification of Pae azurin with $a_4Ru(py)$

b. $[a_4Ru(py)(imz)]Cl_3$

c. Difference spectrum (modified azurin - native azurin). See text.

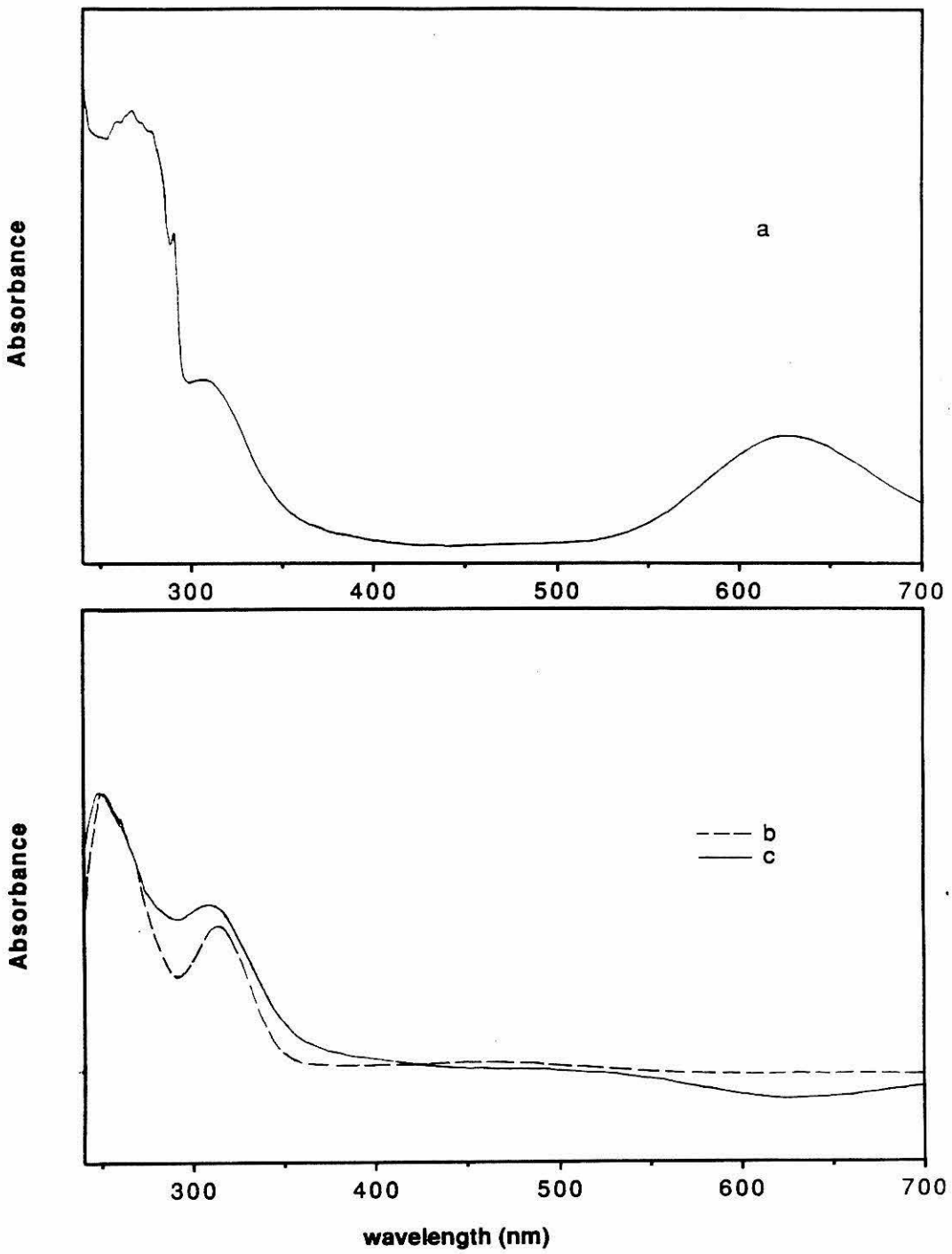
Absorbance
a
300
400
500
600
700
Absorbance
b
c
300
400
500
600
700
wavelength (nm)

Ru(III)-Cu(I) will be produced in the initial reduction by $Ru(bpy)_3^{2+*}$; $Ru(bpy)_3^{3+}$ is then scavenged by EDTA.[46] Intramolecular electron transfer will then occur in the azurin molecule, to produce an equilibrium mixture of reduced and oxidized Ru and Cu. The change in Cu(II) concentration with time is monitored at 625 nm. Since the potential of the copper is 308 mV vs NHE[47] and the potential of the ruthenium site is estimated to be ~317 mV (based on the model complex), approximately equal concentrations of Cu(I) and Ru(II) will exist at equilibrium.

Figure 7 shows the results of a flash experiment at 25°C; native azurin is shown in Figure 7a, and band 2c in Figure 7b. In native azurin, an initial decrease in absorbance at 625 nm is observed immediately after the flash, due to direct reduction of the copper by $Ru(bpy)_3^{2+*}$. The initial decrease in absorbance in the modified azurin sample is followed by a gradual decrease in absorbance, due to reduction of the copper by the bound Ru(II). A fit of this data to a first order plot yields a value of k_{obs} of $\sim 0.01 s^{-1}$. If the redox potentials of the copper and ruthenium sites are approximately equal, then the rate of electron transfer from ruthenium to copper will be $\sim 0.005 s^{-1}$, since $k_{obs} = k_1 + k_{-1}$. This preliminary rate constant can be compared with the rate constant of 2 s^{-1} obtained in a_5Ru-(His 83) azurin in previous work;[11] the thermodynamic driving force in the a_5Ru system was 280 mV. Thus, the rate of intramolecular electron transfer in azurin is found to decrease as the driving force decreases, in accord with theoretical predictions.[1,2]

Conclusions

The amount of the desired product, band 2c, which could be prepared was limited by the formation of a large amount (~25%) of band 2a during each preparation. In addition, definite characterization of band 2a as containing a single a_4Ru(py)

Figure 7. The change in absorbance at 625 nm after a ~5μs flash

a. Native Pae azurin

b. Band 2c from the modification of Pae azurin with $a_4Ru(py)$

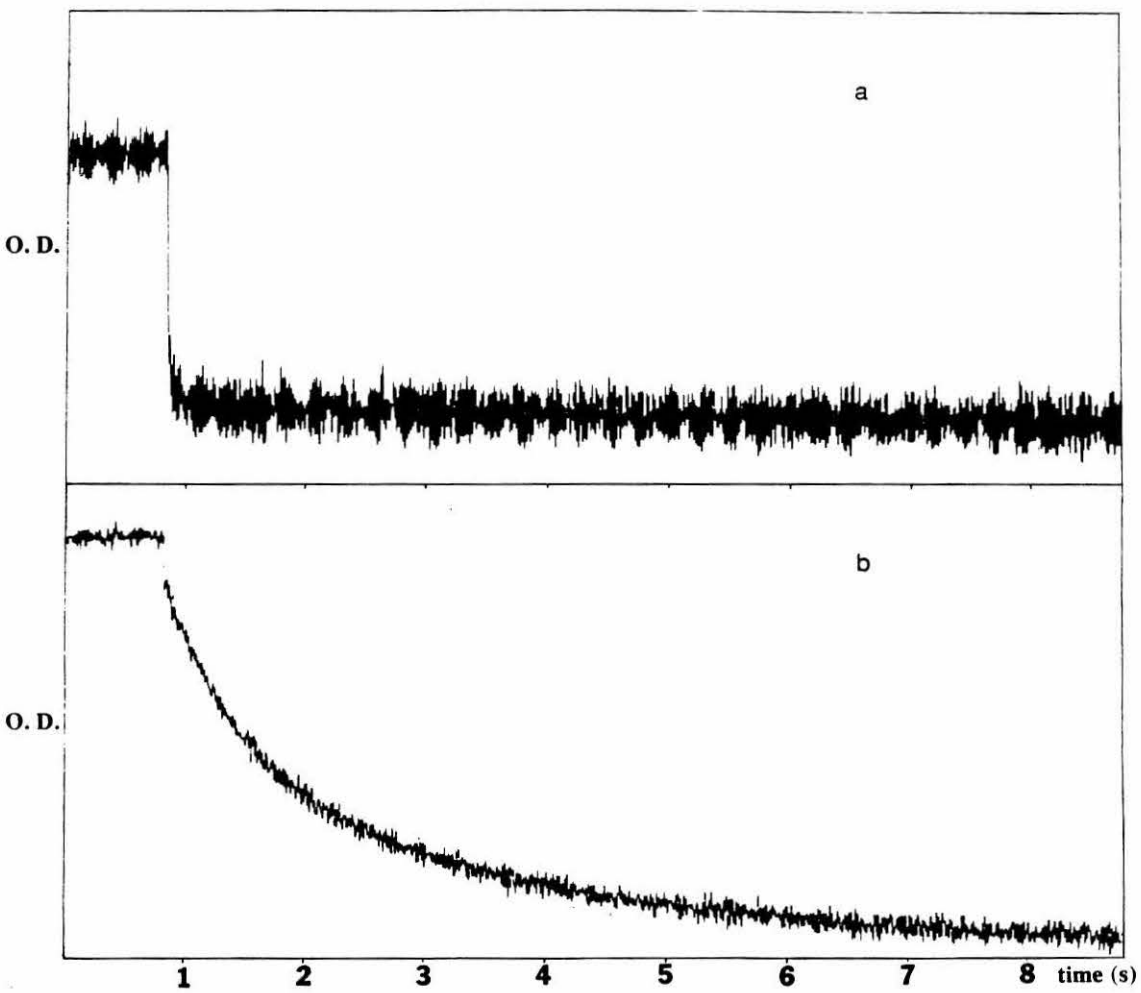
a
O. D.
b
O. D.
1
2
3
4
5
6
7
8
time (s)

modification at His 83 was not possible, due to the ambiguity of the NMR spectrum and the infeasibility of tryptic mapping experiments with $a_4Ru(py)$-labeled proteins.

Modification of Ade azurin

The modification of Ade azurin with $[a_5Ru(H_2O)]^{2+}$ proceeds rapidly at pH 7.2 and 25°C. A chromatogram of the separation of the modified products by cation exchange FPLC is shown in Figure 8. Native azurin elutes at the void volume with Na[Co(edta)].

The UV-visible spectrum of band 2 is shown in Figure 9a. Subtraction of the native Ade azurin spectrum (Figure 9b) yields the difference spectrum shown in Figure 9c. The difference spectrum exhibits a strong absorption at ~300 nm and a weaker band near 450 nm; these absorptions are characteristic of $a_5Ru(His)$.[30] An approximate concentration of the ruthenium complex can be calculated based on the extinction coefficients of the model complex.[30] In this way, a Ru:azurin ratio of 1:1 is obtained.

The results of a computer simulation of the solvent accessibility of the histidine residues in Ade azurin are shown in Figure 10. Using a probe radius of 1.4 Å, the surface areas of the His 32 and His 83 side chains were found to be identical (46 $Å^2$). His 35 is not accessible to solvent according to the simulation, and ^1H-NMR results indicate that His 35 cannot be protonated except at very low pH (~4.5). Thus, band 2 must contain an a_5Ru modification at either His 32 or His 83. Band 3 exhibits a UV-visible spectrum very similar to that of band 2, and thus probably contains an a_5Ru-histidine modification as well.

Since the histidine resonances in the NMR spectrum of oxidized azurin have been assigned,[48] the identification of the sites of modification in Ade azurin should be possible by NMR. Characterization of the products and measurement of the electron transfer rates are currently in progress.

Figure 8. An elution profile for the separation of the products of modification of Ade azurin with a_5Ru. Buffer A is 0.05 M NH_4OAc, pH 5.2; buffer B is buffer A + 1.0 M NaCl.

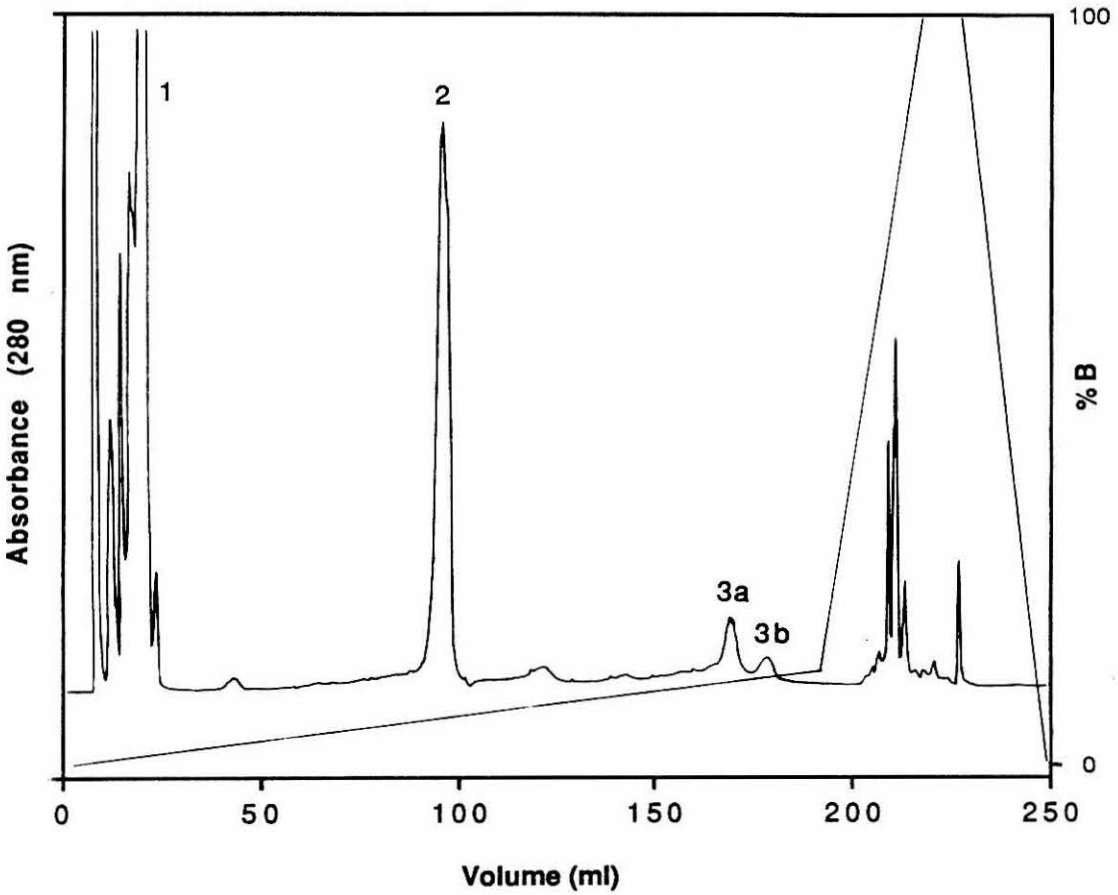
1
2
3a
3b
Absorbance (280 nm)
%B
100
0
0
50
100
150
200
250
Volume (ml)

Figure 9. UV-visible spectra of Ade azurin

a. Band 2 from the modification of Ade azurin with a_5Ru

b. Native Ade azurin

c. Difference spectrum (modified azurin - native azurin), shown at four times the sensitivity of spectra (a) and (b). See text.

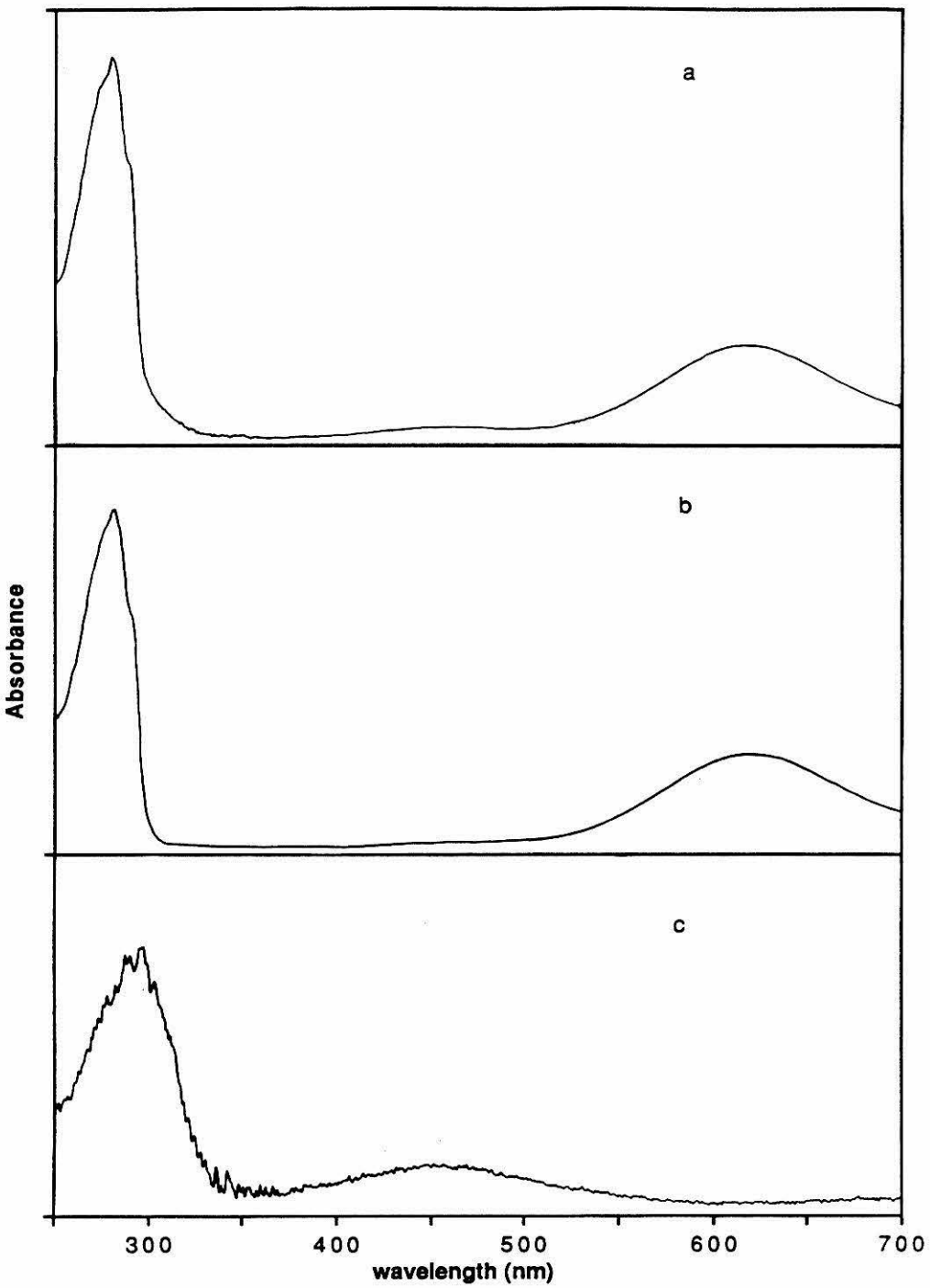
a
b
c
Absorbance
300
400
500
600
700
wavelength (nm)

Figure 10. View of the Ade azurin structure showing the solvent accessibility of the non-ligand histidine residues. The dotted regions indicate the surface accessible to a 1.4 Å probe. The simulation was performed using the program Biograf (BioDesign, Pasadena, CA). The side chain of His 35 is completely inaccessible to solvent, according to the simulation.

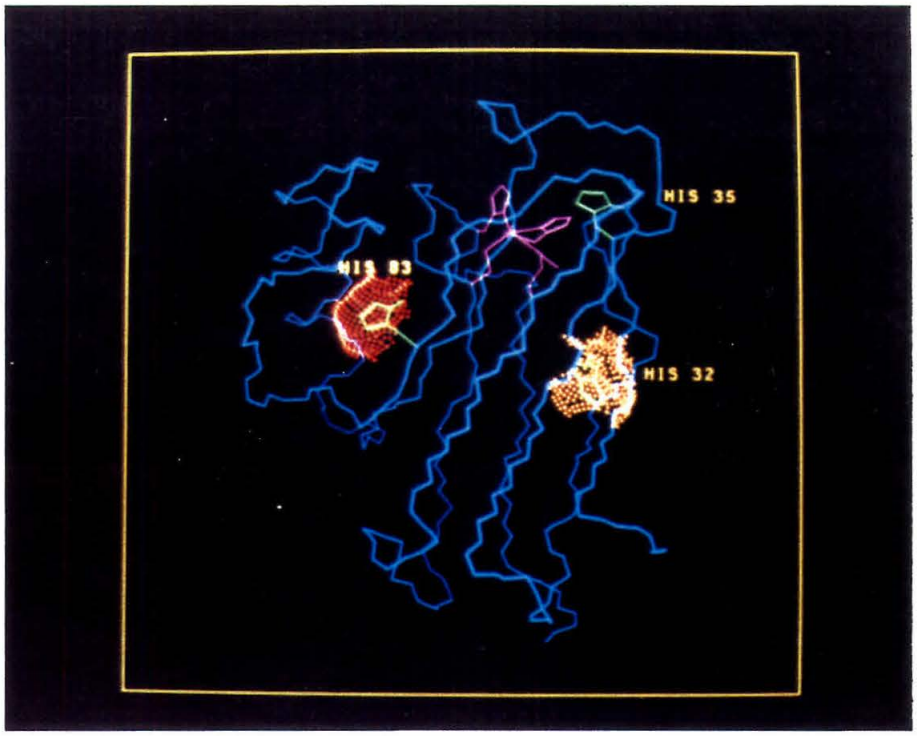
HIS 35
HIS 83
HIS 32

REFERENCES AND NOTES

1. (a) Marcus, R. A. *Annu. Rev. Phys. Chem.* **1964,** *15,* 155; (b) Sutin, N. *Progr. Inorg. Chem.* **1983,** *30,* 441; (c) Marcus, R. A.; Sutin, N. *Biochim. Biophys. Acta* **1985,** *811,* 265.

2. DeVault, D. "Quantum Mechanical Tunneling in Biological Systems", 2nd ed.; Cambridge University Press: Cambridge, 1984.

3. Onuchic, J.; Beratan, D. *J. Am. Chem. Soc.* **1987,** *109,* 6771.

4. Liang, N.; Mauk, A. G.; Pielak, G. J.; Johnson, J. A.; Smith, M.; Hoffman, B. M. *Science 1988,* **240,** 311.

5. Axup, A. W.; Albin, M.; Mayo, S. L.; Crutchley, R. J.; Gray, H. B. *J. Am. Chem. Soc.* **1988,** *110,* 435.

6. Elias, H.; Chou, M. H.; Winkler, J. R. *J. Am. Chem. Soc.* **1988,** *110,* 429.

7. Karas, J. L.; Lieber, C. M.; Gray, H. B. *J. Am. Chem. Soc.* **1988,** *110,* 599.

8. Lieber, C. M.; Karas, J. L.; Gray, H. B. *J. Am. Chem. Soc.* **1987,** *109,* 3778.

9. Crutchley, R. J.; Ellis, W. R.; Gray, H. B. *J. Am. Chem. Soc.* **1986,** *108,* 5002.

10. Mayo, S. L.; Ellis, W. R.; Crutchley, R. J.; Gray, H. B. *Science* **1986,** *233,* 948.

11. Kostic, N. M.; Margalit, R.; Che, C.-M.; Gray, H. B. *J. Am. Chem. Soc.* **1983,** *105,* 7765.

12. Margalit, R.; Kostic, N. M.; Che, C.-M.; Blair, D. F.; Chiang, H. J.; Pecht, I.; Shelton, J. B.; Shelton, J. R.; Schroeder, W. A.; Gray, H. B. *Proc. Natl. Acad. Sci. U.S.A.* **1984,** *81,* 6554.

13. Cowan, J. A.; Gray, H. B. *Chem. Scripta* **1988,** *28A,* 21.

14. (a) Yocom, K. M.; Shelton, J. B.; Shelton, J. R.; Schroeder, W. A.; Worosila, G.; Isied, S. S.; Bordignon, E.; Gray, H. B. *Proc. Natl. Acad. Sci.* **1982,** *79,* 7052; (b) Winkler, J. R.; Nocera, D. G.; Yocom, K. M.; Bordignon, E.; Gray, H. B. *J. Am. Chem. Soc.*

1982, *104,* 5798; (c) Nocera, D. G.; Winkler, J. R.; Yocom, K. M.; Bordignon, E.; Gray, H. B. *J. Am. Chem. Soc.* **1984,** *106,* 5145.

15. Taube, H. *Comm. Inorg. Chem.* **1981,** *1,* 17.

16. Taube, H. *Survey Prog. Chem.* **1973,** *6,* 1.

17. Adman, E. T.; Jensen, L. H. *Isr. J. Chem.* **1981,** *21,* 8.

18. Adman, E. T.; Stenkamp, R. E.; Sieker, L. C.; Jensen, L. H. *J. Mol. Biol.* **1978,** *123,* 35.

19. Baker, E. N. *J. Mol. Biol.* **1988,** *203,* 1071.

20. Norris, G. E.; Anderson, B. F.; Baker, E. N. *J. Mol. Biol.* **1983,** *165,* 501.

21. Norris, G. E.; Anderson, B. F.; Baker, E. N. *J. Am. Chem. Soc.* **1986,** *108,* 2784.

22. Adman, E. T. In "Topics in Molecular and Structural Biology"; Harrison, P., Ed.; VCH Verlagsgesellschaft: Weinheim, BRD, 1984; Vol. 1, Chapter 1.

23. Rosen, P.; Pecht, I. *Biochemistry* **1976,** *15,* 775.

24. Fife, T.; Bruice, T. J. *J. Phys. Chem.* **1961,** *65,* 1079.

25. Milder, S. J.; Goldbeck, R. A.; Kliger, D. S.; Gray, H. B. *J. Am. Chem. Soc.* **1980,** *102,* 6762.

26. Vogt, L. H.; Katz, J. L.; Wiberley, S. E. *Inorg. Chem.* **1965,** *4,* 1157.

27. Curtis, J. C.; Sullivan, B. P.; Meyer, T. J. *Inorg. Chem.* **1983,** *22,* 224.

28. Ford, P.; Rudd, D. F. P.; Gaunder, R.; Taube, H. *J. Am. Chem. Soc.* **1968,** *90,* 1187.

29. Krogh-Jespersen, K.; Schugar, H. J. *Inorg. Chem.* **1984,** *23,* 4390.

30. Sundberg, R. J.; Gupta, G. *Bioinorg. Chem.* **1973,** *3,* 39.

31. Sundberg, R. J.; Bryan, R. F.; Taylor, I. F., Jr.; Taube, H. *J. Am. Chem. Soc.* **1974,** *96,* 381.

32. Isied, S. S.; Taube, H. *Inorg. Chem.* **1976,** *15,* 3070.

33. Allen, R. J.; Ford, P. C. *Inorg. Chem.* **1974,** *13,* 237.

34. Shepherd, R. E.; Taube, H. *Inorg. Chem.* **1973,** *12,* 1392.

35. Solomon, E. I.; Hare, J. W.; Dooley, D. M.; Dawson, J. H.; Stephens, P. J.; Gray, H. B. *J. Am. Chem. Soc.* **1980,** *102,* 168.

36. Canters, G. W.; Hill, H. A. O.; Kitchen, N. A.; Adman, E. T. *Eur. J. Biochem.* **1984,** *138,* 141.

37. Allen, G. "Sequencing of Proteins and Peptides"; North-Holland: Amsterdam, 1981.

38. Rudd, D. P.; Taube, H. *Inorg. Chem.* **1971,** *10,* 1543.

39. Che, C.-M.; Margalit, R.; Chiang, H.-J.; Gray, H. B. *Inorg. Chim. Acta* **1987,** *135,* 33.

40. The compound for which a redox potential is available is the complex of pentaammineruthenium with the methyl ester of methionine: Kuehn, C. G.; Taube, H. *J. Am. Chem. Soc.* **1976,** *98,* 689.

41. Stein, C. A.; Taube, H. *Inorg. Chem.* **1979,** *18,* 1168.

42. Hin-Fat, L.; Higginson, C. E. *J. Chem. Soc. A.* **1967,** 298.

43. (a) Jackman, M. P.; McGinnis, J.; Powls, R.; Salmon, G. A.; Sykes, A. G. *J. Am. Chem. Soc.* **1988,** *110,* 5880; (b) Jackman, M. P.; Sykes, A. G.; Salmon, G. A. *J. Chem. Soc., Chem. Commun.* **1987,** 65.

44. (a) Hill, H. A. O.; Smith, B. E. *J. Inorg. Biochem.* **1979,** *11,* 79; (b) Ugurbil, K.; Bersohn, R. *Biochemistry* **1977,** *16,* 3016.

45. Sutin, N.; Creutz, C. *Adv. Chem. Ser.* **1978,** *168,* 1.

46. Whitten, D. G. *Acc. Chem. Res.* **1980,** *13,* 83.

47. Taniguchi, V. T.; Sailasuta-Scott, N.; Anson, F. C.; Gray, H. B. *Pure Appl. Chem.* **1980,** *52,* 2275.

48. Groeneveld, C. M.; Ouwerling, M. C.; Erkelens, C.; Canters, G. W. *J. Mol. Biol.* **1988,** *200,* 189.